

UNIVERSITY OF CALIFORNIA, SAN DIEGO

Climatic and oceanographic controls on the burial and
preservation of organic matter in equatorial Pacific
deep-sea sediments.

A dissertation submitted in partial satisfaction of the
Requirements for the degree Doctor of Philosophy in

Earth Sciences

by

Helen M. Perks

Committee in charge:

Professor Ralph F. Keeling, Chair
Professor Christopher D. Charles
Professor Ellen R. M. Druffel
Professor Joris M. Gieskes
Professor Andrew C. Kummel

1999

UNIVERSITY OF CALIFORNIA, SAN DIEGO

Climatic and oceanographic controls on the burial and
preservation of organic matter in equatorial Pacific
deep-sea sediments.

A dissertation submitted in partial satisfaction of the
Requirements for the degree Doctor of Philosophy in

Earth Sciences

by

Helen M. Perks

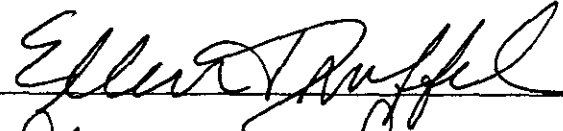
Committee in charge:

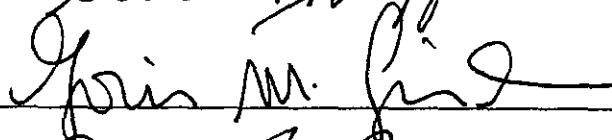
Professor Ralph F. Keeling, Chair
Professor Christopher D. Charles
Professor Ellen R. M. Druffel
Professor Joris M. Gieskes
Professor Andrew C. Kummel

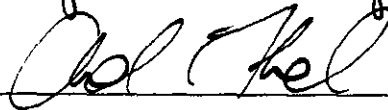
1999

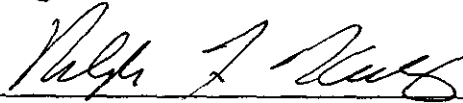
The dissertation of Helen M. Perks is approved, and it is acceptable in quality and form for publication on microfilm:











Chair

University of California, San Diego

1999

To know that we know what we know, and that we do not know what we do not know,
that is true knowledge.

- Confucius

The path is the goal.

- Eastern wisdom

This thesis is dedicated to the memory of my aunt, Lucy Dickens.

TABLE OF CONTENTS

Signature Page		iii
Table of Contents		v
List of Figures and Tables		vii
Acknowledgements		ix
Vita and Publications		xiii
Abstract.....		xv
Chapter 1. Introduction.....		1
1.1 References.....		7
Chapter 2. A 400 kyr record of combustion oxygen demand in the western equatorial Pacific: Evidence for a precessionally forced climate response		10
2.1 Introduction.....		11
2.2 Methods and samples		14
2.3 Results and discussion		16
2.4 Summary.....		24
2.5 References		27
Chapter 3. Coherent synchronous precessional forcing in the eastern and western equatorial Pacific		30
3.1 Introduction		30
3.2 Method and Results		32
3.3 Discussion		39
3.4 Summary		42
3.5 References		44
3.6 Tables		48
Chapter 4. Sedimentological studies with the combustion oxygen demand instrument in box and piston cores from the eastern and western equatorial Pacific		57
4.1 Introduction.....		58
4.2 Size fraction study in RC17-177 from the Ontong-Java Plateau		61
4.3 Box core studies on the Ontong-Java Plateau		65
4.3.1 ERDC 112Bx		65
4.3.2 ERDC 128Bx		71

4.4	Box core studies in the eastern equatorial Pacific	73
4.4.1	PLDS 66Bx	73
4.5	A comparison of COD in core-top and core-bottom samples from ERDC (Ontong-Java Plateau) box cores	75
4.6	COD in PLDS (eastern/central equatorial Pacific) box and piston cores.....	79
4.7	A 4 Million-Year COD record from the Ontong-Java Plateau and eastern equatorial Pacific	85
4.8	Summary	89
4.9	References	91
4.10	Tables.....	93
Appendix A	<i>The combustion oxygen demand method: Instrument performance and calibration</i>	103

LIST OF FIGURES AND TABLES

Figure 1.1	Map of equatorial Pacific showing location of RNDB 74P and ODP 849.....	3
Figure 2.1	Map of the Ontong-Java Plateau	13
Figure 2.2	Experimental setup of the combustion oxygen demand (COD) apparatus	15
Figure 2.3	COD in RNDB 74P	17
Figure 2.4	COD in ERDC 112Bx	20
Figure 2.5	Power spectral analysis of COD and $\delta^{18}\text{O}$ in RNDB 74P	22
Figure 3.1	Map of the tropical Pacific showing core locations	33
Figure 3.2	COD in RNDB 74P and ODP 849	34
Figure 3.3	Cross-spectral analysis of COD and $\delta^{18}\text{O}$ in RNDB 74P and ODP 849	36
Figure 3.4	Comparison of COD in RNDB 74P and ODP 849 with atmospheric methane concentration in the Vostok ice core	38
Table 3.1	COD and oxygen isotope data for RNDB 74P	48
Table 3.2	COD and oxygen isotope data for ODP 849	52
Figure 4.1a	Ontong-Java Plateau sites	59
Figure 4.1b	Eastern equatorial Pacific core sites	60
Figure 4.2	COD in different size fractions in RC 17-177	63
Figure 4.3	COD in RNDB 74P against sand concentration	65
Figure 4.4	COD in sub-cores from box core ERDC 112Bx	66
Figure 4.5	COD in ERDC 128Bx	72
Figure 4.6	COD in PLDS 66Bx	74
Figure 4.7a	COD against water depth for near core-top samples from box cores from the Ontong-Java Plateau	76
Figure 4.7b	COD against water depth for near core-top samples from box cores from the Ontong-Java Plateau	76
Figure 4.7c	COD against water depth for LGM samples from box cores from the Ontong-Java Plateau	77
Figure 4.8	COD against benthic foraminifer accumulation rates in near core-top and LGM samples from box cores from the Ontong-Java Plateau	77
Figure 4.9a	COD in PLDS 73PV	80
Figure 4.9b	COD in PLDS 69PV	80
Figure 4.9c	COD in PLDS 16PV	82
Figure 4.9d	COD in PLDS 15PG	82
Figure 4.9e	COD in PLDS 92Bx	84
Figure 4.9f	COD in PLDS 107Bx	84
Figure 4.10	COD in ODP 806B plotted with RNDB 74P for the last ~4Myr	86
Figure 4.11	COD in ODP 851B for the last ~3.7Myr	87
Table 4.1a	Site data for Ontong-Java Plateau cores	93
Table 4.1b	Site data for eastern and central equatorial Pacific cores	94
Table 4.2	Data for RC17-177 appearing in Figure 4.2	95
Table 4.3	Data for ERDC 112Bx appearing in Figure 4.3	96

Table 4.4	Data for ERDC 128Bx appearing in Figure 4.4	100
Table 4.5	Data for ERDC cores appearing in Figures 4.7 and 4.8	101
Figure A.1	Measured O ₂ consumption for different concentrations of urea solution	105
Figure A.2	Measured O ₂ consumption for elemental sulfur	105
Figure A.3	Typical oxygen depletion peak	107
Figure A.4	Calibration curve for KHP solution.....	108
Figure A.5	COD in standards of KHP on calcium carbonate	108

ACKNOWLEDGEMENTS

Firstly, I would like to acknowledge Ralph Keeling, my advisor for my 6+ years at Scripps. Ralph provided the opportunity for me to pursue my Ph.D. studies, and always made himself available for discussions whilst encouraging me to be truly independent, for which I know I will be very grateful in the future. He also appreciated my attempts in my final months in La Jolla to discover the until-then mysterious lure of surfing. You'll see me on my board in Lake Superior! Many thanks also to Chris Charles who gave me much input and advice during my Ph.D. time, especially in the final year, taught me some of the basics of Zen foram picking, and a baptism in intense (harsh) grading sessions, but unfortunately failed to instill in me very much appreciation for his music tastes (no music test for me!). I am very grateful for all of his help and always appreciated his dry humor. Thank-you to Ellen Druffel, Joris Gieskes and Andy Kummel for serving on my doctoral committee and for their interest and very valuable input.

I thank Tracy Quan, Jason Giordano and Selene Eltgroth for their help and enthusiasm, and for teaching me a little about teaching others. This made my time in the lab burning mud far more rewarding.

Special thanks to Juan Carlos Herguera for all his help and interest. I'm sorry that I didn't visit Ensenada many more times, but I will be back... Also thank-you to Memorie Yasuda and Warren Smith.

For his always very generous help and lending of expertise in the lab I would like to say a big thank-you to Bill Paplowsky. I am always amazed by his seemingly

endless knowledge of lab procedures and ability to fix just about anything. Also many thanks to Elizabeth McEvoy, for keeping our lab a cheery sociable place and baking many very delicious and creative cakes.

I would like to acknowledge Ray Weiss, Gustaf Arrhenius and the Scripps Analytical Facility for the generous loan of lab equipment and supplies.

I am very grateful to Nick Shackleton at Cambridge University for his enthusiasm, support and advice during my Ph.D. studies, from which I learned much. Thank-you also to John Hayes and Dan McCorkle at WHOI for their support and help, and to Jack Gudeman in John Hedges' lab at the University of Washington for making comparative measurements. Also to Tim Herbert, Luc Beaufort and Amos Winter.

Chapter 2 is reproduced with slight modifications from Perks, H. M. and R.F. Keeling, A 400 kyr record of combustion oxygen demand in the western equatorial Pacific: Evidence for a precessionally forced climate response, *Paleoceanography*, 13, 63-69, 1998. I was the primary investigator and lead author for this paper, and conducted all of the analyses presented therein. Chapter 3, in slightly revised form, will be submitted to *Paleoceanography* as Perks, H. M., C. D. Charles and R.F. Keeling, Coherent and synchronous precessional forcing in the eastern and western equatorial Pacific. I was the primary investigator and lead author for this manuscript, and conducted all of the analyses presented therein.

My years in San Diego at Scripps have very much been life-shaping ones and I feel I have learned much and gained many memories which will forever enrich my life. I have been very lucky to have shared this time with some special people who

have become very close friends to me. Andrew, I would like to say a very big thank-you to you for being a shining example of what true friendship is all about, and for conveying a small understanding of what life is like in the Deaf World. A very big *Dankeschoen* to Conny and Christine for all the times we have spent together and also for being very dear friends to me. To Ulli, for your friendship before we both had to leave San Diego, when we weren't quite ready and still had much surfing to do. To Kim, who has tried to instill her "work-hard-play-hard" mentality in me, and her love of dancing the night away. To Jon for being a great friend, making me laugh, and laughing at me all the time. Many thanks to Kriszta, Aivo, Aave, and Dave Hamm for your friendship. To Sanford for his smiling face and kind words of support. Also to Ule, Graham, David Hunter, and to Hernán, Thom, Julianna, Peter, Kati, Scott and Justin for fun times this past year. And to all friends who attended that fateful ("5 P's") party (*Poisoned and Puking from Perks' Ph.D. Party*) that had everyone keeling over. We will probably never know...

Of course, the fact that I am here and could write this thesis at all is owed to the love, support and encouragement of my parents, Jean Dellow and Trevor Perks, and my brother John Perks.

I would like to thank Tim Lueker for all the experiences we went through together, and his children, Tom and Evi, for teaching me some very important life lessons.

Thank-you to the person who helped me in a time of crisis and caused me to think hard, from which I have learned much.

And finally, fitting as to where I find myself as I finish up my thesis, I would like to say a very big thank-you to Sandia Man, the Pumpkin Murderer, for inspiring me through the final weeks, often in crazy ways. Thank-you!!! It will feel oh so good to board that plane.

And to the Beach, Baja, Björk, Broadcasts from Europe and Bierspucken...

Vita

- 1991 B.Sc. (1st Class Hons.) University of Sussex, Brighton, U.K.
Physics with European Studies (German)
- 1993 - 1997 Research Assistant,
University of California, San Diego
- 1997 - 1999 JOI/USSAC Ocean Drilling Fellow
University of California, San Diego
- 1998 - 1999 Research and Teaching Assistant
University of California, San Diego
- 1999 Ph.D., Scripps Institution of Oceanography,
University of California, San Diego

PUBLICATIONS

Articles:

Perks, H. M. and R. F. Keeling, A 400 kyr record of combustion oxygen demand in the western equatorial Pacific: Evidence for a precessionally forced climate response, *Paleoceanography*, 13, 63-69, 1998.

Eltgroth, S.F., H.M. Perks, M.D. Moore, and R.F. Keeling, Organic carbon concentrations in corals determined from combustion oxygen demand measurements, submitted to *Geophys. Res. Letters*, 1999.

Abstracts:

Perks, H.M. and R.F Keeling, Late Pleistocene climatic forcing of combustion oxygen demand in the equatorial Pacific Ocean: A comparison between east and west. Poster, AGU Fall Meeting, San Francisco, USA, Dec 1998.

Perks, H.M. and R.F Keeling, Late Pleistocene climatic forcing of combustion oxygen demand in the equatorial Pacific Ocean: A comparison between east and west. Poster, 6th International Conference on Paleocyanography, Lisbon, Portugal, Aug 1998.

Perks, H.M., Late Pleistocene climatic forcing in the equatorial Pacific Ocean: A comparison between east and west. Poster, Past Global Changes (PAGES) 1st

Open Science Meeting, London, UK, Apr 1998.

Perks, H.M. and R.F. Keeling, Oxygen demand as a new tool for investigating sediment paleochemistry: The Quaternary record of the Ontong-Java Plateau. Oral presentation, AGU Fall Meeting, San Francisco, USA, Dec 1996.

Perks, H.M. and R.F. Keeling, Sediment oxygen demand as a proxy for paleoproductivity: The Quaternary record of the Ontong-Java Plateau. Poster, 5th International Conference on Paleoceanography, Halifax, Canada, Oct 1995.

ABSTRACT OF THE DISSERTATION

Climatic and oceanographic controls on the burial and preservation of organic matter in equatorial Pacific deep-sea sediments.

by

Helen M. Perks

Doctor of Philosophy in Earth Sciences

University of California, San Diego, 1999

Professor Ralph F. Keeling, Chair

The tropical Pacific plays a key role in global climate because of its contribution to the planetary heat and moisture budgets. However, we know little about the behavior of this region in the past under different global climate conditions. Chapters 2 and 3 present two 400,000 yr records of “combustion oxygen demand (COD)”, in deep-sea sediment cores, one from the western equatorial Pacific (160°E) and one from the eastern equatorial Pacific (110°W), to study the interaction of the upper-ocean dynamics, productivity and burial efficiency of organic matter. The COD method was developed as part of my thesis work and measures the total amount of oxygen consumed upon complete combustion of the sediment sample. In the carbonate-rich sediments which lie beneath much of the tropical ocean, COD

approximates closely the organic carbon concentration, measurement of which is complicated with existing techniques because of the difficulty in distinguishing the typically small amount of organic carbon from the large inorganic carbon background. I show that the COD time series are highly coherent with each other over this period and show pronounced precessionally forced peaks of higher productivity during globally colder periods that are in phase in the two cores, suggesting a common insolation forcing mechanism across the equatorial Pacific basin. COD is in phase with global ice volume, as indicated by oxygen isotopes, and with atmospheric methane in the Vostok ice core.

Chapter 4 presents various studies in box and piston cores from sites close to those presented in the previous two chapters, which provide important information for understanding fluctuations in COD down the sediment core and comparing trends between different cores and locations.

1. Introduction.

The tropical oceans, with their role as "heat engines," suppliers of large amounts of latent heat and water vapor to the atmosphere, play a very important role in modern global climate. Variability on seasonal, interannual and longer timescales is increasingly being recognized as spawning teleconnections in far-removed regions of the world (Ropelewski and Halpert, 1987, 1989; Intergovernmental Panel on Climate Change (IPCC), 1995). In particular, due to its large size and its role in producing ENSO events, the tropical Pacific Ocean has been the focus of many studies (e.g. Cane, 1986; Neelin et al., 1998; Seager et al., 1988; Soden, 1997). In addition, the equatorial Pacific plays a major role in the global marine carbon cycle. Vigorous upwelling of nutrient-rich waters along the equator in the eastern and central parts of the ocean gives rise to a strong net flux of CO₂ from the surface waters to the atmosphere. These nutrient-rich waters support high new production (Chavez and Barber, 1987), which draws down the pCO₂ of the surface ocean, and organic matter in turn rains down to deeper waters, a small fraction of it being buried in sea-floor sediments.

In recent years, the role of the tropics in the global climate system over the Last Glacial Maximum (LGM) to Holocene and longer time-scales has been the topic of much research and debate (e.g. Guildersen et al., 1994; Stute et al., 1995; Schrag et al., 1996; Thompson et al., 1998; Cane, 1998). The key to a better understanding of modern tropical climate dynamics lies in improving our knowledge of behavior in the past. Paleoceanographic data sets also provide essential boundary conditions for climate models. Increasing support has recently been gained for the tropical Pacific playing a key role in initiating millennial global climate change and glacial cycles (Cane and Clement, 1998; Cane, 1998). By studying sites in the western and eastern regions of the Pacific, one can obtain information about the basin-

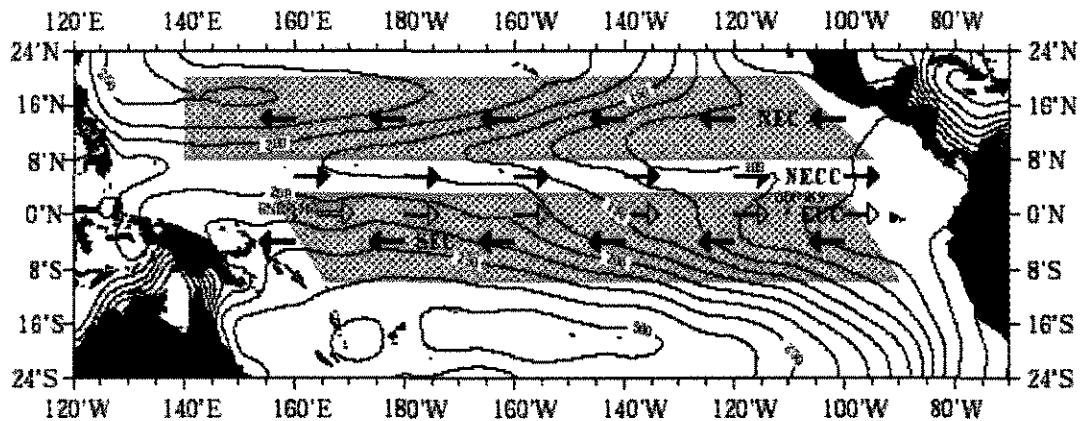
wide responses of the upper ocean along the equator to climatic and oceanographic variability.

This thesis presents studies that have resulted from the development of an instrument to measure the amount of oxygen consumed upon combustion of a sediment sample, a variable that I call the “combustion oxygen demand (COD).” COD is thus a bulk measure of the total amount of reduced materials in the sediment which undergo oxidation during the combustion. Vast areas of the world’s ocean floors, notably in the tropics, are covered by carbonate-rich sediment types. In such sediment types, with high carbonate and low organic carbon, COD closely approximates the organic carbon concentration. These sites have been popular targets of deep-sea drilling expeditions, since the carbonate yields stable isotope records, the paleoceanographer’s prime tool. It is a well-known problem that precise determination of organic carbon in high-carbonate sediments using existing techniques is complicated because the procedures require the separation of the organic carbon and carbonate contributions to the measured carbon. Organic carbon time series are therefore lacking in climatologically and oceanographically important regions where $\delta^{18}\text{O}$ and $\delta^{13}\text{C}$ records can be readily obtained. The organic carbon accumulation rate has been shown to be controlled by the productivity in the overlying surface waters (Pedersen and Calvert, 1990; Pedersen, 1983; Müller & Suess, 1979), knowledge of which aids our understanding of upper-ocean dynamics, surface-wind strength, and responses of the ocean-atmosphere system to Milankovitch forcing.

The data sets that I present in greatest detail in this thesis (Chapters 2 and 3) are from two deep-sea cores for the last 400,000 years. One lies in the western equatorial Pacific on the Ontong-Java Plateau beneath the West Pacific Warm Pool, and the second lies in the

eastern equatorial Pacific on the flanks of the East Pacific Rise (a map of the sites is shown in Figures 1.1 and 3.1). The two sites are in very different oceanographic settings.

Figure 1.1. A map showing the two sites in the equatorial Pacific for which 400,000 yr time series of COD were obtained, RNDB 74P in the west ($0^{\circ}20'N$, $159^{\circ}22'E$, 2547m) and ODP 849 in the east ($0^{\circ}11'N$, $110^{\circ}34'W$, 3851m). The arrows indicate the main ocean currents in the tropical Pacific: the South Equatorial Current (SEC), the North Equatorial Current (NEC), the North Equatorial Countercurrent (NECC), and the Equatorial Undercurrent (EUC) (denoted by the clear arrows). The contours show the annual average thermocline ($18^{\circ}C$ isotherm) depth (in meters) derived from the world ocean atlas of Levitus (1982). The map is adapted from Andreasen and Ravelo (1997).



The upper-ocean circulation of the modern tropical Pacific has been nicely summarized by Philander (1990). It is characterized by four current systems: the westward flowing North Equatorial Current (NEC) located at $10^{\circ}N$; the eastward flowing North Equatorial Countercurrent (NECC), centered at about $6^{\circ}N$; the westward flowing South Equatorial Current (SEC), between $8^{\circ}S$ and $3^{\circ}N$; and the eastward flowing subsurface Equatorial Undercurrent (EUC) at 0° (Figure 1.1). The currents are a manifestation of a dynamic ocean-atmosphere coupling with marked seasonal variability.

The eastern equatorial Pacific (EEP) site, ODP (Ocean Drilling Program) 849, lies at 110°W on the western flank of the East Pacific Rise at 3851m. The sea-floor sediments contain at least >80% (wt) calcium carbonate and <0.2% (wt) organic carbon. The site sits beneath the “cold tongue” upwelling region, one of the strongest open ocean upwelling areas. Maximum upwelling occurs at ~120°W during boreal summer when the southeast trade winds are at their strongest. The trade winds weaken during boreal spring causing a shallowing of the mixed layer, a reversal of the SEC and a shoaling of the EUC (Murtugudde et al., 1999). In contrast, RNDB (Roundabout Cruise) 74P at 2547m and 160°E in the western equatorial Pacific (WEP) lies beneath the West Pacific Warm Pool which has low seasonal variability of winds, surface and subsurface currents and thermal structure. A “barrier layer” of isothermal waters below the mixed layer and above the thermocline reduces the cooling of sea surface temperature (SST) by entrainment of mixed layer waters and may also inhibit the mixing of colder, nutrient-rich thermocline waters into the euphotic zone (Murtugudde et al., 1999; Blanchot et al., 1992). Primary production is higher in the strongly upwelled, nutrient-rich waters of the east and decreases as one progresses westward. Modern-day primary productivity values for 110°W, 0° are of the order of $950 \text{ mgCm}^{-2}\text{day}^{-1}$ (Paytan, 1995), at least a factor of 3 greater than the surface waters at the site in the WEP. In the western equatorial Pacific (WEP) the modern-day thermocline is deep and lies at a depth of 200-225m (Levitus, 1982). The thermocline shoals as one goes further east to a depth of only 75-100m (Levitus, 1982) at site ODP 849. Modern-day primary productivity values for 162°E, 0° are around $300 \text{ mgCm}^{-2}\text{day}^{-1}$ (Paytan, 1995). Our sites, sitting on the equator, should reflect the efficiency of the supply of nutrient-rich waters through equatorial upwelling, driven by surface winds.

Existing measurements in deep-sea sediments from the tropical Pacific indicate that productivity was higher during glacial periods relative to interglacial periods, by a factor of around two (Paytan et al., 1996; Pedersen, 1983; Pedersen et al., 1991; Isern, 1991; Snoeckx, 1995; Herguera and Berger, 1991). It is generally believed that this enhanced productivity was in response to increased upwelling along the equator caused by stronger trade winds (Sarnthein et al, 1988; Berger et al., 1989). The stronger trade winds resulted from a stronger meridional temperature gradient with northern hemisphere ice sheets and have been demonstrated in paleoclimate models (e.g. Bush and Philander, 1998; Ganopolski et al., 1998). However, the sediment results generally have not provided us with enough information to say anything about the effects of forcing on productivity across the full spectrum of Milankovitch timescales. How did insolation changes in the Pleistocene affect the surface-ocean dynamics in the equatorial Pacific? Did this response differ on different sides of the Pacific? Did the nature of the response remain constant over longer periods? The records of COD in this thesis help us to answer such questions to improve our understanding of upper ocean-atmosphere responses to climatic changes induced by astronomically forced fluctuations in insolation. Chapters 2 and 3 discuss COD data from both the WEP and EEP, describe the factors that are most likely driving the signal and speculate on the oceanographic and climatic controls on these time series.

In Chapter 4 I discuss various sedimentological studies I carried out with the COD instrument in box and piston cores from sites close to the cores presented in Chapters 2 and 3. These studies provide information about the effects on COD of factors such as changes in water depth, distance from the equator, depth below the sediment-water interface, content of calcium carbonate, clays and volcanic minerals, and conditions of storage of the sediment

cores and samples. Such information is important if one is to understand fluctuations in COD down the sediment core and compare trends seen in different cores.

The COD instrument introduces a fast, simple technique which provides paleoceanographic time series of a variable that is closely linked to the organic matter content of the carbonate-rich deep sea sediments which characterize vast areas of the sea floor beneath the world's tropical oceans. I have applied the method to the equatorial Pacific Ocean, which plays a key role in global climate, and is an area which is the focus of many climate modeling studies and for which there is a paucity of paleoceanographic data. The instrument has potential for full automation, which would enable the rapid collection of long time series. Refinement of the COD apparatus to provide simultaneous measurement of the CO₂ evolved during the combustion process, would allow studies of redox conditions in sediments from e.g. the more organic matter rich environments of continental shelves and coastal margins. In studies not presented in this thesis, the instrument was used to estimate the very low organic carbon variations in corals (Eltgroth et al., 1999). COD also has applications in the non-oceanographic environment, e.g. for studying soils and C:O₂ exchange ratios in plant material. In terms of applying the method most usefully to deep-sea sediments, the data in Chapter 4 of this thesis have demonstrated the degradation of samples and the need to dry and/or freeze samples as quickly as possible after retrieval from the sea floor if comparison of absolute values is to be useful. The COD instrument would also lend itself well to shipboard use.

1.1 References

- Andreasen, D.J., and A. C. Ravelo, Tropical Pacific Ocean thermocline depth reconstruction for the Last Glacial Maximum, *Paleoceanography*, *12*, 395-413, 1997
- Berger, W. H., V. S. Smetacek, G. Wefer, Smetacek, V. S., editor; Wefer, G., editor (Dahlem workshop on Productivity of the ocean; present and past Berlin, Federal Republic of Germany), Ocean productivity and paleoproductivity; an overview In: Berger, W. H. , editor Productivity of the ocean; present and past. Berlin, Heidelberg, New York, Tokyo: Springer, *Life Sciences Research Reports* Vol. 44 p. 1-34, 1989.
- Blanchot, J., M. Rodier, and A. Le Bouteiller, Effect of El Niño Southern Oscillation events on the distribution and abundance of phytoplankton in the Western Pacific Tropical Ocean along 165°E, *J. of Plankton Res.*, *14*, 137-156, 1992.
- Bush, A. B. G., and S. G. H. Philander, The role of ocean-atmosphere interactions in Tropical cooling during the last glacial maximum, *Science*, *279*, 1341-1344, 1998.
- Cane, M., El Niño, *Annu. Rev. Earth Planet Sci.*, *14*, 43-70, 1986.
- Cane, M. A., Climate change: A role for the tropical Pacific, *Science*, *282*, 59-61, 1998.
- Cane, M. A., and A. C. Clement, A role for the tropical Pacific coupled ocean-atmosphere system on Milankovitch and millennial timescales. Part II: Global impacts, *AGU Monograph: Mechanisms of Millennial-Scale Global Climate Change*, in prep., 1998.
- Chavez, F. P., and Barber R. T., An estimate of new production in the equatorial Pacific, *Deep-Sea Res.*, *34*, 1229-1243, 1987.
- Eltgroth, S. F., H. M. Perks, M D. Moore, and R. F. Keeling, Organic carbon concentrations in corals determined from combustion oxygen demand measurements, submitted to *Geophys. Res. Letters*, 1999.
- Ganopolski, A., S. Rahmstorf, V. Petoukhov, and M. Claussen, Simulation of modern and glacial climates with a coupled global model of intermediate complexity, *Nature*, *391*, 351-356, 1998.
- Guildersen, T. P., R. G. Fairbanks, and J. L. Rubenstone, Tropical temperature variations since 20 000 years ago: Modulating interhemispheric climate change, *Science*, *263*, 663-665, 1994.
- Herguera, J. C., and W. H. Berger, Paleoproductivity from benthic foraminifera abundance: Glacial to postglacial change in the west-equatorial Pacific, *Geology*, *19*, 1173-1176, 1991.

- Houghton, J. T., L. G. Meira Filho, B. A. Callander, N. Harris, A. Kattenberg, and K. Maskell, *Climate Change 1995: The science of climate change. Contribution of Working Group I to the Second Assessment Report of the Intergovernmental Panel on Climate Change*, pp. 572, Cambridge University Press, Cambridge, 1996.
- Isern, A. R., *Calcium carbonate and organic carbon accumulation in the central equatorial Pacific*, M.S. thesis, 200 pp., Univ. of R. I., Providence, 1991.
- Levitus, S., *Climatological atlas of the world ocean, NOAA Prof. Pap. 13*, 173 pp., U. S. Gov. Print. Off., 1982.
- Müller, P. J. and E. Suess, Productivity, sedimentation rate and sedimentary organic matter in the oceans-I. Organic carbon preservation, *Deep-Sea Res.*, 26A, 1347-1362, 1979.
- Murtugudde, R. G., S. R. Signorini, J. R. Christian, A. J. Busalacchi, C. R. McClain, and J. Picaut, Ocean color variability of the tropical Indo-Pacific basin observed by SeaWiFS during 1997-1998., *J. Geophys. Res.*, 104, 18,351-18,366., 1999.
- Neelin, J. D., D. Battisti, A. Hirst, F. Jin, Y. Wakata, T. Yamagata, and S. Zebiak, ENSO Theory, *J. Geophys. Res.*, 103, 14,261-14,290, 1998.
- Paytan, A., *Marine barite, a recorder of oceanic chemistry, productivity and circulation*, Ph.D. thesis, 111 pp., Univ. of Calif. at San Diego, 1995.
- Paytan, A., M. Kastner, and F. P. Chavez, Glacial to interglacial fluctuations in productivity in the equatorial Pacific as indicated by marine barite, *Science*, 274, 1355-1357, 1996.
- Pedersen, T. F., Increased productivity in the eastern equatorial Pacific during the last glacial maximum (19,000 to 14,000 yr B.P.), *Geology*, 11, 16-19, 1983.
- Pedersen, T. F., and S. E. Calvert, Anoxia vs. productivity: What controls the formation of organic-carbon-rich sediments and sedimentary rocks? *Am. Assoc. Petr. Geol. Bull.*, 74, 454-466, 1990.
- Pedersen, T. F., B. Nielsen, and M. Pickering, Timing of late Quaternary productivity pulses in the Panama Basin and implications for atmospheric CO₂, *Paleoceanography*, 6, 657-677, 1991.
- Philander, S.G.H., *El Niño, La Niña, and the Southern Oscillation*. Academic Press, Inc, 293 pp., 1990.
- Ropelewski, C. F., and M. S. Halpert, Global and regional scale precipitation patterns associated with the El Niño/Southern Oscillation., *Mon. Weather Rev.*, 114, 2352-2362, 1987.

- Ropelewski, C. F., and M. S. Halpert, Precipitation patterns associated with the high index phase of the Southern Oscillation, *J. Clim.*, 2, 268-284, 1989.
- Sarnthein, M., K. Winn, J.-C. Duplessy, and M. R. Fontugne, Global variations of surface ocean productivity in low and mid latitudes: Influence on CO₂ reservoirs of the deep ocean and atmosphere during the last 21,000 years, *Paleoceanography*, 3, 361-399, 1988.
- Schrag, D., G. Hampt, and D. Murray, Pore fluid constraints on the temperature and oxygen isotopic composition of the glacial ocean, *Science*, 272, 1930-1931, 1996.
- Seager, R., S. E. Zebiak, and M. A. Cane, A model of tropical Pacific sea surface temperature climatology, *J. Geophys. Res.*, 93, 1265-1280, 1988.
- Snoeckx, H., Late Pleistocene history of ocean-atmosphere interaction in the eastern equatorial Pacific, Ph.D. thesis, 199 pp., Univ. of Mich., Ann Arbor, 1995.
- Soden B. J., Variations in the tropical greenhouse effect during El Niño, *J. Climate*, 10, 1050-1055, 1997.
- Stute, M., M. Forster, H. Frischkorn, A. Serejo, J. Clark, P. Schlosser, W. Broecker, and G. Bonani, Cooling of tropical Brazil during the Last Glacial Maximum, *Science*, 269, 379-383, 1995.
- Thompson, L. G., M. E. Davis, E. Mosley-Thompson, T. A. Sowers, K. A. Henderson, V. S. Zagorodnov, P. N. Lin, V. N. Mikhalenko, R. K. Campen, J. F. Bolzan, J. Cole-Dai, B. Francou, A 25,000-year tropical climate history from Bolivian ice cores, *Science*, 282, 1858-1864, 1998.

2. A 400 kyr record of combustion oxygen demand in the western equatorial Pacific: Evidence for a precessionally forced climate response.¹

Abstract

We have developed a combustion analysis technique for sediments which measures the amount of O₂ consumed by the reduced species. We have measured this quantity, which we call “combustion oxygen demand (COD),” on a carbonate-rich sediment core from the Ontong-Java Plateau in the western equatorial Pacific back to marine oxygen isotope stage 11. The precision of the COD technique is $\pm 6.3 \mu\text{mol O}_2 \text{ g}^{-1}$, which corresponds to $\sim \pm 0.0076\%$ wt C_{org}, assuming oxidation of organic carbon dominates the signal. The COD time series is characterized by values which are about twice as high during glacials as during interglacials, the largest shift occurring from 401 $\mu\text{mol O}_2 \text{ g}^{-1}$ in midstage 6 to 144 $\mu\text{mol O}_2 \text{ g}^{-1}$ at 5e, and is coherent with the oxygen isotope curve of *Globigerinoides sacculifer* in the same core at the Milankovitch frequencies of 100 and 41 kyr. Pronounced variations in the 19-23 kyr band suggest that the climate of the western equatorial Pacific is sensitive to precessional forcing, a response not apparent from other records obtained in this region.

¹ This chapter is reproduced with slight modifications from Perks, H. M. and R. F. Keeling, A 400 kyr record of combustion oxygen demand in the western equatorial Pacific: Evidence for a precessionally forced climate response, *Paleoceanography*, 13, 63-69, 1998.

2.1 Introduction

In this paper we present a method for characterizing sediment chemistry based on measuring the total amount of oxygen consumed upon complete combustion of the sediment per unit mass of sample. This quantity, which we call combustion oxygen demand (COD), measures the amount of reduced materials in the sample which are oxidized under the conditions of combustion. This includes organic carbon as well as any other reduced components such as sulfides and reduced iron and manganese. We apply our technique to a high-carbonate sediment core from the Ontong-Java Plateau spanning the last ~400 kyr. The application of traditional organic carbon measurement techniques is problematic in high-carbonate cores because of the difficulty in distinguishing a small amount of organic carbon from the large inorganic carbon background (Hedges and Stern, 1984). The COD method is advantageous because the separation of organic and inorganic carbon is unnecessary (the pyrolysis of carbonate does not consume O_2). We argue that in these sediments, organic carbon is the dominant contributor to oxygen demand.

The high-carbonate sediments on the Ontong-Java Plateau provide us with an ideal location in which to apply the combustion oxygen demand technique. Much of the seafloor beneath the tropical oceans consists of carbonate-rich (>80% wt $CaCO_3$) sediments, and many of these regions have been targeted by deep-sea drilling projects to retrieve samples which have been used to obtain detailed stratigraphic records of the isotopic content of benthic and planktonic foraminifera and to examine preservation and accumulation cycles in calcium carbonate (Shackleton and Opdyke, 1973; Berger et al., 1993a). Notably lacking in many high-carbonate regions, however, are detailed records of sediment organic carbon content, which, although generally present in very low amounts (<0.4% wt), may be an

important indicator of the rates of productivity of surface waters (e.g., Pedersen, 1983; Sarnthein et al., 1988; Pedersen and Calvert, 1990; Lyle et al., 1992). The stability of tropical climate is a leading issue in paleoclimate research because of the importance of the tropics to the energy and moisture budgets of the planet (Hastenrath, 1985).

The Ontong-Java Plateau, a mid-oceanic submarine plateau covered with >1000 m Mesozoic and Cenozoic carbonate deposits, straddles the equator to the north of the Solomon Islands in the western Pacific (Figure 2.1). The Plateau is located beneath the West Pacific Warm Pool (WPWP), which contains the warmest waters of the global oceans and is the Earth's major convective region with an important role in the dynamics of climate in the modern equatorial Pacific. However, despite well-studied cores from the Ontong-Java Plateau (e.g. Berger et al., 1993a), there has been little evidence for significant changes in the characteristics of the WPWP in the late Quaternary. This region of the equatorial Pacific lies near the boundaries of an extensive area extending across from SE Asia that is affected by a combination of monsoon-circulation- and trade-wind-influenced climate patterns. Just to the west of the WPWP lie the shallow shelf areas of the Indonesia-North Australia region, which are very sensitive to ice-volume-change-induced sea level fluctuations and became land during glacial periods. Milankovitch cyclicity at 41 and 100 kyr has been demonstrated by several data sets from the Ontong-Java Plateau (e.g., Berger et al., 1993b). Sensitivity of low-latitude climatic and oceanographic signals to precessional forcing (19-23 kyr) has been demonstrated by data sets at several different locations and simulated by models (e.g., Prell and Kutzbach, 1987; Anderson and Prell, 1993; McIntyre and Molfino, 1996; Beaufort, 1996). However, a clear precession signal has not been detected in the western equatorial

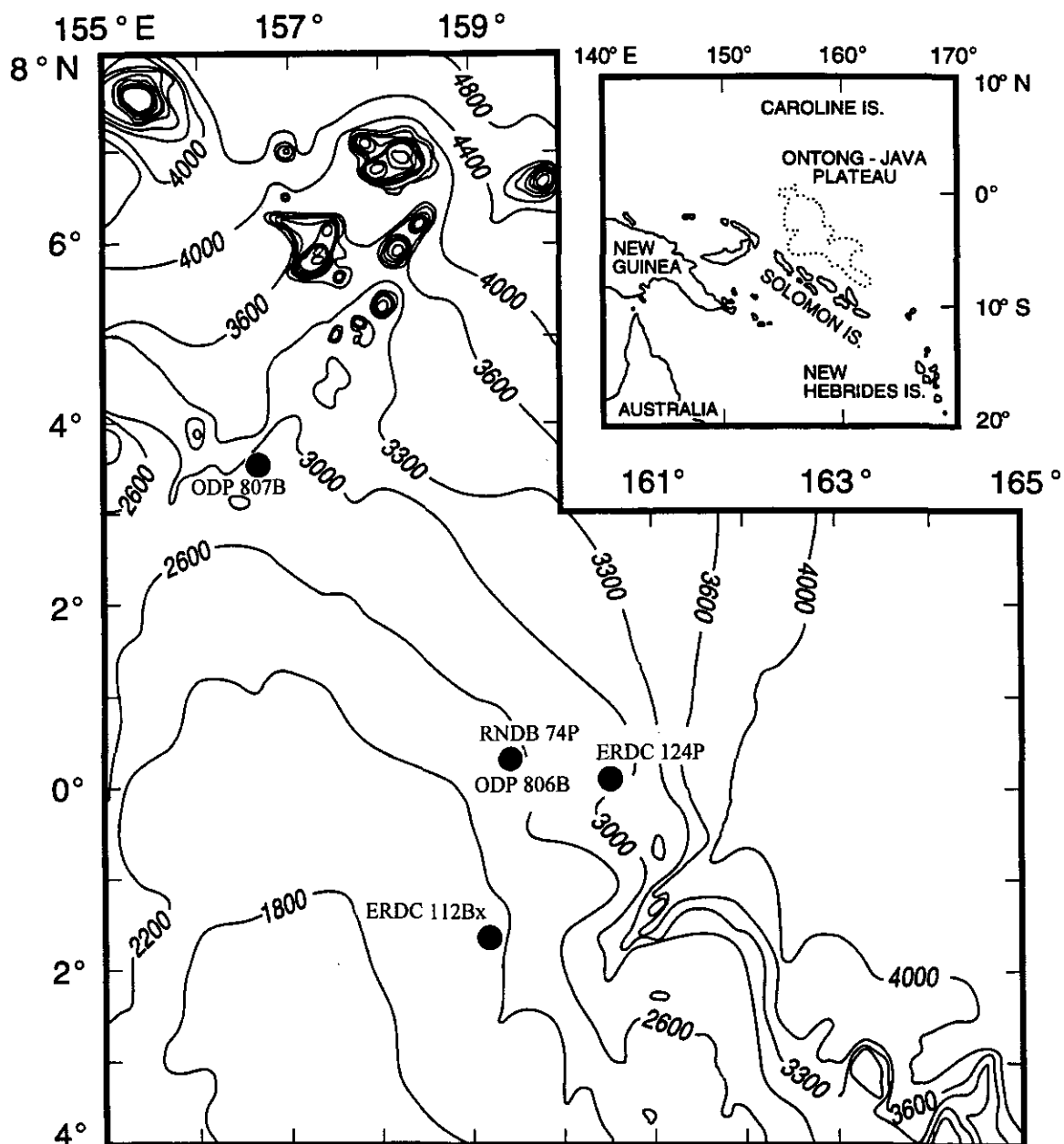


Figure 2.1. Map of the Ontong-Java Plateau showing the locations of the core sites referred to in the text: RNDB 74P ($0^{\circ}20.48'N$, $159^{\circ}22.49'E$ and 2547 m water depth); ERDC 112Bx ($1^{\circ}37'S$, $159^{\circ}14'E$ and 2169 m water depth); ERDC 124P ($0^{\circ}0'S$, $160^{\circ}24'E$ and 2946 m water depth); Ocean Drilling Program (ODP) 806B ($0^{\circ}19.11'N$, $159^{\circ}21.69'E$ and 2519.9 m water depth), and ODP 807B ($3^{\circ}36.39'N$, $156^{\circ}37.49'E$ and 2806.1 m water depth).

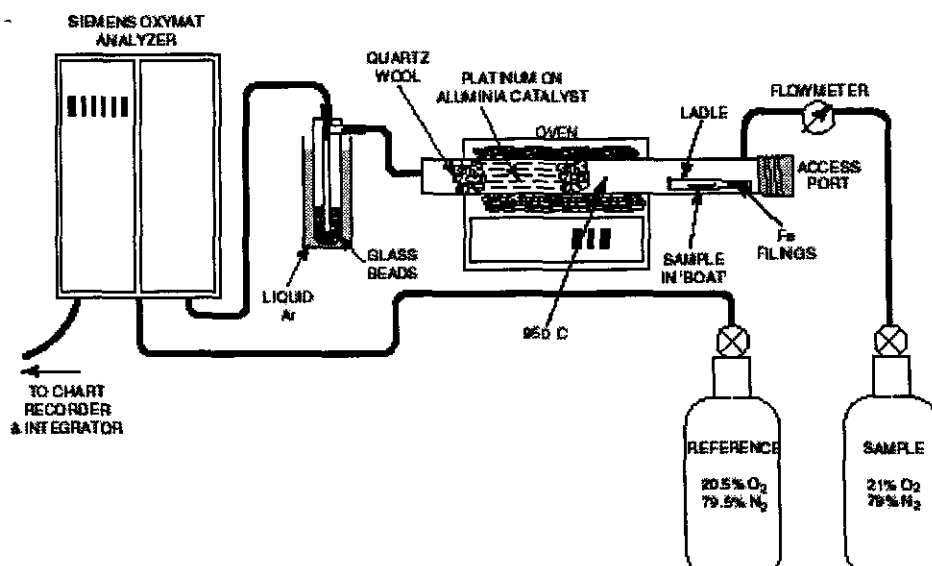
Pacific in the Quaternary. Evidence for precessional forcing here could provide a link between the responses of the Asian monsoon, trade wind dynamics, and the climate of the western equatorial Pacific to solar forcing in the past.

2.2 Methods and Samples

The COD method utilizes a paramagnetic oxygen analyzer connected downstream from an oven in which the sample is combusted. The experimental setup is shown in Figure 2.2. The sample is dried, weighed, and burned in an air stream flowing at a measured rate in a quartz tube heated to 950°C. The exhausted air is run through a liquid argon cold trap (87.5 K) to freeze out water vapor, CO₂, and other trace gases (but not O₂) and then passed through a Siemens Oxymat 5F O₂ analyzer which records the O₂ mole fraction. The “depletion peak” of the O₂ concentration caused by the combustion is integrated over the duration of the combustion and multiplied by the flow to yield the total moles of O₂ consumed because of the oxidation of the reduced material in the sample. The Oxymat analyzer is operated in a high-sensitivity mode in which the sample air stream is compared against a reference of slightly lower mole fraction (20.5% versus 21.0%). For carbonate-rich sediment types we typically use a sample size of 50-80 mg, on which the method achieves a precision on duplicate samples of $\pm 6.3 \mu\text{mol O}_2 \text{ g}^{-1}$ corresponding to $\sim \pm 0.0076\%$ wt C_{org} (assuming only organic C consumes the O₂ and with an O₂:C ratio of 1 to 1). The signal-to-noise ratio of the oxygen demand values on a typical sediment sample containing the equivalent of $\sim 0.3\%$ wt C_{org} is $\sim 40:1$. The sensitivity of the instrument based upon combustion of a “pure” calcium carbonate “blank” is $\sim 1 \mu\text{mol O}_2$. The COD analyzer is calibrated by burning known amounts

of reference materials: for the Ontong-Java Plateau samples we generally used 100 μL aliquots of different concentrations of potassium hydrogen phthalate (KHP) solutions in

Figure 2.2. Experimental setup of the combustion oxygen demand (COD) apparatus.



water purified by a “milli-Q” system. The time required per sample measurement, including weighing and analysis, is ~10 mins.

Piston core RNDB 74P ($0^{\circ}20.48'N$, $159^{\circ}22.49'E$) was taken during Roundabout Cruise 11 (Mayer et al., 1991), the site survey cruise for Ocean Drilling Program (ODP) Leg 130 (Figure 2.1). The core is 805 cm in length extending back to ~400 ka and is from 2547 m water depth, which is above the present-day lysocline at 3400 m. The core was analyzed at 5 cm intervals corresponding to a time resolution of 2-3 kyr, close to the limits allowed by bioturbation. In order to better resolve trends through the Holocene, which is largely missing from the piston core, samples were also analyzed from box core ERDC 112Bx ($1^{\circ}37'S$,

159°14'E and 2169 m water depth) at 1 cm intervals to a depth of 38 cm (which corresponds to an age of ~ 15 ^{14}C ka). The box core was analyzed using solid benzoic acid standards for calibration of the COD instrument before the calibration was improved using KHP standard solutions, and the precision was estimated to be ± 21.6 $\mu\text{mol O}_2 \text{ g}^{-1}$ corresponding to $\sim \pm 0.026\%$ wt C_{org} .

2.3 Results and Discussion

Figure 2.3 shows values of combustion oxygen demand versus depth in RNDB 74P plotted with the $\delta^{18}\text{O}$ record (in the same core) from *Globigerinoides sacculifer*. The COD record displays a sawtooth pattern, similar to that of the $\delta^{18}\text{O}$, with higher values generally occurring during glacial periods and lower COD occurring during interglacial conditions. The oxygen demand is higher during glacials than during interglacials by at least a factor of 2 with the highest value of 401 $\mu\text{mol O}_2 \text{ g}^{-1}$ in midstage 6 and the lowest value of 144 $\mu\text{mol O}_2 \text{ g}^{-1}$ at stage 5e. The 400 kyr COD time series does not display any obvious overall down-core trend, indicating that any long-term losses due to oxidative degradation of organic matter in the sediment are small.

Organic carbon is clearly an important contributor to the oxygen demand observed, but how significant are the contributions from other elements? With respect to iron the total iron concentration measured in samples in the top 3 m of core ERDC 124P ($0^\circ 0' \text{S}$, $160^\circ 24' \text{E}$ and 2946 m water depth) ranges from 1356 to 3007 $\mu\text{g g}^{-1}$ (salt-free) (T. Fitts, personal communication, 1997). As an upper bound corresponding to this maximum range, if all the iron were oxidized from Fe(+2) to Fe(+3), then the change in COD would be ~ 7 $\mu\text{mol O}_2 \text{ g}^{-1}$, or $< 5\%$ of the COD changes observed across glacial-interglacial transitions.

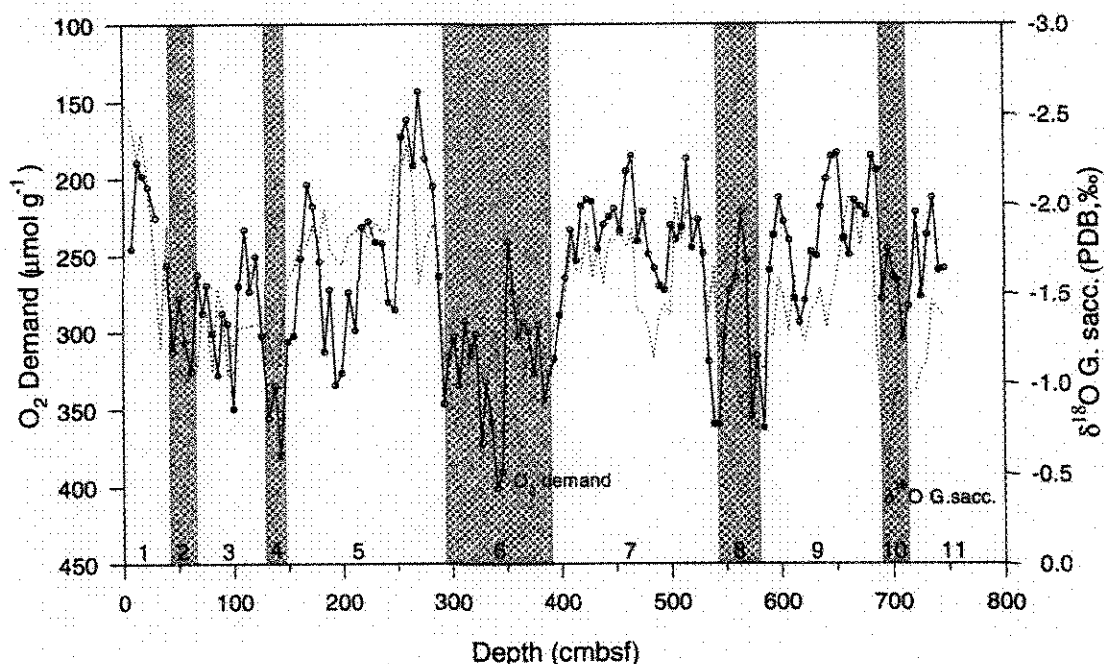


Figure 2.3. COD (solid line) in piston core RNDB 74P from the Ontong-Java Plateau plotted with $\delta^{18}\text{O}$ (*Globigerinoides sacculifer*) (dashed line) from the same core (M. Yasuda, personal communication, 1996) versus depth below sea floor. The shading indicates marine oxygen isotope stages for glacial periods (Shackleton and Opdyke, 1973). The COD values are reported in $\mu\text{mol O}_2$ per g of (dry) sediment sample, and the COD axis is in descending magnitude for comparison with the $\delta^{18}\text{O}$ which are plotted according to the usual convention. The COD data show similar trends to the $\delta^{18}\text{O}$, with higher COD generally occurring during glacials (shaded areas) and lower COD occurring during interglacials. The largest transition in COD is from midstage 6 to 5e. In addition, COD exhibits proportionally larger higher-frequency fluctuations than the $\delta^{18}\text{O}$.

Concentrations of Mn(+2) mobilized in pore waters are negligible in neighboring ODP 806B ($0^\circ 19.11' \text{N}$, $159^\circ 21.69' \text{E}$ and 2519.9 m water depth) (Kroenke et al., 1991). Measurements of total sulfur concentration in late Quaternary samples from ODP 807B ($3^\circ 36.39' \text{N}$, $156^\circ 37.49' \text{E}$ and 2806.1 m water depth) vary by $\sim 0.02\%$ (Lind et al., 1993). In the extreme case, if the full range of sulfur variability in RNDB 74P were attributable to pyrite, the resulting range in COD would be $\sim 23 \mu\text{mol O}_2 \text{ g}^{-1}$, which is $<10\%$ of the range observed. Therefore we conclude that organic carbon must dominate the COD variations.

Generally, since COD includes the oxygen consumed by oxidation of any pyrite and other electron acceptors in the sediment additional to organic carbon, we would expect COD to be a more conservative variable in sediments than organic carbon. The reactions that form, for example, Mn^{2+} , Fe^{2+} , and S^{2-} by reducing equivalents supplied by the oxidation of organic carbon, where the change in oxidation state is transferred from the organic carbon to the electron acceptors, simply trade off between the oxygen demand caused by organic carbon and that caused by the reduced ions. However, this situation may be complicated by the mobility of reduced species in the pore waters. Although we see no evidence for such processes in our samples from the Ontong-Java Plateau, the occurrence of concentrations of reduced precipitate, such as pyrite in carbonate-rich sediments, may be possible, and these would lead to large excursions in COD, which would then require further analysis.

Kroenke et al. (1991) report measurements of total organic carbon in ODP 806B by the difference between total carbon, determined by means of a Carlo Erba NCS Analyzer, and inorganic carbon, determined using a Coulometrics coulometer. Only three results which lie within the range of core depths covered by RNDB 74P are recorded, 0.13, 0.17, and 0.40% wt, and these are stated as being near the detection limit of the method (Kroenke et al., 1991). Assuming an oxidation ratio of 1:1 for the organic carbon, the values of organic carbon concentration calculated from COD in RNDB 74P range from 0.17 to 0.48% wt. The actual organic carbon contents are probably slightly smaller than this because of the presence of reduced nitrogen in the organic matter and because carbon is likely to be in a more reduced oxidation state than C(0). The exact conversion factor between combustion oxygen demand and organic carbon concentration is not well known and will be the subject of further study.

In the box core (Figure 2.4) we observe a decrease, with some apparent oscillation, in COD from $\sim 210 \mu\text{mol O}_2 \text{ g}^{-1}$ at the core top to $\sim 140 \mu\text{mol O}_2 \text{ g}^{-1}$ at 26 cm ($\sim 11.5 \text{ }^{14}\text{C ka}$). This trend may be due to true variations caused by climatic changes in the region, but the measurements also place an upper bound on the possible extent of remineralization of organic matter in the core of $< 70 \mu\text{mol O}_2 \text{ g}^{-1}$. The average COD of $\sim 150 \mu\text{mol O}_2 \text{ g}^{-1}$ from the top of the box core down to 24 cm ($\sim 11 \text{ }^{14}\text{C ka}$) compares with an average of $\sim 200 \mu\text{mol O}_2 \text{ g}^{-1}$ for interglacial periods in the piston core and is similar to the lowest oxygen demand in the piston core which occurs during stage 5e. (The resolution of sampling in the Holocene in the piston core is too low to allow comparison of Holocene values between both cores). The lowest COD values ($\sim 125 \mu\text{mol O}_2 \text{ g}^{-1}$) are observed in samples from the box core from 8 to 26 cm (~ 6.5 to $11.5 \text{ }^{14}\text{C ka}$). The oxygen demand rises from this low value at 26 cm ($\sim 11.5 \text{ }^{14}\text{C ka}$) to $\sim 300 \mu\text{mol O}_2 \text{ g}^{-1}$ across the boundary back into the last glacial period. This is consistent with the measured oxygen demand into the last glacial transition in the piston core.

Surface sediments on the ocean floor are a sink for dissolved oxygen because of the oxidation of the reduced sediment components. Estimates of the proportion of these species not oxidized in the top layer of sediment can be derived by comparing COD with pore water O_2 flux measurements. Hales and Emerson (1996) observed a diffusive O_2 flux of $10\text{-}21 \mu\text{mol cm}^{-2} \text{ yr}^{-1}$ in waters from a few centimeters above the sediment-water interface down to a maximum depth of 9 cm at three sites between 2000 and 3000 m water depth on the Ontong-Java Plateau. A COD of $200 \mu\text{mol O}_2 \text{ g}^{-1}$, typical of values in the top 8 cm of the box core, multiplied by the dry bulk sediment density (0.8 g cm^{-3}) and sedimentation rate (2.5 cm kyr^{-1}), yields a flux of reduced material into the sediment equivalent to an oxygen flux of ~ 0.4

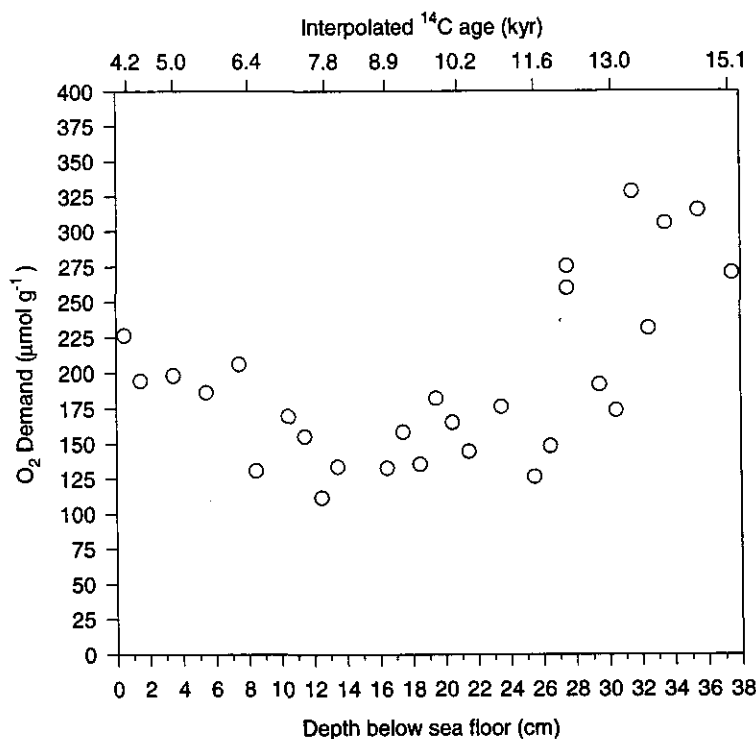


Figure 2.4. COD in box core ERDC112Bx from the Ontong-Java Plateau versus depth below sea floor. Carbon-14 ages in uncorrected radiocarbon years are interpolated from data by Berger and Killingley (1982).

$\mu\text{mol cm}^{-2} \text{ yr}^{-1}$. Dividing this number by $10\text{-}21 \mu\text{mol cm}^{-2} \text{ yr}^{-1}$ (Hales and Emerson, 1996) yields a ratio of 0.02-0.04, implying that 96-98% of the reduced material is consumed above the depth range resolved by the box core. This evidence for very shallow oxidation of the majority of the reduced species, leaving a highly refractory component that is then conserved down core, is consistent with a lack of apparent down-core decrease in COD.

Figure 2.5 shows that the COD data contain information about the effects of astronomical forcing in the Ontong-Java Plateau region, which can be compared with the $\delta^{18}\text{O}$ time series controlled by global ice volume and, to a lesser extent, with local sea surface temperatures (SST). In the COD time series there is a pronounced signal at the precessional

period of 23 kyr, which was found to be significant at the 95% confidence limit. In the $\delta^{18}\text{O}$ a small signal can be detected at this period, but it is not significant even at the 80% limit. (Both multitaper and Blackman-Tukey methods (Yiou et al., 1996) were applied to the two data sets).

The variations in COD we detect could either be driven by changes in the amounts or types of organic material delivered to the seafloor from the surface waters or by changes in the deep water environment that affect preservation. One possible deep water mechanism that may cause changes in the sediment organic matter content is changes in the amount of CaCO_3 preserved in the sediment driven by changes in deep water CO_3^{2-} concentration. Carbonate dissolution is higher during interglacials (Wu and Berger, 1991) which, by concentrating the residual sediment constituents, would tend to increase the oxygen demand signal and organic carbon weight percentage during interglacial conditions. In fact, we see the opposite. In addition, the constancy of the sedimentation rate (see below) does not allow for great enough fluctuations in calcium carbonate weight percentages to cause the factor of 2 changes in COD values that we observe. It is also possible that changes in deep water temperature or dissolved O_2 could produce changes in deep water metabolic activity, although it is hard to imagine how the changes could have been large enough to cause the observed variations in oxygen demand without producing pronounced features in other paleoceanographic records in the western equatorial Pacific. Further support for the COD signal not being significantly affected by bottom water O_2 changes is provided by Pedersen and Calvert (1990), who conclude that oxygen minima do not appear to have any direct effect on carbon accumulation today in low oxygen environments such as continental margins and marginal seas. We conclude therefore

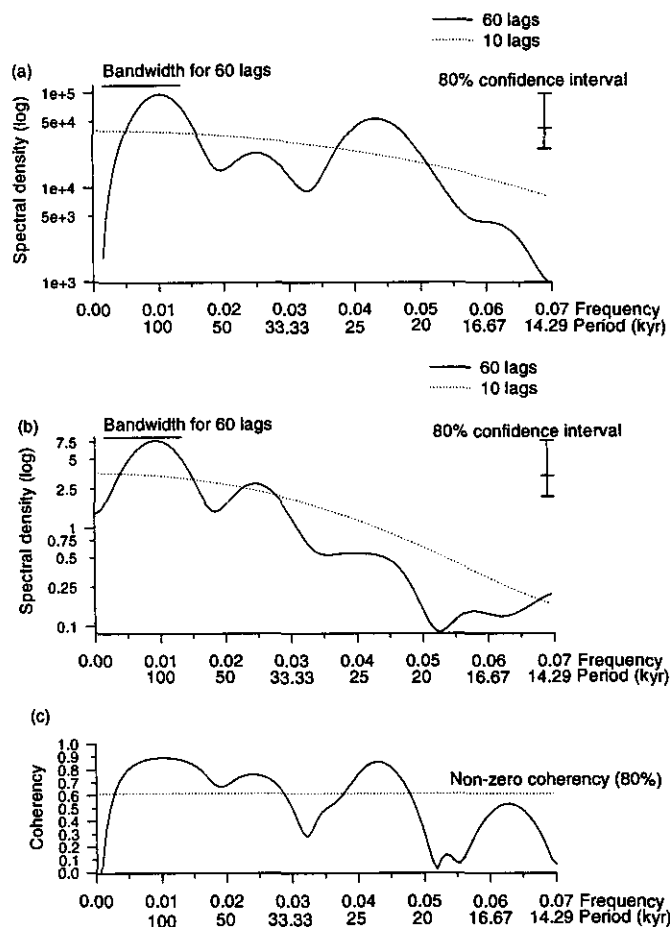


Figure 2.5. Power spectral analysis of (a) COD and (b) $\delta^{18}\text{O}$ (*Globigerinoides sacculifer*) in piston core RNDB 74P from the Ontong-Java Plateau presented in Figure 3. The analysis was performed with unfiltered data sets. Ages were assigned for both data sets by fitting them to the age model for ODP Hole 806B (Berger, 1996) and interpolation. 195 data points were used in each analysis with a sampling interval of 4 kyr. Graphs show variance spectra as spectral density ($\sigma^2 f^1$, where σ^2 is variance and frequency f is 1 per period) against frequency (not plotted to the Nyquist frequency as spectral densities at frequencies higher than those plotted were very low) and period at 60 lags (solid line) and 10 lags (dotted line). Spectral density is plotted on a logarithmic scale. The 80% confidence limit and bandwidth for the variance spectra are given in the upper right and left of the graphs, respectively. The low-lag spectra provide a baseline against which the significance of peaks in the high-lag spectra can be assessed. Significant peaks occur at 100 kyr for both data sets and 23 kyr in the COD time series. The 23 kyr peak is not significant at the 80% confidence limit in the $\delta^{18}\text{O}$ time series and could be placed over the range 21–26 kyr and is markedly stronger and narrower in COD. Figure 5c shows the coherency output from a cross-spectral analysis (Blackman-Tukey method) of Figures 5a and 5b (60 lags). The 80% coherency significance level is indicated by the horizontal line. Coherency between two time series can be assigned when both series exhibit significant spectral peaks that are coherent with a significant peak in the coherency function.

that the observed variation in COD cannot be driven by changes in bottom water environment.

Considering possible changes in surface water export, a mechanism which could be driving the COD signal is variations in nonorganic particle fluxes from the surface waters (dilution). The calculated sedimentation rates for the Ontong-Java Plateau are remarkably constant over the last 400 kyr, varying between 1.85 and 2.1 cm kyr⁻¹ (Berger, 1994]. This represents a maximum variation of a factor of just 1.16 over the course of the presented COD record and indicates that variations in COD are not primarily controlled by variations in the dilution of organic matter.

Another possible surface water mechanism is changes in the export of organic matter from the surface waters to the seafloor affecting the amount of organic matter ultimately preserved in the sediment column. Organic matter export rates could change in association with changes in population abundances or changes in the amount or type of organic matter associated with a particular species. Although conclusive proof is lacking, we believe this the most likely mechanism. Additional support for this mechanism is provided by similarities in COD data with benthic foraminiferal abundance from the Ontong-Java Plateau (S. Burke, personal communication, 1996), which has been correlated to the organic carbon flux arriving at the seafloor (Herguera and Berger, 1991, 1994). Ohkouchi et al. (1997) analyzed lipid class compounds and measured $\delta^{13}\text{C}_{\text{org}}$ in a core from the Caroline Basin in the western tropical Pacific. They conclude that there was a decrease during the last deglaciation in the export of organic matter from the surface waters, from both marine organisms and terrestrial sources, and that the terrestrial component of this organic matter was very small.

An approximate doubling in organic carbon mass accumulation rate (MAR) (Pedersen, 1983; Pedersen et al., 1991), calcium carbonate MAR (Isern, 1991; Snoeckx, 1995) and barite MAR (Paytan, 1995; Paytan et al., 1996) has been recorded for glacial conditions in the Quaternary in the eastern and central equatorial Pacific. Increases in biogenic sedimentation rates in these regions during glacials are also described by Lyle et al. (1988) and Rea et al. (1991). Although on the basis of an independent method, our results suggest that similar changes in organic matter content (and because of the low variation in sedimentation rate, organic matter MAR) occurred in the western equatorial Pacific. The eastern and central Pacific data sets have been interpreted as reflecting changes in organic carbon export from surface waters, and if this interpretation is valid, our results suggest that similar changes also occurred in the western equatorial Pacific. The increases in organic carbon export from the waters above the Ontong-Java Plateau during glacial periods may have been caused by increased trade wind strength resulting in enhanced equatorial upwelling and thus supply of nutrients to surface waters (Pedersen et al., 1991; Sarnthein et al., 1988) and may indicate changes in the structure of the WPWP over the last 400 kyr.

2.4 Summary

We have described a chemical analysis technique for the study of deep-sea sediments, which records the total amount of oxidizable species in the sediment sample, and applied it to carbonate-rich sediments on the Ontong-Java Plateau in the western equatorial Pacific. This variable, combustion oxygen demand (COD), is dominated by the organic carbon content in such sediment types, precise measurement of which is difficult with conventional techniques. The COD method provides a better signal-to-noise ratio than most other lithological

measurements that have been made in these sediments. We have demonstrated large changes in COD over the last 400 kyr on the Ontong-Java Plateau, with at least a doubling of oxygen demand during glacials as compared to interglacials. We conclude that such variations in COD in these sediments are caused by changes in the amount or types of organic matter exported from surface waters, suggesting that changes in organic carbon export similar in magnitude and timing to those previously inferred in the central and eastern equatorial Pacific in the late Quaternary also took place in the western equatorial Pacific. The COD record displays strong Milankovitch forcing, including marked forcing in the precessional frequency band. This is the first data set from the region to show such precessional structure in the late Quaternary, indicating that the organic carbon signal here may be controlled by the responses of low-latitude climate processes to astronomical forcing. The COD measurements imply that the West Pacific Warm Pool may not have been a stable feature during the late Quaternary.

We have demonstrated here the usefulness of the COD method in carbonate-rich sediments; the method may also be useful for characterizing more organic carbon-rich sediments. The COD apparatus could be employed as a shipboard instrument, which might allow analysis prior to any oxidative degradation of highly reduced sediments since it is quick and fairly insensitive to vibration.

Acknowledgments

We wish to thank M. Yasuda for many helpful discussions. The original manuscript was improved by comments and reviews from C. Charles, M. Delaney, J. Gieskes, J. C. Herguera, R. Jahnke, T. Pedersen, N. Pias, and N. Shackleton. We are grateful to R. Weiss and the staff of Scripps Analytical Facility. We acknowledge W. Paplawsky and also U. Ninnemann and D. Hunter. Finally, we are indebted to T. Herbert, who first suggested the potential of applying the new method to carbonate-rich sediment types, specifically those of the Ontong-Java Plateau.

This chapter is reproduced with slight modifications from

Perks, H. M. and R. F. Keeling, A 400 kyr record of combustion oxygen demand in the western equatorial Pacific: Evidence for a precessionally forced climate response, *Paleoceanography*, 13, 63-69, 1998.

I was the primary investigator and lead author for this paper, and conducted all of the analyses presented therein.

2.5 References

- Anderson, D. M., and W. L. Prell, A 300 kyr record of upwelling off Oman during the late Quaternary: Evidence of the Asian Southwest Monsoon, *Paleoceanography*, 8, 193-208, 1993.
- Beaufort, L., Dynamics of the monsoon in the equatorial Indian Ocean over the last 260,000 years, *Quat. Int.*, 31, 13-18, 1996.
- Berger, W. H., and J. S. Killingley, Box cores from the equatorial Pacific: ¹⁴C sedimentation rates and benthic mixing, *Mar. Geol.*, 45, 93-125, 1982.
- Berger, W. H., et al., *Proceedings of the Ocean Drilling Program Scientific Results vol.*, 130, 867 pp., Ocean Drill. Program, College Station, Texas, 1993a.
- Berger, W. H., T. Bickert, H. Schmidt, G. Wefer, and M. Yasuda, Quaternary oxygen isotope record of pelagic foraminifers: Site 805, Ontong Java Plateau, *Proc. Ocean Drill. Prog. Sci. Results*, 130, 363-379, 1993b.
- Berger, W. H., Quaternary time scale for the Ontong Java Plateau: Milankovitch template for Ocean Drilling Program Site 806, *Geology*, 22, 463-467, 1994.
- Berger, W. H., Reconstruction of atmospheric CO₂ from ice-core data and the deep-sea record of Ontong Java Plateau - The Milankovitch Chron, *Geologische Rundsch.*, 85, 466-495, 1996.
- Hales, B., and S. Emerson, Calcite dissolution in sediments of the Ontong Java Plateau: In situ measurements of pore water O₂ and pH, *Global Biogeochem. Cycles*, 10, 527-541, 1996.
- Hastenrath, S., *Climate and Circulation of the Tropics*, 455 pp., Kluwer Acad., Norwell, Mass., 1985.
- Hedges, J. I., and J. H. Stern, Carbon and nitrogen determinations of carbonate-containing solids, *Limnol. Oceanogr.*, 29, 657-663, 1984.
- Herguera, J. C., and W. H. Berger, Paleoproductivity from benthic foraminifera abundance: Glacial to postglacial change in the west-equatorial Pacific, *Geology*, 19, 1173-1176, 1991.
- Herguera, J. C., and W. H. Berger, Glacial to postglacial drop in productivity in the western equatorial Pacific: Mixing rate vs. nutrient concentrations, *Geology*, 22, 629-632, 1994.
- Isern, A. R., Calcium carbonate and organic carbon accumulation in the central equatorial Pacific, M.S. thesis, 200 pp., Univ. of R. I., Providence, 1991.

- Kroenke, L. W., et al., *Proceedings of the Ocean Drilling Program Initial Report vol.*, 130, 867 pp., Ocean Drill. Program, College Station, Texas, 1991.
- Lind, I. L., T. R. Janecek, L. A. Krissek, M. L. Prentice, and R. Stax, Color bands in Ontong Java Plateau carbonate oozes and chalks, *Proc. Ocean Drill. Prog. Sci. Results*, 130, 453-470, 1993.
- Lyle, M., D. W. Murray, B. P. Finney, J. Dymond, J. M. Robbins, and K. Brooksforce, The record of late Pleistocene biogenic sedimentation in the eastern tropical Pacific Ocean, *Paleoceanography*, 3, 39-59, 1988.
- Lyle, M., R. Zahn, F. Prahl, J. Dymond, R. Collier, N. Pisias, and E. Suess, Paleoproductivity and carbon burial across the California current: The multitracers transect, 42°N, *Paleoceanography*, 7, 251-272, 1992.
- Mayer, L. A., T.H. Shipley, E. L. Winterer, D. Mosher, and R. A. Hagen, Seabeam and seismic reflection surveys on the Ontong Java Plateau, edited by L.W. Kroenke et al., *Proc. Ocean Drill. Program Initial Rep.*, 130, 45-75, 1991.
- McIntyre, A., and B. Molino, Forcing of Atlantic equatorial and subpolar millennial cycles by precession, *Science*, 274, 1867-1870, 1996.
- Ohkouchi, N., K. Kawamura, and A. Taira, Fluctuations of terrestrial and marine biomarkers in the western tropical Pacific during the last 23,300 years, *Paleoceanography*, 12, 623-630, 1997.
- Paytan, A., Marine barite, a recorder of oceanic chemistry, productivity and circulation, Ph.D. thesis, 111 pp., Univ. of Calif. at San Diego, 1995.
- Paytan, A., M. Kastner, and F. P. Chavez, Glacial to interglacial fluctuations in productivity in the equatorial Pacific as indicated by marine barite, *Science*, 274, 1355-1357, 1996.
- Pedersen, T. F., Increased productivity in the eastern equatorial Pacific during the last glacial maximum (19,000 to 14,000 yr B.P.), *Geology*, 11, 16-19, 1983.
- Pedersen, T. F., and S. E. Calvert, Anoxia vs. productivity: What controls the formation of organic-carbon-rich sediments and sedimentary rocks? *Am. Assoc. Petr. Geol. Bull.*, 74, 454-466, 1990.
- Pedersen, T. F., B. Nielsen, and M. Pickering, Timing of late Quaternary productivity pulses in the Panama Basin and implications for atmospheric CO₂, *Paleoceanography*, 6, 657-677, 1991.
- Prell, W. L., and J. E. Kutzbach, Monsoon variability over the past 150,000 years, *J. Geophys. Res.*, 92, 8411-8425, 1987.

- Rea, D. K., N. G. Pisias, and T. Newberry, Late Pleistocene paleoclimatology of the central equatorial Pacific: Flux patterns of biogenic sediments, *Paleoceanography*, 6, 227-244, 1991.
- Sarnthein, M., K. Winn, J.-C. Duplessy, and M. R. Fontugne, Global variations of surface ocean productivity in low and mid latitudes: Influence on CO₂ reservoirs of the deep ocean and atmosphere during the last 21,000 years, *Paleoceanography*, 3, 361-399, 1988.
- Shackleton, N., Timescale calibration, ODP 677, IGBP Pages/World Data Center-Paleoclimatology Data Contribution Series #96-018. NOAA/NGDC Paleoclimatology Prog., Boulder, CO, USA, 1996.
- Shackleton, N. J., and N. D. Opdyke, Oxygen isotope and paleomagnetic stratigraphy of equatorial Pacific core V28-238: Oxygen isotope temperatures and ice volumes on a 10⁵ year and 10⁶ year scale, *Quat. Res.*, 3, 39-55, 1973.
- Snoeckx, H., Late Pleistocene history of ocean-atmosphere interaction in the eastern equatorial Pacific, Ph.D. thesis, 199 pp., Univ. of Mich., Ann Arbor, 1995.
- Wu, G., and W. H. Berger, Pleistocene $\delta^{18}\text{O}$ records from Ontong-Java Plateau: Effects of winnowing and dissolution, *Mar. Geol.*, 96, 193-209, 1991.
- Yasuda, M., Foraminifera as indicators of Quaternary carbonate saturation and productivity in the western equatorial Pacific, the last million years, Ph.D. thesis, Univ. of Calif. at San Diego, 1999, in prep.
- Yiou, P., E. Baert, and M. F. Loutre, Spectral analysis of climate data, *Surv. Geophys.*, 17, 619-663, 1996.

3. Coherent synchronous precessional forcing in the eastern and western equatorial Pacific.

Abstract

The tropical oceans play a major role in modern global climate, but their behavior on Milankovitch timescales is poorly understood. Measurements of combustion oxygen demand (COD) in two sediment cores provide a record of paleoproductivity driven by surface-ocean dynamics in the equatorial eastern and western Pacific for the past 400,000 years. The two COD time series are highly coherent with each other over this period and show pronounced precessionally forced peaks of higher productivity during globally colder periods. The phase of this signal in the two cores is identical, suggesting a common insolation forcing mechanism across the equatorial Pacific. COD is also in phase with global ice volume, as indicated by oxygen isotopes, and with atmospheric methane in the Vostok ice core.

3.1 Introduction

The tropics, as a source of large amounts of heat and water vapor, play a major role in global climate. However, our knowledge of the behavior of the tropical climate system on glacial-interglacial timescales is still unclear, and there is a shortage of data sets for climate models, particularly those that extend beyond the Last Glacial Maximum (LGM). Beginning with the first investigations of deep-sea sediments, scientists have sought to clarify the relationship between climate and surface-water productivity in the tropical oceans. The Pacific Ocean contains the largest area of tropical waters on the planet, and is additionally of

interest because of its role today in ENSO events. Although the physics of the tropical Pacific with respect to ENSO cycles has been well studied in recent years (e.g. Cane, 1986; Zebiak and Cane, 1987), there is little information on the variation of biological processes on these timescales. Interannual and seasonal variations have been even less well quantified, especially in the western part of the basin, which is the largest body of warm water on Earth. The majority of existing records of paleoproductivity in the tropical Pacific have been produced from the eastern part of the Ocean, in particular from sites within the Peru Basin (Lyle et al., 1988; Pedersen, 1983; Pedersen et al., 1991; Farrell et al., 1995) which do not necessarily reflect the major dynamical processes of the equatorial Pacific as a whole. Only a few records exist from the central and western equatorial Pacific (Herguera and Berger, 1991; 1994; Yasuda et al., 1993; Paytan et al., 1996). These records indicate higher productivity coincident with glacial conditions. To date, discussions of such productivity fluctuations have been restricted to the influence of ice sheets and colder temperatures at high latitudes, which can increase meridional temperature gradients and thus increasing trade wind strength. This would have intensified equatorial upwelling, increasing productivity by enhancement of nutrient supplies from deeper waters (Sarnthein et al., 1988; Berger et al., 1989). However, it is widely held that tropical surface-ocean dynamics and hence productivity should, if anything, be strongly influenced more by precessional insolation forcing (Cane, 1998). In addition, since ENSO is highly sensitive to the seasonal cycle in the tropics (Zebiak and Cane, 1987; Tziperman et al., 1997) then it would also be expected to be influenced by such forcing (Clement et al., 1999). Existing paleoceanographic data sets from the tropical Pacific generally show a weaker response in the precessional band than at the other Milankovitch frequencies of 100 and 41 kyr (Pisias and Mix, 1997; Pisias and Rea,

1988; Lyle et al., 1988; Hagelberg et al., 1995). In this study we present data from both the western and eastern equatorial Pacific and advance the paleoproductivity record beyond the LGM to 400 ka. We demonstrate that the productivity pattern does not simply display glacial to interglacial contrasts, but does indeed have a pronounced in-phase response in the precessional band throughout the equatorial Pacific.

3.2 Method and Results

The COD method (Perks and Keeling, 1998) offers a fast, high-precision measurement of the amount of oxygen consumed upon combustion, which is closely related to the organic carbon content of the sediment and thus productivity in the overlying surface waters. It provides a higher signal-to-noise ratio (the signal-noise ratio of COD on a typical sediment sample containing the equivalent of $\sim 0.3\%$ wt C_{org} is $\sim 40:1$) than many other proxies, especially in the low sedimentation rate, carbonate-rich environments typical of vast areas of the tropical ocean.

We present COD measurements back to ~ 400 ka in piston core RNDB 74P from the Ontong-Java Plateau ($0^{\circ}20'N$, $159^{\circ}22'E$, 2547m) beneath the West Pacific Warm Pool, and in ODP 849 from the open-ocean eastern equatorial Pacific ($0^{\circ}11'N$, $110^{\circ}34'W$, 3851m) on the western flank of the East Pacific Rise. Our sites, sitting on the equator (Figure 3.1) should reflect the efficiency of the supply of nutrient-rich waters by equatorial divergence and upwelling, driven by surface winds. The upwelled waters originate from the eastward flowing Equatorial Undercurrent (EUC) which carries water thought to originate in higher latitudes, including Subantarctic Mode Water in the southwest Pacific (Toggweiler et al., 1991). From the observed glacial-interglacial patterns, we would expect to see higher surface

water production when the tropical Pacific was in a mean colder state. However, given the paucity of data for the modern ocean, the nature of the expected phase behavior between the

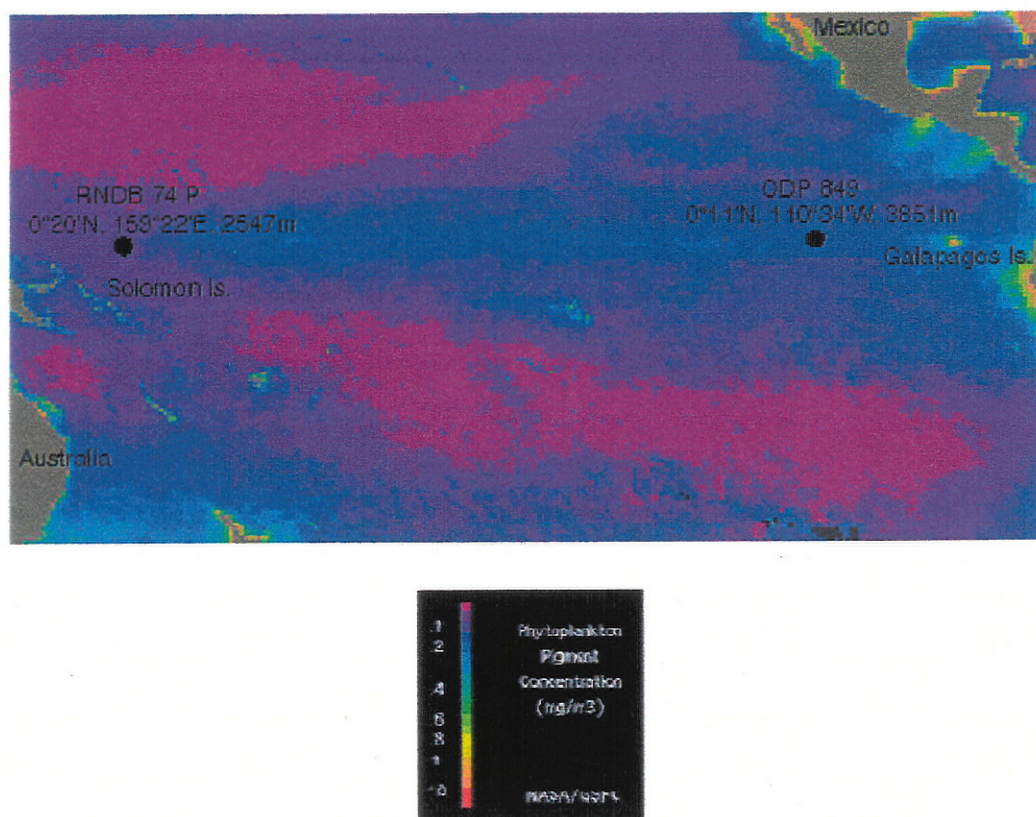


Figure 3.1. Map of the tropical Pacific showing the locations of the cores used in this study and the surface-water phytoplankton pigment concentration. The map is modified from a map on the SeaWiFS website, NASA's global ocean color monitoring mission, obtained from composite data from the Nimbus-7 Coastal Zone Color Scanner satellite between November 1978 and June 1986. The phytoplankton pigment concentration is expected to generally reflect primary production, higher pigment concentration corresponding to higher primary production. In contrast to the WEP, the thermocline shoals as one goes further east so that it lies at a depth of only 75-100m (Levitus, 1982) above ODP 849, compared with 200-225 m above RNDB 74P (Levitus, 1982). Primary production is higher in the strongly upwelled, nutrient-rich waters of the east and falls away as one progresses westward. Modern-day primary productivity values for 110°W, 0° are of the order of $950 \text{ mgCm}^{-2}\text{day}^{-1}$ (Paytan, 1995), at least a factor of 3 greater than above our site in the WEP.

west and east sides of the equatorial Pacific is unclear based on an analogy with shorter time-scale processes, such as the modern-day El Niño-La Niña variability.

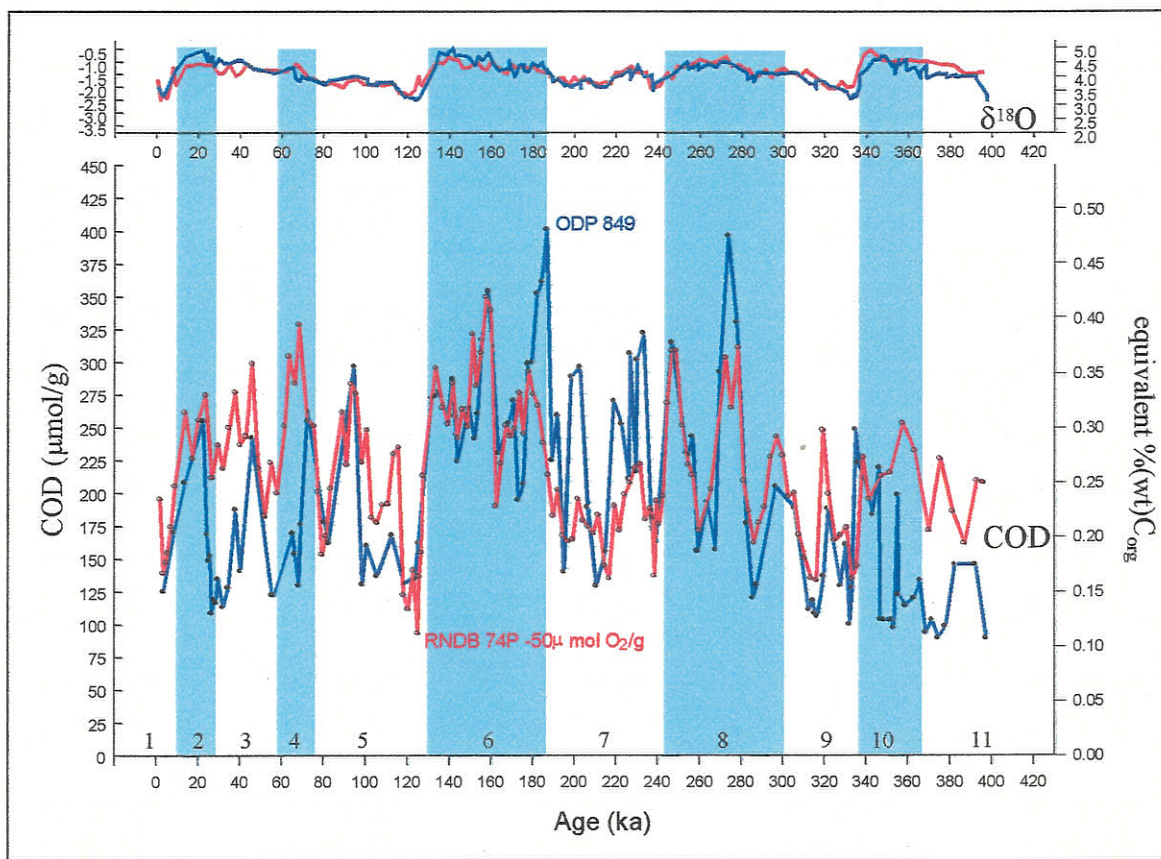
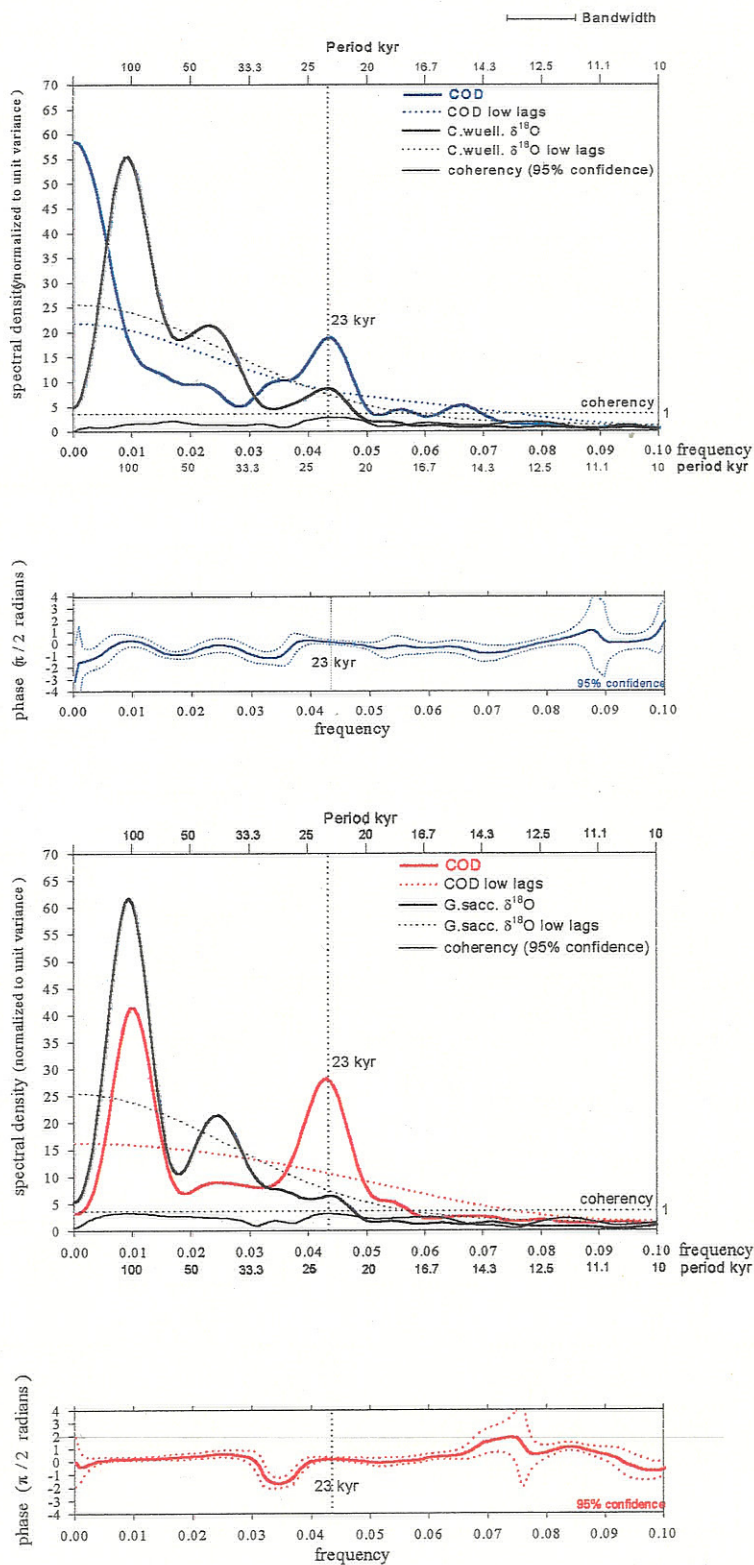


Figure 3.2. Combustion oxygen demand (COD) in piston-core RNDB 74P (red solid line) from the Ontong-Java Plateau ($0^{\circ}20'N$, $159^{\circ}22'E$, 2547m) beneath the West Pacific Warm Pool, and ODP Hole 849 (blue solid line) in the eastern equatorial Pacific ($0^{\circ}11'N$, $110^{\circ}34'W$, 3851m) versus age in thousand years before present (kya). The COD values are reported in $\mu\text{mol O}_2$ per g of (dry) sediment sample, with the record of RNDB 74P offset by subtracting $50\mu\text{mol O}_2/\text{g}$ from each data point. The shading indicates marine oxygen isotope stages for glacial periods (even numbers). The top plot shows $\delta^{18}\text{O}$ in each core. Ages were assigned for RNDB 74P by fitting the *Globigerinoides sacculifer* $\delta^{18}\text{O}$ record to the age model for ODP Hole 806B (Berger, 1996), and for ODP 849 by matching the *Cibicides wuellerstorfi* $\delta^{18}\text{O}$ age model of Mix et al. (1995) to the RNDB 74P $\delta^{18}\text{O}$ record. The match of the $\delta^{18}\text{O}$ curves was then refined by matching both $\delta^{18}\text{O}$ records to the age model of ODP 677 (Shackleton, 1996). Within each core the $\delta^{18}\text{O}$ and COD were measured at the same depths. The average sampling resolution is 2.7 kyr for RNDB 74P and 3.2 kyr for ODP 849. Although we present COD as a concentration rather than as a bulk property (such as accumulation rate), sedimentation rates over this interval only vary within less than a few %, averaging 2.0 cm/kyr for RNDB 74P and 3.1 cm/kyr for ODP 849. At both sites, the sea-floor sediments contain at least $>80\%$ (wt) calcium carbonate and $<0.2\%$ (wt) organic carbon. The right-hand axis shows the equivalent organic carbon (C_{org}) concentrations as dry weight percentages, where we have assumed that only C_{org} consumes the O_2 and with an $\text{O}_2:\text{C}$ ratio of 1 to 1. The actual C_{org} contents are probably slightly smaller than this because of the presence of reduced nitrogen in the organic matter and because carbon is likely to be in a more reduced oxidation state than $\text{C}(0)$.

Both records display a sawtooth pattern, with higher values generally occurring during glacial periods and lower COD coinciding with interglacials, a similar pattern to that displayed by the $\delta^{18}\text{O}$ in each core (Figure 3.2). However, COD exhibits more higher frequency variability, with pronounced precessional peaks, which are synchronous in both cores to within the resolution provided by sampling interval and dating uncertainties, around 3 kyr. Glacial COD is higher than interglacial values by at least a factor of 2. The highest COD values occur in stage 6 in both cores ($400.6 \mu\text{molO}_2/\text{g}$ in RNDB 74P, and $402.0 \mu\text{molO}_2/\text{g}$ in ODP 849), and the lowest value in stage 5e in RNDB 74P ($143.9 \mu\text{molO}_2/\text{g}$), when there is a similarly low value in ODP 849 ($136.1 \mu\text{molO}_2/\text{g}$). The mean COD in RNDB 74P is $267.2 \mu\text{molO}_2/\text{g}$, and in ODP 849 $188.2 \mu\text{molO}_2/\text{g}$. The EEP core appears to have longer periods of lower COD after stage 5e than the WEP. Both cores display the same main features, which occur synchronously to within the resolution provided by sampling interval and dating uncertainties (around 3 kyr). Blackman-Tukey cross-spectral analysis (Paillard et al., 1996) does not reveal a 100 kyr response in COD in ODP 849 (Fig. 3.3a.), and power in the obliquity band is not significant. In RNDB 74P, there is likewise no significant obliquity response (Figure 3.3b.). However, here there is a strong 100 kyr signal in COD. The most striking feature in Figures 3.2 and 3.3 is the pronounced, in-phase, response displayed in both cores to forcing at the precessional frequency of 23 kyr, with more power concentrated in this band in RNDB 74P than in ODP 849. Neither time series displays any obvious overall down-core trend, indicating that any long-term losses due to oxidative degradation of organic matter in the sediment are small. This also supports the assumption that the organic matter that we are measuring is highly refractory, having survived long-term exposure to oxygenated bottom waters and consumption by bottom-dwelling fauna and bacteria (sedimentation rates are of the order of 2-3 cm/kyr).



Figures 3a (blue) and 3b (red).

Figure 3.3. Blackman-Tukey cross-spectral analysis (Paillard et al., 1996) of COD and $\delta^{18}\text{O}$ data sets presented in Figure 3.2 in RNDB 74P from the Ontong-Java Plateau (a) and ODP Hole 849 from the eastern equatorial Pacific (b). Phasing between COD and $\delta^{18}\text{O}$ is shown at the base of the plots, with positive phase indicating COD leading $\delta^{18}\text{O}$. Phase is in units of $\pi/2$ radians. The analysis was performed with unfiltered data sets. Ages were assigned as described in Figure 3.2. The sampling interval was 2 kyr. Graphs show variance spectra as spectral density ($\sigma^2 f^1$, where σ^2 is variance and frequency f is 1 per period) against frequency (not plotted to the Nyquist frequency as spectral densities at frequencies higher than those plotted were very low) and period at 60 lags (solid line) and 10 lags (dotted line). Spectral density is plotted on a logarithmic scale. The low-lag spectra provide a baseline against which the significance of peaks in the high-lag spectra can be assessed. Significant peaks occur at 23 kyr in COD for both data sets. The 41 kyr peak is not significant at the 95% confidence limit in the COD time series and the 100 kyr peak is only significant in RNDB 74P. The $\delta^{18}\text{O}$ data show significant peaks at 100, 41 and 23 kyr, although the 23 kyr peak is broad and not significant at the 95% confidence limit in RNDB 74P. The 95% coherency significance level is indicated by the horizontal line. Coherency between two time series can be assigned when both series exhibit significant spectral peaks that are coherent with a significant peak in the coherency function. Our COD data do not display the 31 kyr cycle observed by Pisias and Rea (1988) and Pisias and Mix (1997) in the central and eastern equatorial Pacific, respectively.

COD in both cores is highly coherent with methane in the Vostok ice-core (Petit et al., 1999) (Figure 3.4): high COD coincides with low methane. We also compared our COD data with the model NINO3 index response of Clement et al. (1999). For both the EEP and WEP, COD and model NINO3 are highly coherent. However, high values of COD are in phase with model *warm* events, as indicated by high NINO3 index, suggesting that periods of higher productivity coincided with warmer mean conditions (more El Niño-like) over the past 150 kyr. This is the opposite phasing than what we would infer from the coincidence of colder mean conditions with higher productivity from the glacial-interglacial trend in paleoproductivity proxies. Similar patterns of modeled warm periods coinciding with higher productivity occur when we compare the model NINO3 index with another paleoproductivity proxy from the central equatorial Pacific (Paytan et al., 1996).

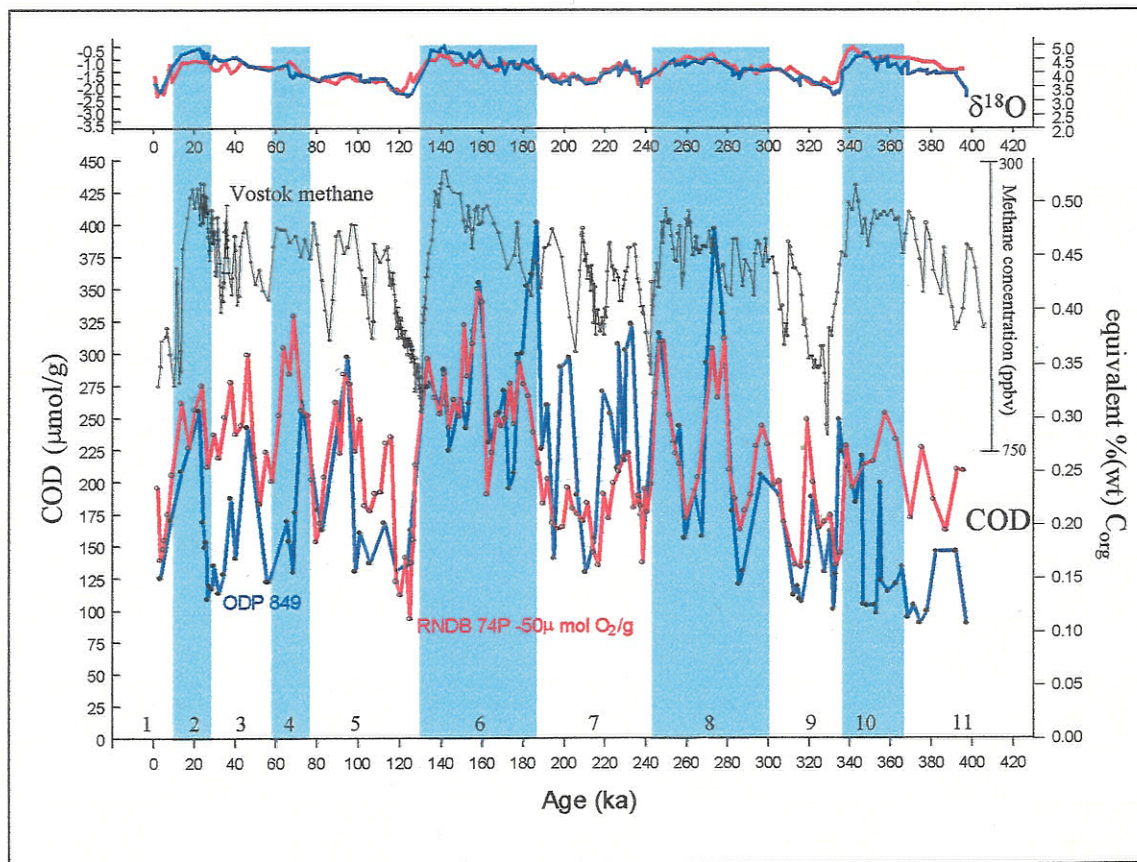


Figure 3.4. Comparison of the COD data sets presented in Figure 3.2 in RNDB 74P from the Ontong-Java Plateau (red line) and ODP Hole 849 (blue line) in the eastern equatorial Pacific with atmospheric methane concentration (parts per billion by volume (ppbv)) trapped in air bubbles in the Vostok ice core (Petit et al., 1999). CH_4 shows Milankovitch periodicity at 100, 41 and 23 kyr (Petit et al., 1999). The strong 23 kyr variability supports the conclusion by Chapellaz et al. (1993) that atmospheric CH_4 responds primarily to changes in sources in the tropics. COD at both sites and Vostok CH_4 are highly coherent, particularly for the last ~300 kyr, but are anti-phased: peaks of *lower* CH_4 , occurring during globally cooler conditions, are in phase with *higher* COD. (The phasing of the 23 kyr response between COD and CH_4 is indistinguishable from 180° given the precision of both age models). This implies that lower CH_4 coincided with a colder mean tropical Pacific.

3.3 Discussion

It is important to assess whether the COD signal results from a sedimentary artifact, as opposed to being a measure of surface-ocean dynamics. We are measuring very small amounts of organic carbon (generally $<0.35\%$ (wt)) and the higher COD we observe during

glacials might indicate that higher COD just reflects enhanced preservation of organic matter with higher sedimentation rate, and/or increased CaCO_3 dissolution. However, the fact that we see the same patterns in both the east and west cores, which are at different depths and have different sedimentation rates and dissolution histories, indicates that this is unlikely to be the case, although such factors may contribute to differences in relative amplitude in COD observed between the two cores. This provides support for our conclusion that higher COD in these cores corresponds to higher productivity in the overlying surface waters. It is unclear why COD in the WEP core is some 20% higher than in the EEP, especially given that modern-day surface primary production values are at least 3 times higher in the EEP. It is possible that storage conditions after retrieval of the core and in the core locker affect the absolute magnitude of the COD signal, a feature which we have observed in other cores from these regions, although the down-core trend does remain preserved in these cores (Chapter 4). Besides the factors mentioned above, another explanation for this difference may be that RNDB 74P contains a higher background clay signal than ODP 849. We estimate an extreme upper bound for the contribution from any reduced iron to be <5% of the COD changes observed across glacial-interglacial transitions, from reduced sulfur to be <10% of the observed range, and a negligible contribution from $\text{Mn}(+2)$ (Perks and Keeling, 1998).

Nevertheless, the general pattern observed in both cores, COD values which are at least twice as high during glacial periods as during interglacials, is consistent with paleoproductivity patterns inferred from other proxy data in the equatorial Pacific (e.g. Pedersen, 1983; Pedersen et al., 1991; Isern, 1991; Snoeckx, 1995; Paytan et al., 1996). The coherent, in-phase 23,000 year variability we observe in COD implies a Pacific-wide response in productivity along the equator to precessional insolation forcing. We suggest that

the observed COD variations in the EEP and WEP are consistent with a response to low-latitude insolation changes of the intensity and westward extent of upwelling of cool, nutrient-rich water in the eastern equatorial Pacific. During cold periods, this "tongue" of upwelled water apparently extended across into the West Pacific Warm Pool, supporting higher productivity across the equatorial Pacific. During warm periods, the upwelling in the east was less vigorous, advection of these waters did not reach as far westward, and productivity was lower. The more vigorous upwelling presumably would have been driven by stronger trade winds during globally colder periods (Bush and Philander, 1998; Bigg et al., 1998).

These are relatively standard conclusions derived from the comparison of glacial and interglacial productivity patterns (Sarnthein et al., 1988; Berger et al., 1989). However, our work refines the description of this behavior to be primarily a precessional signal that extends to the basin-wide equatorial Pacific. From existing data, it is unclear whether such a mechanism is consistent with the nutrient behavior in surface waters during El Niño and La Niña events in the modern Pacific Ocean, or whether the mechanisms that control productivity over ENSO timescales may be similar to those taking place over precessional timescales. Data from Blanchot et al. (1989, 1992); Radenac and Rodier (1996); and Murtugudde et al. (1999) in the west, and Barber and Chavez (1983) in the east could be interpreted as evidence for generally increased primary productivity during La Niña relative to El Niño conditions, indicating that primary production variations in the eastern equatorial Pacific (EEP) and western equatorial Pacific (WEP) might be in phase during El Niño and La Niña conditions. The model of Clement et al. (1999) does show that tropical Pacific interannual SST's, driven by changes in wind-driven upwelled water at the equator, are

coherent across the open-ocean Pacific. This observation is consistent with the in-phase behavior of COD between the EEP and WEP. However, the fact that COD and the model output appear to be 180° out of phase from what we would expect from glacial-interglacial productivity proxies may imply that the model is not accurately reproducing past conditions in the tropical Pacific. Clement et al. (1999) discuss limitations of their model, the most important of which may very well be the fact that it is very closely tied to modern tropical Pacific climate. *If* the dominant factor affecting tropical Pacific climate in the past was insolation changes, *and* production in the equatorial surface waters was responding to more strongly upwelled cooler, nutrient-rich waters, then this suggests that we cannot simply extrapolate our present understanding of modern tropical Pacific climate variability back into the recent Pleistocene. The COD data also suggest that Andreasen and Ravelo's (1997) interpretation of thermocline shoaling in the east and deepening in the west during glacials may be wrong, since from this we would infer productivity in the EEP and WEP to be 180° out of phase with one another. Alternatively, the thermocline depth might not be a major factor in controlling Late Pleistocene productivity in both EEP and WEP simultaneously.

The fact that the phasing of COD in both EEP and WEP is similar to that of ice volume might imply that high-latitude ice volume changes are driving the signal. One possible scenario would be if surface-ocean dynamics were being forced by sea-level fluctuations, such as the effects of the exposure and flooding of the maritime continent of the Indonesian archipelago. However, absence of significant obliquity in both cores, and eccentricity in the east, suggests that high-latitude forcing mechanisms may not play a main role in forcing COD. The phase behavior of COD and ice volume is consistent with the theory that a cool tropical Pacific favors northern hemisphere ice sheet growth (Cane and Clement, 1998, Cane,

1998). The high coherency of COD and atmospheric CH₄ in the Vostok ice-core (Chapellaz et al., 1993; Petit et al., 1999) (Figure 3.4) over precessional cycles is consistent with both being forced by low-latitude insolation changes. Low COD in phase with high CH₄ implies that high CH₄ occurs when equatorial upwelling in the Pacific is weaker and the mean state of the tropical Pacific is warmer, which would by analogy with modern conditions correspond to warmer tropics in general.

We might expect that, because of its proximity to Asia, the WEP was more strongly affected by changes in monsoon strength than the EEP. We speculate that the monsoon over the Australian and maritime continent (which would have been exposed during glacial conditions) may have strengthened and increased upwelling in the WEP in phase with that taking place in the EEP. The role of this monsoon may also account for the differences in amplitude observed over some intervals between the WEP and EEP data sets. Another possible mechanism may be changes in the supply of nutrients along the equator from overturning of the mid-latitude Subantarctic Mode Waters (Pisias and Mix, 1997). The fact that our data do not resemble the 100 and 41 kyr peaks observed in the Vostok CO₂ record (Petit et al., 1999), provides evidence to suggest that the solubility pump driven by changes in the intensity of equatorial upwelling in the Pacific is not driving global CO₂ variations on Milankovitch timescales (Keir, 1993).

3.4 Summary

We have demonstrated a highly coherent variation in surface-water production, as recorded by combustion oxygen demand, with Milankovitch-scale global climate fluctuations, in particular a pronounced precessional response, which is in phase in both the

eastern and western equatorial Pacific Ocean over the last 400 kyr. We conclude that the surface waters of the equatorial Pacific displayed a basin-wide response to low-latitude insolation changes in the Late Pleistocene, which was synchronous to within the limits set by our sampling resolution and age model (3-4 kyr). We suggest that the implied increases in productivity were caused by more vigorous equatorial upwelling which extended westward into the West Pacific Warm Pool, driven by stronger trade winds, possibly analogous to modern-day La Niña conditions. We speculate that changes in the Australian monsoon and exposure of the maritime continent of Indonesia may have played a role in affecting surface-water conditions, at least in the western equatorial Pacific. Improved interpretation of paleoceanographic data sets from the region requires the development of more sophisticated models which are also less tightly tied to modern climate conditions. It is also clear that the development and testing of such models, and a better understanding of the tropical Pacific climate system and oceanographic conditions in the past, necessitates the generation of more proxy records from the region, at all levels of resolution, from Milankovitch to seasonal.

This chapter will be submitted with slight modifications to *Paleoceanography* as

Perks, H. M., C. D. Charles, and R. F. Keeling, Coherent and synchronous precessional forcing in the eastern and western equatorial Pacific.

I was the primary investigator and lead author for this manuscript, and conducted all of the analyses presented therein.

3.5 References

- Andreasen, D.J., and A. C. Ravelo, Tropical Pacific Ocean thermocline depth reconstruction for the Last Glacial Maximum, *Paleoceanography*, *12*, 395-413, 1997.
- Barber, R.T., and F. P. Chavez, Biological consequences of El Niño, *Science*, *222*, 1203-1210, 1983.
- Berger, W. H., Reconstruction of atmospheric CO₂ from ice-core data and the deep-sea record of Ontong Java Plateau - The Milankovitch Chron, *Geologische Rundsch.*, *85*, 466-495, 1996.
- Berger, W. H., V. S. Smetacek, G. Wefer, Smetacek, V. S., editor; Wefer, G., editor (Dahlem workshop on Productivity of the ocean; present and past Berlin, Federal Republic of Germany), Ocean productivity and paleoproductivity; an overview In: Berger, W. H. , editor Productivity of the ocean; present and past. Berlin, Heidelberg, New York, Tokyo: Springer, *Life Sciences Research Reports* Vol. 44 p. 1-34, 1989.
- Bigg, G. R., M. R. Wadley, D. P. Stevens, and J. A. Johnson, Simulations of two last glacial maximum ocean states, *Paleoceanography*, *13*, 340-351, 1998.
- Blanchot, J., R. Le Borgne, A. Le Bouteiller, and M Rodier, Enso events and consequences on the nutrient planktonic biomass and production in the Western Pacific Tropical Ocean, *Proceedings of TOGA-COARE meeting, May 1989, Nouméa*, 785-790, 1989.
- Blanchot, J., M. Rodier, and A. Le Bouteiller, Effect of El Niño Southern Oscillation events on the distribution and abundance of phytoplankton in the Western Pacific Tropical Ocean along 165°E, *J. of Plankton Res.*, *14*, 137-156, 1992.
- Bush, A. B. G., and S. G. H. Philander, The role of ocean-atmosphere interactions in Tropical cooling during the last glacial maximum, *Science*, *279*, 1341-1344, 1998.
- Cane, M. A., El Niño, *Ann. Rev. Earth Planet Sci.*, *14*, 43-70, 1986.
- Cane, M. A., Climate change: A role for the tropical Pacific, *Science*, *282*, 59-61, 1998.
- Cane, M. A., and A. C. Clement, A role for the tropical Pacific coupled ocean-atmosphere system on Milankovitch and millennial timescales. Part II: Global impacts, *AGU Monograph: Mechanisms of Millennial-Scale Global Climate Change*, in prep., 1998.
- Chapellaz, J., T. Blunier, D. Raynaud, J. Barnola, J. Schwander, and B. Stauffer, Synchronous changes in atmospheric CH₄ and Greenland climate between 40 and 8 kyr BP, *Nature*, *366*, 443-445, 1993.

- Clement, A. C., R. Seager, and M. A. Cane, Orbital controls on the El Niño/Southern Oscillation and the tropical climate, *Paleoceanography*, 14, 441-456, 1999.
- Farrell, J., T. Pedersen, S. Calvert, and B. Nielsen, Glacial-interglacial changes in the equatorial Pacific Ocean, *Nature*, 377, 514-517, 1995.
- Hagelberg, T., N. Pisias, L. Mayer, N. Shackleton, and A. Mix, Spatial and temporal variability of the late Neogene equatorial carbonate: Leg 138, *Proc. Ocean Drill. Program Sci. Res.*, 138, 321-336, 1995.
- Herguera, J. C., and W. H. Berger, Paleoproductivity from benthic foraminifera abundance: Glacial to postglacial change in the west-equatorial Pacific, *Geology*, 19, 1173-1176, 1991.
- Herguera, J. C., and W. H. Berger, Glacial to postglacial drop in productivity in the western equatorial Pacific: Mixing rate vs. nutrient concentrations, *Geology*, 22, 629-632, 1994.
- Isern, A. R., Calcium carbonate and organic carbon accumulation in the central equatorial Pacific, M.S. thesis, 200 pp., Univ. of R. I., Providence, 1991.
- Keir, R. S., Cold surface ocean ventilation and its effect on atmospheric CO₂, *J. Geophys. Res.*, 98, 849-856, 1993.
- Lyle, M., D. W. Murray, B. P. Finney, J. Dymond, J. M. Robbins, and K. Brooksforce, The record of late Pleistocene biogenic sedimentation in the eastern tropical Pacific Ocean, *Paleoceanography*, 3, 39-59, 1988.
- Mix, A.C., N.G. Pisias, W. Rugh, J. Wilson, A. Morey, T. Hagelberg, Benthic foraminiferal stable isotope record from Site 849, 0-5 Ma: Local and global climate changes. In: N.G. Pisias, L. Mayer, T. Janecek, A. Palmer-Julson, T.H. van Andel (eds.) *Proc. ODP, Scientific Results 138*, College Station TX (Ocean Drilling Program), 371-412, 1995.
- Murtugudde, R. G., S. R. Signorini, J. R. Christian, A. J. Busalacchi, C. R. McClain, and J. Picaut, Ocean color variability of the tropical Indo-Pacific basin observed by SeaWiFS during 1997-1998., *J. Geophys. Res.*, 104, 18,351-18,366., 1999.
- Paillard, D., L. Labeyrie, and P. Yiou, Macintosh program performs time-series analysis, *Eos. Trans., AGU*, 77, 379, 1996.
- Paytan, A., Marine barite, a recorder of oceanic chemistry, productivity and circulation, Ph.D. thesis, 111 pp., Univ. of Calif. at San Diego, 1995.
- Paytan, A., M. Kastner, and F. P. Chavez, Glacial to interglacial fluctuations in productivity in the equatorial Pacific as indicated by marine barite, *Science*, 274, 1355-1357, 1996.

- Pedersen, T. F., Increased productivity in the eastern equatorial Pacific during the last glacial maximum (19,000 to 14,000 yr B.P.), *Geology*, *11*, 16-19, 1983.
- Pedersen, T. F., B. Nielsen, and M. Pickering, Timing of late Quaternary productivity pulses in the Panama Basin and implications for atmospheric CO₂, *Paleoceanography*, *6*, 657-677, 1991.
- Perks, H. M. and R. F. Keeling, A 400 kyr record of combustion oxygen demand in the western equatorial Pacific: Evidence for a precessionally forced climate response, *Paleoceanography*, *13*, 63-69, 1998.
- Petit, J. R., J. Jouzel, D. Raynaud, N. I. Barkov, J.-M. Barnola, I. Basile, M. Bender, J. Chappellaz, M. Davis, G. Delaygue, M. Delmotte, V. M. Kotlyakov, M. Legrand, V. Y. Lipenkov, C. Lorius, L. Pépin, C. Ritz, E. Saltzman, and M. Stievenard, Climate and atmospheric history of the past 420,000 years from the Vostok ice core, Antarctica, *Nature*, *399*, 429-438, 1999.
- Pisias, N. G. and A. C. Mix, Spatial and temporal oceanographic variability of the eastern equatorial Pacific during the late Pleistocene: Evidence from Radiolaria microfossils, *Paleoceanography*, *12*, 381-393, 1997.
- Pisias, N. G. and D. K. Rea, Late Pleistocene paleoclimatology of the central equatorial Pacific: Sea surface response to the southeast trade winds, *Paleoceanography*, *3*, 21-37, 1988.
- Radenac, M.-H., and M. Rodier, Nitrate and chlorophyll distributions in relation to thermocline and current structures in the western tropical Pacific during 1985-1989, *Deep-Sea Res. II*, *43*, 725-752, 1996.
- Sarnthein, M., K. Winn, J.-C. Duplessy, and M. R. Fontugne, Global variations of surface ocean productivity in low and mid latitudes: Influence on CO₂ reservoirs of the deep ocean and atmosphere during the last 21,000 years, *Paleoceanography*, *3*, 361-399, 1988.
- Shackleton, N., Timescale calibration, ODP 677, IGBP Pages/World Data Center-Paleoclimatology Data Contribution Series #96-018. NOAA/NGDC Paleoclimatology Prog., Boulder, CO, USA, 1996.
- Snoeckx, H., Late Pleistocene history of ocean-atmosphere interaction in the eastern equatorial Pacific, Ph.D. thesis, 199 pp., Univ. of Mich., Ann Arbor, 1995.
- Toggweiler, J. R., K. Dixon, and W. S. Broecker, The Peru Upwelling and the ventilation of the South Pacific thermocline, *J. Geophys. Res.*, *96*, 20,467-20,497, 1991.
- Tziperman, E., S. E. Zebiak, and M. Cane, Mechanisms of seasonal-ENSO interaction, *J. Atmos. Sci.*, *54*, 61-71, 1997.

Yasuda, M., Foraminifera as indicators of Quaternary carbonate saturation and productivity in the western equatorial Pacific, the last million years, Ph.D. thesis, Univ. of Calif. at San Diego, in prep., 1999.

Yasuda, M., W. H. Berger, G. Wu, S. Burcke, and H. Schmidt, Foraminifer preservation record for the last million years: Site 805, Ontong Java Plateau, *Proc. Ocean Drill. Prog. Sci. Results*, 130, 491-508, 1993.

Zebiak, S. E., and M. A. Cane, A model El Niño-Southern Oscillation, *Mon. Weather Rev.*, 115, 2262-2278, 1987.

3.6 Tables

Table 3.1. Combustion oxygen demand and oxygen isotope data for piston core RNDB 74P from the Ontong-Java Plateau.

Depth interval in core	depth in core (mid-point)	age model ¹	COD ² average from duplicates	COD - 50 average from duplicates	COD equivalent Corg	$\delta^{18}\text{O}$ <i>G.sacculifer</i> Yasuda (1999)
cm	cm	kya	$\mu\text{mol/g}$	$\mu\text{mol/g}$	%(wt)	‰,PDB
0-2	1	0.00	373.95	323.95	0.389	-1.630
6-8	7	1.50	246.00	196.00	0.235	-2.470
11.5-13.5	12.5	3.00	189.82	139.82	0.168	-2.240
16-18	17	4.50	198.38	148.38	0.178	-2.390
21-23	22	5.20	205.70	155.70	0.187	-2.130
28-30	29	6.70	225.42	175.42	0.211	-1.627
33-35	34	7.20				-1.202
38-40	39	8.50	256.45	206.45	0.248	-1.878
44-46	45	13.28	312.54	262.54	0.315	-1.127
50-52	51	16.82	277.78	227.78	0.274	-1.096
55-57	56	19.77	307.00	257.00	0.309	-1.011
61-63	62	23.31	326.00	276.00	0.332	-1.095
66-68	67	26.26	262.80	212.80	0.256	-1.067
71-73	72	29.21	287.88	237.88	0.286	-1.414
75-77	76	31.57	269.68	219.68	0.264	-1.398
80-82	81	34.52	301.16	251.16	0.302	-1.064
85-87	86	37.46	328.08	278.08	0.334	-1.532
89-91	90	39.82	288.07	238.07	0.286	-1.415
94-96	95	42.77	294.63	244.63	0.294	-1.052
99-101	100	45.72	349.62	299.62	0.360	-1.228
104-106	105	48.67	270.29	220.29	0.265	-1.307
109-111	110	51.62	233.41	183.41	0.220	-1.311
114-116	115	54.57	274.03	224.03	0.269	-1.318
119-121	120	57.52	251.28	201.28	0.242	-1.329
125-127	126	61.06	302.65	252.65	0.303	-1.342
131-133	132	63.00	355.43	305.43	0.367	-1.263
137-139	138	66.00	334.67	284.67	0.342	-1.062
142-144	143	68.00	379.69	329.69	0.396	-1.192
148.5-150.5	149.5	72.00	306.37	256.37	0.308	-1.585
154-156	155	75.00	302.54	252.54	0.303	-1.639
160-162	161	77.00	252.50	202.50	0.243	-1.791
166-168	167	79.00	204.13	154.13	0.185	-1.776
171-173	172	81.00	218.39	168.39	0.202	-1.882
177-179	178	83.00	254.55	204.55	0.246	-1.779
182-184	183	88.69	312.70	262.70	0.316	-1.974
187-189	188	90.75	272.97	222.97	0.268	-1.747

Table 3.1	continued						
192-194	193	92.80	334.45	284.45	0.342	-1.697	
198-200	199	95.27	326.98	276.98	0.333	-1.659	
204.5-206.5	205.5	97.94	274.50	224.50	0.270	-1.826	
210.5-212.5	211.5	100.41	299.22	249.22	0.299	-1.843	
216-218	217	102.67	232.10	182.10	0.219	-1.892	
222-224	223	105.14	228.26	178.26	0.214	-1.803	
228.5-230.5	229.5	107.81	241.84	191.84	0.230	-1.903	
235-237	236	110.48	242.52	192.52	0.231	-1.840	
241-243	242	112.95	280.89	230.89	0.277	-1.857	
247-249	248	115.41	285.78	235.78	0.283	-2.215	
253-255	254	117.88	173.32	123.32	0.148	-2.203	
258-260	259	119.93	162.26	112.26	0.135	-2.327	
264-266	265	122.40	192.04	142.04	0.171	-2.109	
269-271	270	124.46	143.90	93.90	0.113	-1.549	
275-277	276	125.00	187.64	137.64	0.165	-1.758	
282-284	283	126.00	205.40	155.40	0.187	-1.888	
287-289	288	127.00	264.29	214.29	0.257	-1.720	
292-294	293	133.00	346.72	296.72	0.356	-0.974	
296-298	297	136.40	316.38	266.38	0.320	-1.041	
301-303	302	138.75	303.71	253.71	0.305	-0.765	
306-308	307	141.11	334.96	284.96	0.342	-0.866	
311-313	312	143.46	293.03	243.03	0.292	-0.900	
316-318	317	145.82	314.81	264.81	0.318	-1.217	
321-323	322	148.18	301.51	251.51	0.302	-1.198	
326-328	327	150.53	372.57	322.57	0.387	-1.082	
330-332	331	152.42	332.86	282.86	0.340	-0.946	
335-337	336	154.77	358.28	308.28	0.370	-1.217	
340-342	341	157.13	400.62	350.62	0.421	-1.290	
345-347	346	159.48	390.57	340.57	0.409	-0.887	
350-352	351	161.84	240.97	190.97	0.229	-1.149	
355-357	356	164.19	273.84	223.84	0.269	-1.294	
360-362	361	166.55	302.88	252.88	0.304	-1.445	
365-367	366	168.91	294.16	244.16	0.293	-1.047	
369-371	370	170.79	300.37	250.37	0.301	-1.211	
374-376	375	173.15	327.27	277.27	0.333	-1.131	
378-380	379	175.03	295.85	245.85	0.295	-1.152	
383-385	384	177.39	344.03	294.03	0.353	-1.216	
388-390	389	179.74	326.61	276.61	0.332	-1.136	
393-395	394	182.10	317.49	267.49	0.321	-1.326	
398-400	399	184.45	289.32	239.32	0.287	-1.384	
403-405	404	186.81	265.07	215.07	0.258	-1.422	
408-410	409	189.16	233.63	183.63	0.221	-1.781	
413-415	414	191.52	253.37	203.37	0.244	-1.634	
418-420	419	193.96	218.21	168.21	0.202	-1.620	
423-425	424	196.40	213.77	163.77	0.197	-1.895	
428-430	429	198.83	215.11	165.11	0.198	-1.587	
433-435	434	201.27	246.17	196.17	0.236	-1.786	
438-440	439	203.71	229.98	179.98	0.216	-1.548	
443-445	444	206.15	225.12	175.12	0.210	-1.804	

Table 3.1		continued					
448-450	449	208.59	219.83	169.83	0.204	-1.795	
453-455	454	211.03	234.15	184.15	0.221	-1.854	
459-461	460	213.95	195.48	145.48	0.175	-1.758	
464-466	465	216.39	185.70	135.70	0.163	-1.862	
469-471	470	218.83	240.93	190.93	0.229	-1.406	
474-476	475	221.27	221.94	171.94	0.207	-1.397	
479-481	480	223.70	249.54	199.54	0.240	-1.314	
484-486	485	226.14	258.74	208.74	0.251	-1.139	
489-491	490	228.58	270.28	220.28	0.265	-1.372	
494-496	495	231.02	273.10	223.10	0.268	-1.436	
499-501	500	233.46	230.57	180.57	0.217	-1.378	
504-506	505	235.89	239.58	189.58	0.228	-2.042	
509-511	510	237.00	232.12	182.12	0.219	-1.808	
514-516	515	238.00	187.50	137.50	0.165	-1.967	
518.5-520.5	519.5	239.00	245.05	195.05	0.234	-1.910	
524-526	525	240.00	227.02	177.02	0.213	-1.946	
528.5-530.5	529.5	242.00	248.78	198.78	0.239	-1.626	
534-536	535	244.00	319.53	269.53	0.324	-1.398	
538.5-540.5	539.5	246.00	359.97	309.97	0.372	-1.642	
543-545	544	248.00	359.82	309.82	0.372	-1.176	
548-550	549	251.00	302.78	252.78	0.304	-1.163	
553-555	554	254.00	272.74	222.74	0.268	-1.091	
558-560	559	256.00	264.74	214.74	0.258	-1.038	
563-565	564	259.00	222.26	172.26	0.207	-0.864	
568-570	569	265.00	253.97	203.97	0.245	-1.042	
573-575	574	271.87	354.42	304.42	0.366	-0.760	
578-580	579	274.57	316.01	266.01	0.320	-1.134	
584-586	585	277.81	362.12	312.12	0.375	-1.073	
589-591	590	280.51	260.24	210.24	0.253	-1.286	
593-595	594	282.79	237.52	187.52	0.225	-1.253	
598-600	599	285.63	213.07	163.07	0.196	-1.590	
602-604	603	287.90	228.29	178.29	0.214	-1.481	
607-609	608	290.75	240.50	190.50	0.229	-1.286	
612-614	613	293.59	278.41	228.41	0.274	-1.591	
617-619	618	296.43	294.07	244.07	0.293	-1.309	
622-624	623	299.28	279.87	229.87	0.276	-1.230	
627-629	628	302.12	248.17	198.17	0.238	-1.406	
632-634	633	304.96	250.97	200.97	0.241	-1.433	
636-638	637	307.24	219.07	169.07	0.203	-1.529	
641-643	642	310.08	200.76	150.76	0.181	-1.304	
646-648	647	312.93	186.21	136.21	0.164	-1.482	
651-653	652	315.77	184.10	134.10	0.161	-1.655	
656-658	657	318.61	298.84	248.84	0.299	-1.872	
661-663	662	321.46	250.21	200.21	0.240	-2.035	
666-668	667	324.30	214.60	164.60	0.198	-2.023	
671-673	672	327.14	218.87	168.87	0.203	-1.768	
676-678	677	329.99	224.44	174.44	0.210	-1.989	
681-683	682	332.83	185.76	135.76	0.163	-1.918	
685-687	686	335.10	195.29	145.29	0.175	-1.281	

Table 3.1	continued						
690-692	691	337.95	278.61	228.61	0.275	-0.688	
695-697	696	340.79	245.99	195.99	0.235	-0.507	
700-702	701	346.49	264.09	214.09	0.257	-0.888	
704-706	705	351.06	266.65	216.65	0.260	-0.984	
709-711	710	356.76	304.25	254.25	0.305	-0.889	
714-716	715	362.47	283.52	233.52	0.280	-0.932	
720-722	721	369.31	222.33	172.33	0.207	-0.968	
725-727	726	375.01	277.05	227.05	0.273	-1.071	
730-732	731	380.72	236.75	186.75	0.224	-1.116	
735-737	736	386.42	212.60	162.60	0.195	-1.462	
740-742	741	392.13	260.21	210.21	0.252	-1.415	
745-747	746	395.22	259.01	209.01	0.251	-1.375	

¹ The age model was assigned by fitting to the age model for ODP 806B (Berger, 1996) and refined by matching the $\delta^{18}\text{O}$ record (Yasuda, 1999) to ODP 677 (Shackleton, 1996)

² COD data are not corrected for salt.

Table 3.2. Combustion oxygen demand and oxygen isotope data for Ocean Drilling Program core ODP 849 from the eastern equatorial Pacific.

Section	depth interval in core	depth in core (mid-point)	depth in core (mid-point)	age model ²	COD ³ average from duplicates	COD equivalent Corg	$\delta_{18}O$
	cm	mbsf	rmcd ¹	kya	$\mu\text{mol/g}$	%(wt)	‰ , PDB
849B-1H-1	6.5-7.5	0.06		0.00	241.04	0.290	3.66
849B-1H-1	17.0-18.0	0.17		1.00	267.89	0.322	3.49
849B-1H-1	28.0-29.0	0.28		3.00	125.71	0.151	3.31
849B-1H-1	44.0-45.0	0.44		8.00	171.22	0.206	4.17
849B-1H-1	53.5-54.5	0.54		13.28	209.19	0.251	4.69
849B-1H-1	69.0-70.0	0.69		22.00	256.26	0.308	4.92
849B-1H-1	89.0-90.0	0.89		24.00	169.67	0.204	4.55
849B-1H-1	109.0-110.0	1.09		24.80	149.75	0.180	4.59
849B-1H-1	118.0-119.0	1.18		25.50	153.87	0.185	4.55
849B-1H-1	128.0-129.0	1.28		26.26	109.64	0.132	4.72
849B-1H-1	138.0-139.0	1.38		27.30	119.94	0.144	4.36
849B-1H-1	147.0-148.0	1.47		28.30	117.74	0.141	4.46
849B-1H-2	11.0-12.0	1.61		29.21	135.89	0.163	4.63
849C-1H-1	87.0-88.0	1.88		31.57	113.86	0.137	4.47
849B-1H-2	38.0-39.0	1.98		34.00	129.10	0.155	4.45
849C-1H-1	97.0-98.0	2.18		37.46	188.36	0.226	4.54
849B-1H-2	48.0-49.0	2.28		39.82	141.34	0.170	4.57
849C-1H-1	107.0-108.0	2.42		45.72	243.12	0.292	4.27
849C-1H-1	117.0-118.0	2.51		55.00	123.15	0.148	4.14
849B-1H-2	68.0-69.0	2.61		56.00	123.27	0.148	4.10
849B-1H-2	78.0-79.0	1.87		65.00	170.25	0.204	4.32
849B-1H-2	92.0-93.0	2.73		66.00	154.78	0.186	3.95
849C-1H-2	7.0-8.0	1.97		68.00	130.54	0.157	3.83

Table 3.2		continued										
849B-1H-2	101.0-102.0	2.07	2.89	69.00	176.91	0.212	4.00	3.96				
849C-1H-2	17.0-18.0	2.83	2.92	72.00	263.21	0.316	3.90					
849B-1H-2	110.0-111.0	2.17	2.96	80.00	179.23	0.215	3.71	3.84				
849C-1H-2	27.0-28.0	2.96	3.06	82.11	163.34	0.196	3.85					
849B-1H-2	123.0-124.0	2.43	3.15	94.25	297.62	0.357	4.00					
849C-1H-2	37.0-38.0	2.53	3.24	98.14	131.09	0.157	3.95					
849B-1H-2	133.0-134.0	2.63	3.33	100.41	160.95	0.193	3.91	3.73				
849C-1H-2	47.0-48.0	2.73	3.44	105.14	137.40	0.165	3.70	3.79				
849C-1H-2	57.0-58.0	2.83	3.55	112.18	168.63	0.203	3.78					
849B-1H-2	146.0-147.0	2.93	3.66	117.88	131.60	0.158	3.30					
849C-1H-2	67.0-68.0	3.03	3.77	122.40	136.13	0.164	3.23					
849C-1H-2	77.0-78.0	3.13	3.88	123.00	135.53	0.163	3.15					
849C-1H-2	87.0-88.0	3.23	3.98	125.00	163.11	0.196	3.27					
849C-1H-2	97.0-98.0	3.33	4.08	131.00	273.64	0.329	4.13					
849C-1H-2	107.0-108.0	3.43	4.18	133.00	275.14	0.330	4.42					
849C-1H-2	117.0-118.0	3.53	4.28	134.51	278.99	0.335	4.85					
849C-1H-2	127.0-128.0	3.63	4.37	138.75	255.93	0.307	4.75	4.84				
849C-1H-2	137.0-138.0	3.73	4.47	141.00	287.97	0.346	4.98					
849C-1H-2	147.0-148.0	3.83	4.56	142.00	260.12	0.312	4.70					
849C-1H-3	7.0-8.0	3.93	4.67	143.00	246.18	0.296	4.74					
849C-1H-3	17.0-18.0	4.03	4.77	143.46	225.41	0.271	4.76					
849C-1H-3	27.0-28.0	4.13	4.88	148.78	266.48	0.320	4.67					
849D-1H-1	20.5-21.5	4.22	4.98	151.63	242.64	0.291	4.38					
849C-1H-3	36.0-37.0	4.32	5.08	153.00	261.72	0.314	4.72					
849D-1H-1	30.5-31.5	4.43	5.18	155.00	318.27	0.382	4.57					
849C-1H-3	46.0-47.0	4.53	5.28	158.00	355.15	0.427	4.81					
849D-1H-1	41.0-42.0	4.62	5.38	160.00	313.24	0.376	4.52	4.46				
849C-1H-3	57.0-58.0	4.72	5.48	163.00	231.48	0.278	4.21					
849D-1H-1	51.0-52.0	4.83	5.58	168.00	254.49	0.306	4.26	4.54				
849C-1H-3	67.0-68.0	4.93	5.68	170.34	271.76	0.326	3.98					
849D-1H-1	61.0-62.0	5.02	5.78	172.64	195.83	0.235	4.38					
849C-1H-3	76.0-77.0	5.12	5.89	175.04	207.82	0.250	4.39	4.21				
849D-1H-1	70.5-71.5	5.22	5.99	177.19	299.67	0.360	4.16					

Table 3.2 continued								
849D-1H-2	91.0-92.0	5.91	9.27	285.00	120.89	0.145	4.00	3.79
849C-1H-4	106.0-107.0	6.01	9.37	287.00	130.99	0.157	4.13	
849D-1H-2	100.5-101.5	6.1	9.48	296.00	205.96	0.247	4.06	
849C-1H-4	116.0-117.0	6.2	9.6	305.20	189.53	0.228	4.13	
849D-1H-2	110.5-111.5	6.31	9.72	312.00	112.24	0.135	3.72	
849C-1H-4	127.0-128.0	6.41	9.82	314.00	119.18	0.143	3.75	
849D-1H-2	120.5-121.5	6.51	9.9	315.00	108.91	0.131	3.53	3.86
849C-1H-4	137.0-138.0	6.61	9.96	316.00	107.00	0.129	3.85	3.86
849C-1H-4	146.0-147.0	6.7	10.03	319.00	137.42	0.165	3.79	
849D-1H-3	3.0-4.0	6.82	10.12	321.00	188.54	0.226	3.65	
849D-1H-3	13.0-14.0	6.92	10.26	327.15	130.27	0.156	3.54	
849D-1H-3	23.0-24.0	7.02	10.41	329.77	161.79	0.194	3.44	3.42
849D-1H-3	33.5-34.5	7.12	10.52	331.58	100.93	0.121	3.21	
849D-1H-3	43.0-44.0	7.22	10.59	332.74	128.78	0.155	3.25	3.32
849D-1H-3	54.5-55.5	7.34	10.67	334.21	249.39	0.300	3.38	3.28
849D-1H-3	63.0-64.0	7.42	10.75	335.68	224.05	0.269	3.70	4.06
849D-1H-3	71.0-72.0	7.5	10.9	338.85	211.84	0.254	4.24	
849D-1H-3	82.5-83.5	7.61	11.05	342.45	184.70	0.222	4.58	
849D-1H-3	92.5-93.5	7.72	11.17	345.69	220.59	0.265	4.62	
849D-1H-3	102.5-103.5	9.24	11.19	346.23	104.94	0.126	4.64	4.70
849D-1H-3	123.5-124.5	7.82	11.25	348.08	104.12	0.125	4.72	
849B-2H-2	104.0-105.0	9.41	11.37	351.86	104.51	0.126	4.34	4.47
849B-2H-2	121.0-122.0	8.02	11.4	352.80	98.41	0.118	4.30	4.09
849B-2H-2	130.0-131.0	9.5	11.46	354.66	199.78	0.240	4.57	
849B-2H-2	132.0-133.0	9.52	11.47	354.97	123.53	0.148	4.40	
849B-2H-2	143.0-144.0	9.63	11.58	358.38	115.32	0.139	4.59	4.20
849B-2H-3	6.0-7.0	9.76	11.72	362.42	121.14	0.146	4.33	4.32
849B-2H-3	17.0-18.0	9.87	11.82	365.24	134.51	0.162	3.93	4.18
849B-2H-3	26.5-27.5	9.97	11.92	367.94	94.82	0.114	4.40	3.93
849B-2H-3	38.0-39.0	10.08	12.03	371.06	104.16	0.125	4.04	4.07
849B-2H-3	47.0-48.0	10.17	12.12	373.94	90.14	0.108	4.12	4.07
849B-2H-3	57.0-58.0	10.27	12.22	377.38	99.50	0.120	4.09	3.95
849B-2H-3	67.0-68.0	10.37	12.32	381.78	146.18	0.176	4.07	3.97

Table 3.2	continued										
849B-2H-3	86.5-87.5	10.56	12.52	391.54	146.40	0.176	4.02	3.92			
849B-2H-3	96.5-97.5	10.66	12.62	396.79	90.08	0.108	3.35	3.11			

¹ Depths are given in "revised meters composite depth (rmed)" according to Mix et al. (1995).

² The age model was assigned by matching the *Cibicides wuellerstorfi* $\delta^{18}\text{O}$ age model of Mix et al. (1995) to the RNDDB 74P $\delta^{18}\text{O}$ record (Yasuda, 1999). The match of the $\delta^{18}\text{O}$ curves was then refined by matching both $\delta^{18}\text{O}$ records to the age model of ODP 677 (Shackleton, 1996).

³ COD data are not corrected for salt.

4. Sedimentological studies with the combustion oxygen demand instrument in box and piston cores from the eastern and western equatorial Pacific.

Abstract

To gain a better understanding of the factors influencing the COD records in the piston core RNDB 74P from the Ontong-Java Plateau and the ODP core 849 from the eastern equatorial Pacific presented in Chapters 2 and 3, I carried out a collection of studies on various box and piston cores from sites close to these two cores.

Samples from a core from the Ontong-Java Plateau indicate that the COD is dominated by the contribution from the $<63\mu\text{m}$ size fraction. Treatment of these samples with a sodium hypochlorite solution and measurement of COD demonstrates that the amount of organic matter bound within the foraminifer or nannofossil (coccolithophore) calcite lattice is very small, corresponding to around 0.08% (wt) C_{org} (organic carbon), and is roughly the same in both the nannofossil and foraminifer size fractions. Down-core measurements of COD in two box cores from the Ontong-Java Plateau demonstrate an apparent ongoing decay signal in the top 8-12 cm, and then a rise into glacial conditions. COD measured in different sub-cores from the same box core suggest that storage conditions of the cores affect the concentration of organic matter in the sediment, changing the COD by as much as 100%, although the down-core trend appears to be preserved independent of this effect. This result complicates the interpretation of studies I carried out in core tops and Last Glacial Maximum (LGM) samples from the Ontong-Java Plateau and eastern equatorial Pacific to investigate the effect

of water depth, distance from the equator, sediment age and calcium carbonate (CaCO_3) content. These results and measurements carried out in box and piston cores in the eastern equatorial Pacific indicate that CaCO_3 concentration does have an effect on COD and that increased CaCO_3 dissolution enhances COD if the CaCO_3 changes are large enough. The eastern equatorial Pacific cores provide no clear evidence that the existence of reduced phases in volcanic minerals present because of proximity to the East Pacific Rise affects COD. Measurements of COD in ODP cores from the Ontong-Java Plateau and eastern equatorial Pacific back to ~4 Ma (million years before present) show similar values to those for the last 400 kyr (thousand years), although the data do suggest that some diagenesis of organic matter may take place for depths greater than this age. The data for both cores display fluctuations of around a factor of 2 over the course of the records in both cores, but the sampling resolution is too low to allow a study of the role of Milankovitch forcing on the COD values.

4.1 Introduction

In this chapter I present a collection of studies in box and piston cores from the Ontong-Java Plateau and the eastern equatorial Pacific. The first study involves looking at the COD signal from different size fractions in a piston core from the Ontong-Java Plateau. I also examine COD trends through the Holocene in box cores from the Ontong-Java Plateau, including measurements in different sub-cores taken from the same box to investigate the possible effects of storage conditions. In subsequent sections, measurements in a suite of box and piston cores allow comparison of the COD signal at different water depths, distance from the equator, sediment age, and sediment calcium carbonate content in the Holocene and last

glacial, both on the Ontong-Java Plateau and in the eastern equatorial Pacific. The eastern equatorial Pacific cores also enable the study of the contribution of possible input of minerals from nearby volcanic sources associated with the East Pacific Rise, which is of significance when interpreting the COD time-series from ODP Hole 849, presented in Chapter 3. Finally, I present low-resolution combustion oxygen demand data from the Ontong-Java Plateau and the eastern equatorial Pacific going back to approximately 4 Ma. Figures 4.1a and b and Tables 4.1a and b show the locations of all the cores to be discussed in this chapter.

Figure 4.1a. Ontong-Java Plateau core sites (shown in black).

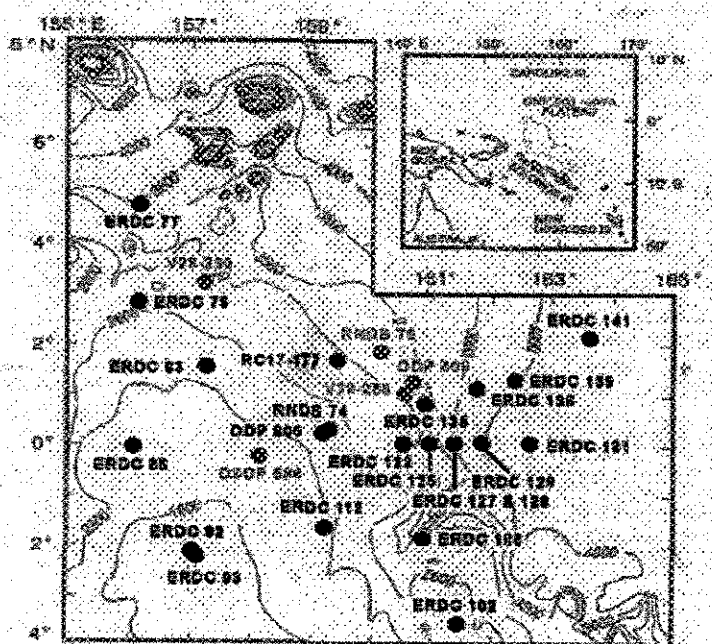
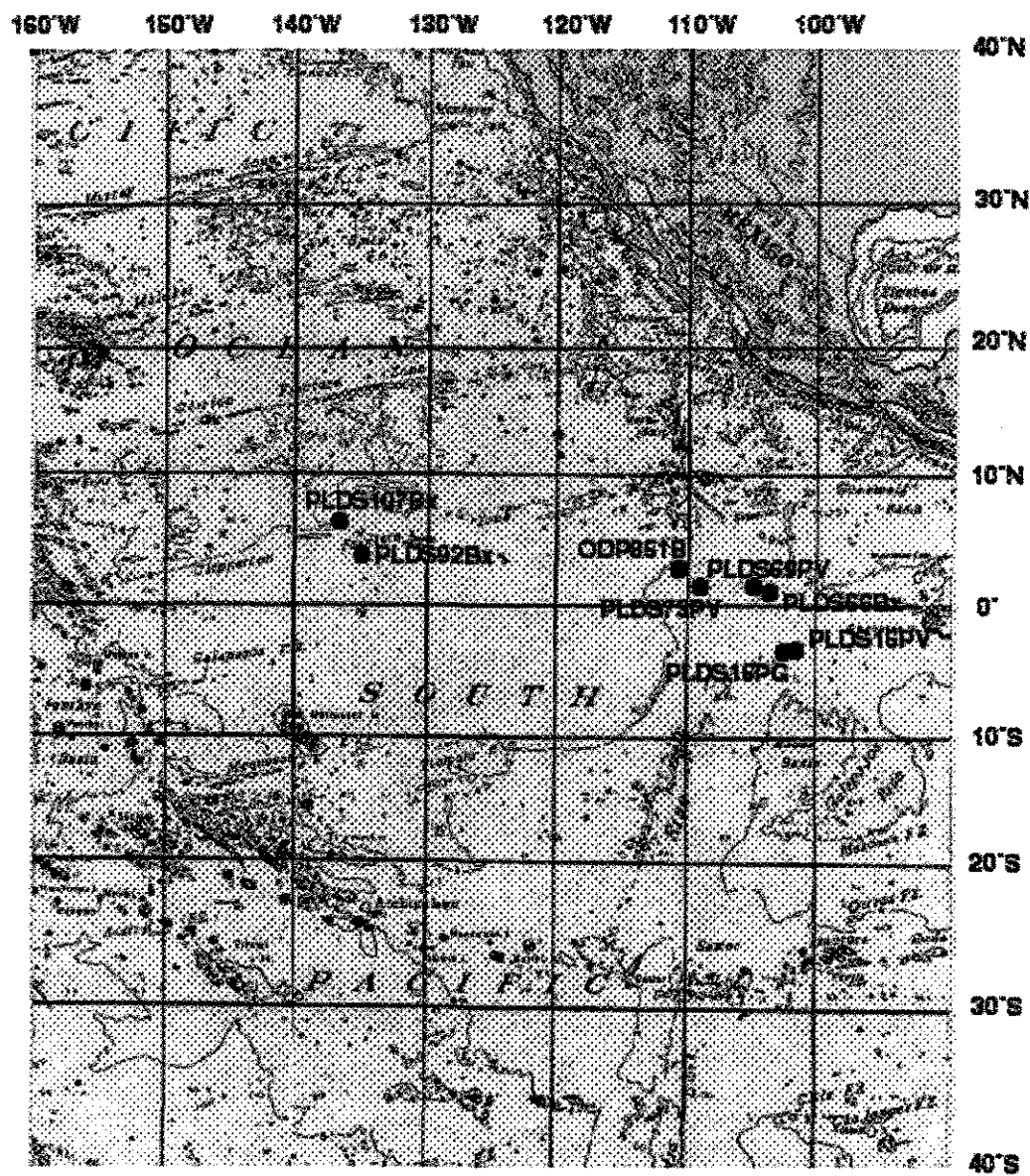


Figure 4.1b. Eastern equatorial Pacific core sites. (Adapted from the map "Topography of the Oceans," T.E. Chase, Scripps Institution of Oceanography, 1975, IMR Technical Report Series TR57).



4.2 Size fraction study in RC17-177 from the Ontong-Java Plateau

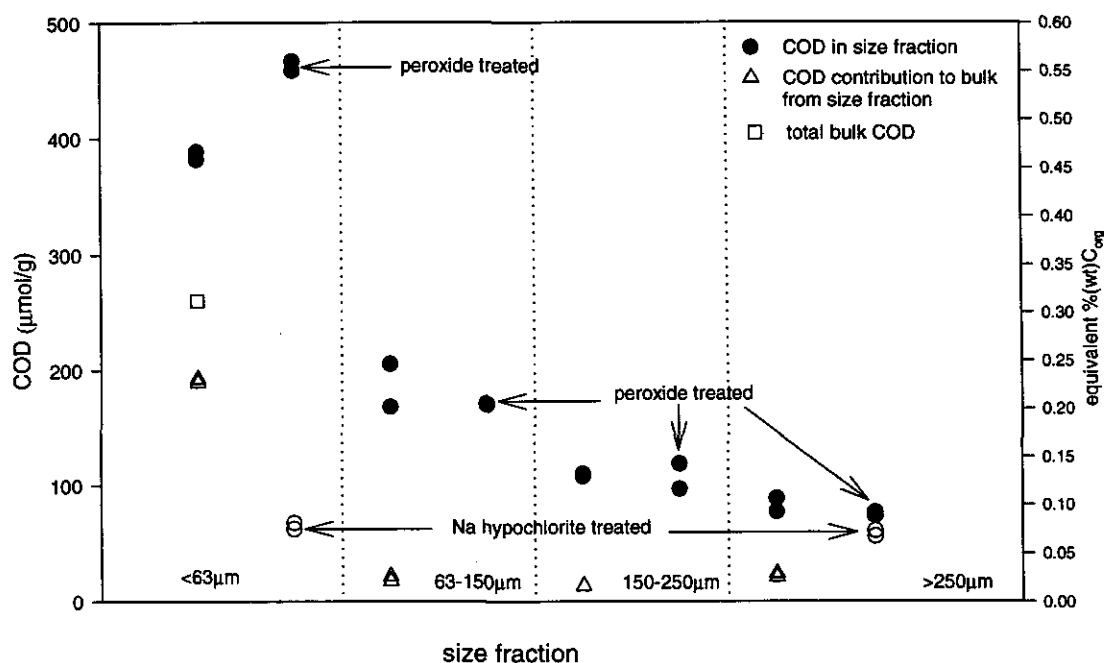
The original aim of this study was to investigate how much of the organic matter that is being detected by measurement of the COD is actually bound inside the foraminifer calcite lattice structure and how much inside the nannofossil calcite lattice. The work was undertaken in collaboration with Professor Nick Shackleton at the University of Cambridge, England, and the sediment samples were sent to SIO from his lab in Cambridge. The samples are from piston core RC17-177 (1°45.3'N, 159°26.9'W, 2600 m). It is of interest to detect how much “residual” organic matter is actually bound inside the shell structure itself since measurement of $\delta^{13}\text{C}$ in this organic material may be able to provide us with a more direct measurement of the carbon isotopic signal in marine organic matter, without influence from any terrestrial material (this provides a possible method to estimate changes in paleo- pCO_2 in surface waters). Measurements of $\delta^{13}\text{C}$ in bulk organic matter only reflect the relative proportions of terrestrial and marine organic matter. Another reason for discovering whether the organic matter is inside the calcite lattice or on the surface is to determine the role of carbonate dissolution on organic matter preservation and COD. If the organic matter is on the surface, one might predict that as dissolution proceeds the more refractory organic matter would just stick onto the particles that are left. If on the other hand the organic matter is bound inside the lattice, then as dissolution proceeds this organic matter may be oxidized and lost as it becomes newly exposed. In addition, sections of some cores from the Ontong-Java Plateau display precession in foraminifer abundance data (Nick Shackleton, pers. comm.), which is the dominant Milankovitch frequency of variation in RNDB 74P from the Ontong-Java Plateau and ODP 849 from the eastern equatorial Pacific, presented in Chapters 2 and 3. The RC17-177 study allowed me to examine how much of the COD signal is associated

either with the amount of organic matter “locked up” in the shell matrix of foraminifera or occurring as coating stuck onto foraminifer shells. Manganese and pyrite nodules are sometimes observed adhered to the surface of foraminifer shells (Stakes et al., 1999). If the signal from the foraminifer size fraction is very small, this provides further evidence to rule out a significant contribution from these sources.

Initially, COD was measured in sieved samples from RC17-177 from the interval 12-14 cm below sea floor (with an age of ~8 kyr). Some of these samples had been washed in Cambridge with 3% hydrogen peroxide solution to remove the organic matter coated on the outside of foraminifer and nannofossil shells, and other particulate organic material not bound inside shell matrices. The results (Figure 4.2, Table 4.2) appeared to indicate little difference between the untreated and peroxide-treated samples, implying that the peroxide treatment had not provided strong enough oxidizing conditions to remove any detectable amount of organic matter in the samples. Alternatively, this observation is also perhaps an indication that the small amount of organic matter that is preserved in these samples, from sites that have low sedimentation rates in well-oxygenated waters, is highly refractory, a fact also supported by data presented below in this chapter.

Figure 4.2 shows that the majority of the contribution to the COD signal comes from the <63 μm size fraction. (This is the size fraction that contains nannofossils, fragmented nannofossils and foraminifera, and various clay components). In fact, when the results are scaled to the contributions from each size fraction to the weight percentages of bulk sample, then ~75% of the COD signal is from the <63 μm size fraction. This indicates that the organic matter is *not* dominated by material associated either within or coating the shells of foraminifera.

Figure 4.2. COD in duplicate samples from different size fractions in untreated, hydrogen-peroxide treated and sodium hypochlorite-treated samples from a depth of 12-14 cmbsf (centimeters below sea floor) in the piston core RC17-177 (1°45.3'N, 159°26.9'W, 2600 m) from the Ontong-Java Plateau. The data appear in Table 4.2. The distribution of the different size fractions in the bulk sediment by weight is 49.6% in the <63 μm , 10.7% in the 63-150 μm , 12.5% in the 150-250 μm , and 27.2% in the >250 μm fraction. The triangles show the contribution of COD from each size fraction to the total COD of the bulk sediment (plotted as the square). The samples were provided by Nick Shackleton's lab at Cambridge University, U.K.



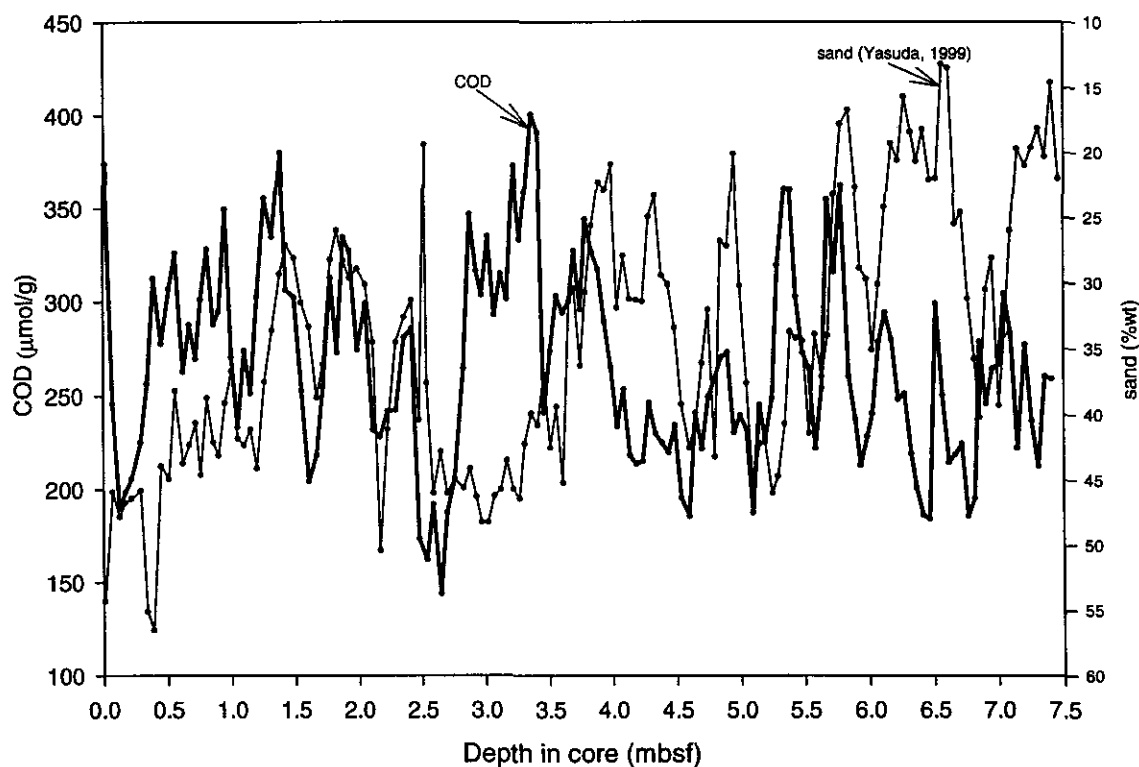
Samples from the same core were treated with a more aggressive oxidizing agent, sodium (Na) hypochlorite solution. The COD for samples from the <63 μm and >250 μm size fractions appear in Figure 4.2, and are 62.12 and 67.68 $\mu\text{mol O}_2/\text{g}$, and 55.95 and 60.59 $\mu\text{mol O}_2/\text{g}$ for duplicate samples for the <63 μm and >250 μm size fractions, respectively. This is equivalent to a concentration of <0.08% (wt) C_{org} .

The COD data from the untreated samples show that the signal is dominated by the <63 μm size fraction and indicate that the organic matter is either (i) bound within the nannofossil shell matrix, or (ii) associated, in a less tightly bound form, with nannofossils, or

(iii) with nannofossil and foraminifer fragments, or (iv) as non-foraminifer or non-nannofossil particulate organic matter. The similar low values for both the $<63 \mu\text{m}$ and $>250 \mu\text{m}$ size fractions treated with Na hypochlorite solution show that very little of the organic matter is bound up within the nannofossil or foraminifer shell matrix ($<17\%$ of the COD for the nannofossil size fraction). The COD results in Figure 4.2 are consistent with previous estimates that the amount of organic carbon bound within fossil foraminifer shells varies from 0.04 to 0.10% (wt) (King and Hare, 1972; L. D. Stott, unpublished data, 1992).

If COD is dominated by nannofossils, this provides support for COD being driven by the productivity in the overlying surface waters, since coccolithophores dominate the material raining down through the water column from the surface. However, the dominance of the COD signal from the $<63 \mu\text{m}$ size fraction may also indicate that the organic matter is associated with fine particles, clays and shell fragments. The larger surface-area of these smaller particles may enhance preservation of organic matter (Suess, 1973; Hedges and Keil, 1995) and this could be a possible explanation for the small size fraction dominating the COD signal. However, this would still not disqualify the hypothesis that COD is being driven by productivity, since it would be very hard to isolate the possible contribution of enhanced preservation. Figure 4.3 shows COD and sand ($>63 \mu\text{m}$ size fraction) concentration in RNDB 74P from the Ontong-Java Plateau (this core is presented in Chapters 2 and 3). The data do suggest that there may be some correlation between a lower weight percentage of sand (i.e. more fine fraction) and higher COD, although they also indicate that COD is being influenced by additional factors.

Figure 4.3. COD in RNDB 74P (0°20'N, 159°22'E, 2547m) from the Ontong-Java Plateau plotted against sand (>63 μm fraction) concentration (Yasuda et al, 1999). The data appear in Table 3.1. Note that the sand axis is in descending magnitude.



4.3 Box core studies on the Ontong-Java Plateau

4.3.1 ERDC 112Bx

Figure 4.4 and Table 4.3 show COD in the box core ERDC 112Bx (1°37'S, 159°14'E, 2169 m). The plot shows data from two different sub-cores (each of diameter 9 cm) from the same box core (which was 50 cm by 50 cm in cross-section) and includes data from measurements made in October 1995 in sub-core Bx1 and also May 1998 in sub-cores Bx's 1, 37 and 47, and December 1997 and May 1998 in Bx5. The ERDC cores were retrieved on the EURYDICE Expedition in 1974-5 (Glockhoff, 1979; Berger and Killingley, 1982). The

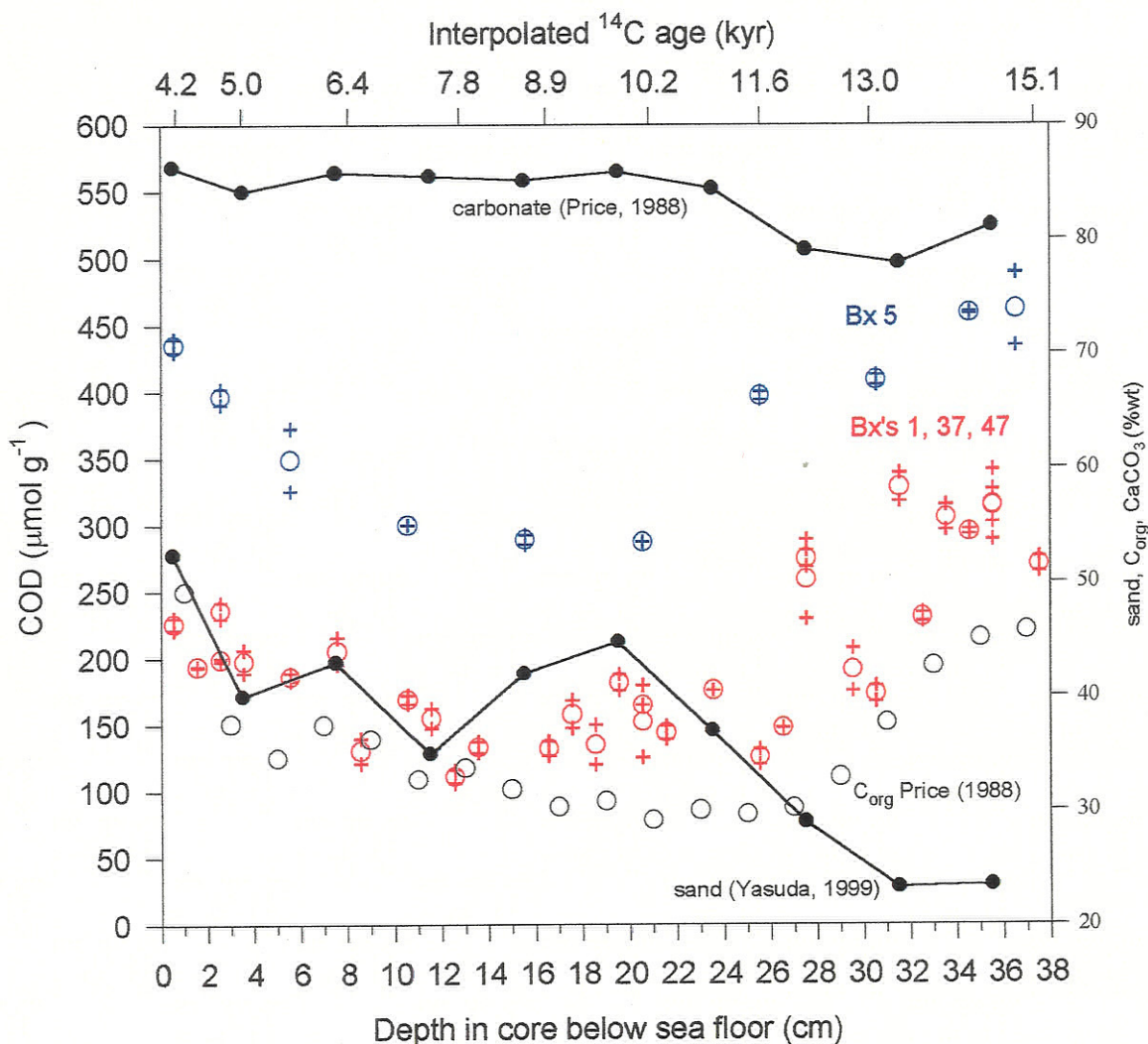


Figure 4.4. COD in duplicate samples from different sub-cores from box core ERDC 112Bx (1°37.5'S, 159°14.1'E, 2168 m) from the Ontong-Java Plateau. Calcium carbonate (Price, 1988) and sand (>63 μm fraction) concentrations (Yasuda, 1999) are also displayed, along with organic carbon concentrations determined by measuring the CO₂ evolved after boiling acid treatment of carbonate-free sediment (Price, 1988). Ages are extrapolated from ¹⁴C data in Berger and Killingley (1982). The data appear in Table 4.3.

samples measured had been subjected to different storage conditions, both with respect to how they had been stored in the core locker at Scripps Institution of Oceanography (SIO) Geological Collections since return from the cruise, and also how they had been stored, and for how long, after removal from the box core.

The trend observed in sub-cores ERDC 112Bx's 1, 37 and 47 is discussed in Chapter 2 (page 19).

The values observed for all the sub-cores appear to be independent of the storage conditions that the samples had been subjected to once they had been removed from the box core in the core locker. Some of the samples, once taken from the box core, had been freeze-dried and then stored at room temperature in unsealed plastic sample bags, some of them for at least 3 years. Some of the samples had been refrigerated (for a maximum of 3 months, often only for a few days) directly after sampling from the core and removal from the core locker. All the samples were, following typical procedure for COD measurements, oven-dried at 45-50°C over 1-2 days, and the COD measured in the dry sample immediately after removal from the oven. The COD data show that the storage conditions *after* sampling from the core and removal from the core locker do not appear to have a significant effect on COD value, nor the date upon which the samples were measured (for the samples from Bx's 1, 37 and 47 that were measured in October 1995, the COD instrument was calibrated using benzoic acid, instead of KHP solution (Appendix A)). However, the data sets from the two different sets of cores (1, 37, 47, and 5) in ERDC 112Bx display a fairly constant offset, which is most likely a result of the conditions of the different box cores in the core locker. COD values in Bx5 are roughly a factor of 2 higher than in Bx's 1, 37 and 47. The samples from all the sub-cores were analyzed randomly, on different days and even different years (Table 4.3), which rules out a systematic calibration effect. Bx5 was visibly more dried out than Bx's 1, 37 and 47 and this may have been the case for several years. The cause of the observed offset is unclear. Some of the cores have been re-moistened during their storage by spraying with distilled water, and this makes it very hard to know how dry the sub-cores have

been in the past, and for how long they were dry. It is also likely that the time that has elapsed since the sub-cores were split in half (lengthways) may affect the extent of dissolution of carbonate and oxidation of organic matter through changes in moistness and direct exposure to air. Another factor to be considered, especially in such old cores, is mold. However, during sampling, every effort was taken to avoid any contact with visibly mold-covered areas.

The measurements in ERDC 112Bx demonstrate that when such carbonate-rich samples are taken from cores for measurement of the organic matter content, the storage conditions can have a significant effect on the total organic carbon concentration and COD. However, it is unclear which factors relating to the storage conditions, and to which extent, affect COD. Ideally, samples should be frozen and/or dried as soon as possible after retrieval from the sea floor. However, although I observed offsets between different sub-cores stored under different conditions, it does appear that the main down-core trends have been preserved in the cores (Figure 4.4). This observation supports the validity of COD trends observed in deep-sea sediment cores, although raises some questions as to the pertinence of comparing the absolute values of COD between different cores, unless they have been stored under very similar conditions for similar lengths of time.

The COD data from ERDC 112Bx display a decay in COD from core top to a depth of around 8-12 cm (roughly to an age of 5-6.5 kya (thousand years before present)). This depth corresponds to approximately the depth of the layer mixed by bioturbation. This pattern is also displayed by ERDC 128Bx, presented below in Section 4.3.2. A possible explanation for this observation is that there could still have been ongoing diagenesis of the organic matter taking place to this depth and the mixing by bioturbation did not destroy the decay trend. A

preferential concentration of C_{org} in the upper 2 cm or so of sediment cores from the equatorial Pacific and then a decay with increasing depth has also been described by Jahnke et al. (1986), and Prahl et al. (1989) observed a similar core-top maximum and then a decay to depths corresponding to ~4 kya in cores from the central equatorial Pacific. Jahnke et al. (1986) suggest that the bioturbating fauna preferentially strip organic matter from the deeper part of the sediment mixed layer and concentrate it in the upper part. Alternatively, the pattern could also reflect an actual increase in the export of organic matter from the surface waters from the mid-Holocene to present. This observed decay trend should, therefore, be considered when looking at the top part of other records. It may be responsible for the particularly high value relative to the rest of the core recorded at the top of the Ontong-Java piston core RNDB 74P (Chapters 2 and 3). I was originally hoping to be able to calibrate COD to organic carbon accumulation rates from sediment trap data using core-top COD values, but this occurrence of higher values relative to lower down in the core makes this difficult. I observed a similar decrease in COD across the top 10 cm in three cores from sites close to the ERDC cores sent to me by Dan McCorkle from the Woods Hole Oceanographic Institution (WHOI). These cores are from water depths ranging from 1773 m to 4330 m and were retrieved in 1997, much later than the ERDC cores, and kept frozen since then so are less likely to have been affected by storage conditions. Below 8-12 cm in ERDC 112Bx, COD appears to level off, with some smaller oscillations, and then rises to around double this mid-Holocene value at the bottom of the core, which lies in the last glacial transition (~15 ka), thus showing a rise in the organic matter content of the sediment under globally colder conditions, which is a feature present in nearly all the deep-sea cores presented in this dissertation.

Figure 4.4 also shows the calcium carbonate (CaCO_3) concentrations in ERDC 112Bx (for Cores 1, 37 and 47) (Price, 1988). CaCO_3 displays only small variations, and the site lies above the lysocline at ~3300 m, but there is no clear indication of any correlation between % (wt) CaCO_3 and % (wt) C_{org} in this core and thus no evidence for an enhancement of COD by dissolution of CaCO_3 . The lowest values of % (wt) CaCO_3 coincide also with low values of COD and a rise in CaCO_3 at the bottom of the core is coincident with a rise in COD. It is also possible that the CaCO_3 concentration does affect the down-core COD trend and that the increase in CaCO_3 % into the deglacial to some extent offsets the increase in COD, and the observed increase would actually be larger under constant CaCO_3 %. The data presented in this chapter are insufficient to determine if this is the case or not. The role of storage conditions on absolute values of COD, discussed above, complicates any interpretation of the role of differences in CaCO_3 concentration on COD in different cores. The sand concentration (% (wt) of $>63 \mu\text{m}$ size fraction) displayed in Figure 4.4 suggests some correlation between lower sand % and higher COD, as discussed above in Section 4.2. Price (1988) also measured the C_{org} concentration in ERDC 112Bx (Bx's 1, 37 and 47) by measurement of the CO_2 evolved during reaction of carbonate-free sediment with boiling sulfuric acid and potassium dichromate, and her results are shown for comparison with the COD values converted into equivalent % (wt) C_{org} (calculated assuming only C_{org} consumes the O_2 and with an $\text{O}_2:\text{C}$ ratio of 1 to 1) in Figure 4.4. The values from the two methods are similar, although the Price (1988) numbers are generally slightly lower than the COD values. Since the actual C_{org} contents are probably smaller than the numbers I calculated from COD because of the presence of reduced nitrogen in the organic matter and because carbon is likely to be in a more reduced oxidation state than $\text{C}(0)$, the COD values and those of Price

(1988) are in fairly good agreement, although the COD data appear to indicate a steeper rise towards the bottom of the core going into the glacial transition. (No information is available about how the samples were stored during the time between removal from the core locker and analysis).

4.3.2 ERDC 128Bx

Figure 4.5 and Table 4.4 display COD and % (wt) CaCO_3 in ERDC 128Bx2 (0°00'S, 161°25'E, 3732m). The samples are all from the same sub-core. The base of this core is older than ERDC112Bx, the bottom sample having an age of ~20 kyr. This core, like ERDC 112Bx, also shows a decrease in COD from the top to a depth of 8-14 cm, possibly reflecting ongoing diagenesis, and then more than a doubling from the low value of 254.73 $\mu\text{mol O}_2/\text{g}$ at 15.5 cm to 591.21 $\mu\text{mol O}_2/\text{g}$ in the bottom sample at 41.5 cm. ERDC 128Bx is closer to the equator and over 1500 m deeper than ERDC 112Bx so is below the lysocline at ~3300m. COD in the core-top sample in ERDC 128Bx2 is within the range of that in ERDC 112Bx5, and the low value is slightly lower than in ERDC 112Bx5. All values of COD in ERDC 128Bx2 are higher than ERDC 112Bx's 1, 37, 47 at corresponding ages. The highest value in ERDC 128Bx2, 591.21 $\mu\text{mol O}_2/\text{g}$, is almost 30% higher than the highest value at the bottom of ERDC 112Bx Core 5, 461.56 $\mu\text{mol O}_2/\text{g}$. This may reflect higher productivity on the equator compared to 1°37'S, but the bottom of the ERDC 128Bx core also goes beyond the deglacial and coincides with the Last Glacial Maximum (LGM). It is also possible that greater CaCO_3 dissolution in ERDC 128Bx2 enhances COD. The differences between the 2 cores may also be due to differences in the conditions that they have been stored in at the SIO Geological Collections, as discussed above in Section 4.3.1. Significantly, all 3 main

cores, ERDC 128Bx2, ERDC 112Bx5 and ERDC 112Bx's 1, 37, 47, display the same down-core trends: A decrease over the top 8-12 cm to a low value (this trend is strongest in ERDC128Bx2), perhaps reflecting continuing diagenesis of organic matter, a leveling off

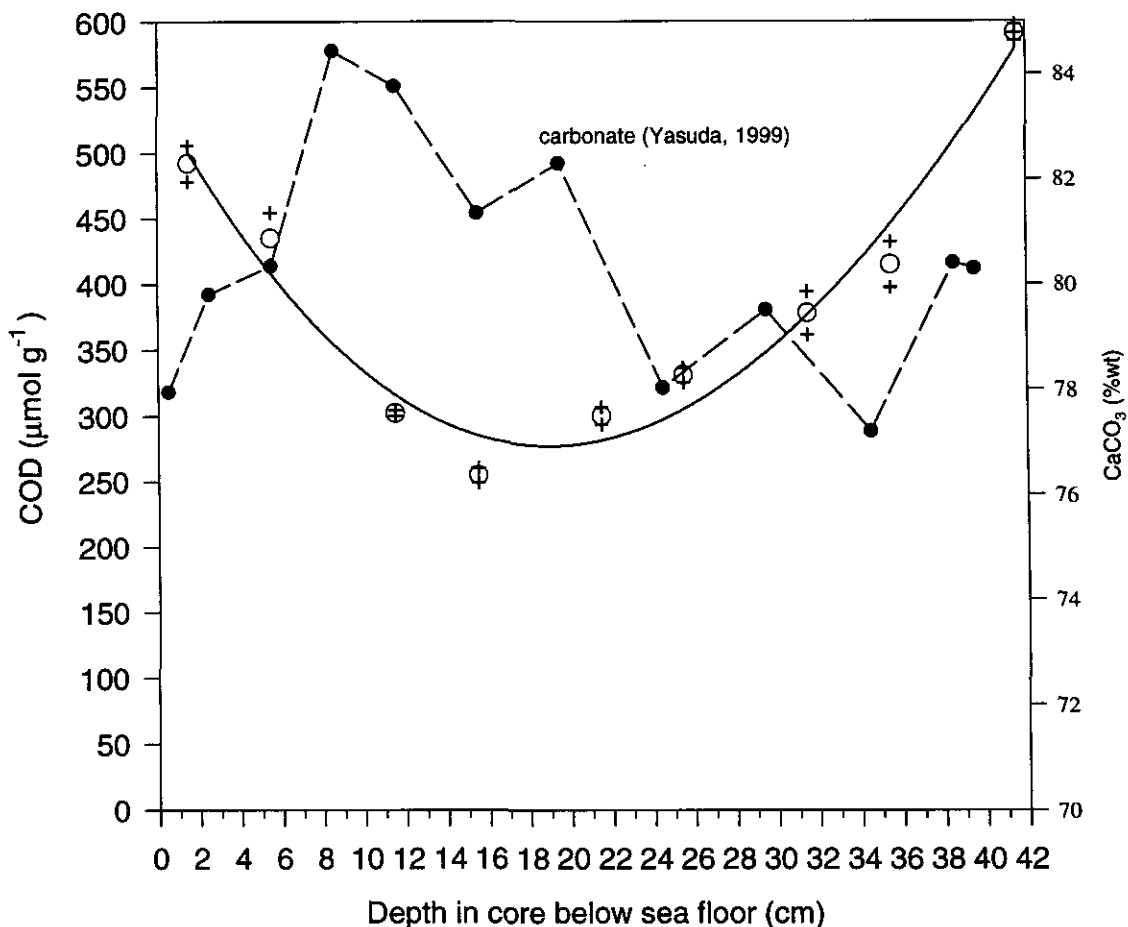


Figure 4.5. COD in duplicate samples from sub-core Bx2 from box core ERDC 128Bx (0°00.3'S 161°25.6'E, 3732 m) from the Ontong-Java Plateau. A polynomial line fit (solid line) is drawn for the averages of the duplicates. Calcium carbonate concentrations are displayed as the dashed line (Yasuda, 1999). The bottom of the core has an approximate age of 20 kyr. The data appear in Table 4.4.

and then a rise to at least double this low value crossing into glacial conditions. All cores, which display only small variation in CaCO₃ concentration, indicate that the CaCO₃ concentration does not have a significant effect on the observed COD trend at these sites.

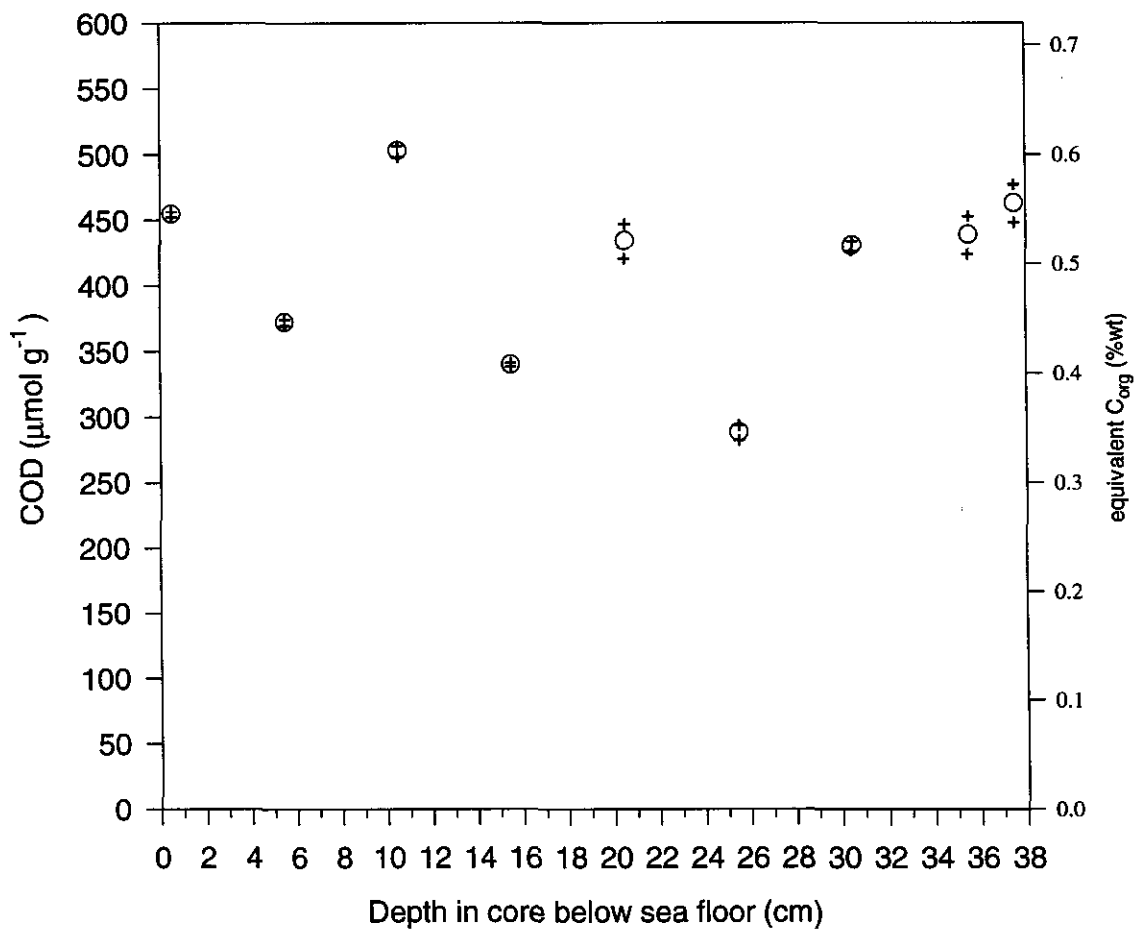
These observations add support to the validity of measuring and comparing the down-core trends in COD in different carbonate-rich deep-sea sediment cores, and are consistent with trends for the past 26 kyr observed in total organic carbon (TOC) by Prahl et al. (1989) in cores from the central equatorial Pacific.

4.4 Box core studies in the eastern equatorial Pacific

4.4.1 PLDS 66Bx

Figure 4.6 shows COD in box core PLDS 66Bx (0°56.6'N, 104°06.1'W, 3496m). The PLDS cores were retrieved on the PLEIADES Expedition in 1976 (Glockhoff 1982; Berger and Killingley, 1982) and since then, as with the ERDC cores, have been stored at the SIO Geological Collections. All samples were taken from the same sub-core Bx1. Although the surface waters above this site in the modern-day support significantly higher production than those above the Ontong-Java Plateau, this feature does not appear to be reflected by greater COD in PLDS relative to the ERDC cores. One theory to explain the lower values in the east is that COD could be a measure of the residual highly refractory organic matter left in the sediment, material that is not eaten or attacked by bacteria. Although it is likely that the amount of this refractory material is correlated to the organic matter rain rate from the surface waters (a fact supported by the increases in COD generally observed in glacial periods in agreement with other paleoproductivity proxies), it is possible that the ratio of rain rate to preserved refractory organic matter concentration in the sediment is not constant over different locations. However, the effects of storage conditions of the cores on the absolute values of COD complicates any comparison of absolute COD between different cores. The down-core decay in the COD signal from the core-top to about 12 cm is not as clear in this

Figure 4.6. COD in duplicate samples from sub-core Bx 1 from PLDS 66Bx (0°56.6'N, 104°06.1'W, 3496m) from the eastern equatorial Pacific. The bottom of the core has an approximate age of 12 kyr.



core as in ERDC 112Bx and ERDC 128Bx. This may be due to insufficient data points in ERDC 128 Bx. The bottom of the core has an age of ~12 kyr, so we have no information about the behavior of COD into the last glacial period at this site.

4.5 A comparison of COD in core-top and core-bottom samples from ERDC (Ontong-Java Plateau) box cores

Figure 4.1a and Table 4.1a show the core locations and water depths for the Ontong-Java Plateau, and Table 4.5 contains COD data for all the cores. I measured COD in a suite of ERDC box cores and one ERDC piston core, taking samples from at or near the core top and from a depth as close as possible to the LGM (estimated from interpolated radiocarbon ages or $\delta^{18}\text{O}$ curves), or the bottom of the core if this was younger than the LGM. Initially, I had wished to compare the COD values in the Holocene and LGM at the different sites, but the results presented above from ERDC 112Bx and ERDC 128Bx show that the core-top values represent organic matter that may still be undergoing oxidation. It is not until depths of below around 8-12 cm that there is no apparent further decay trend. (This is the observation I have made in the ERDC cores, PLDS cores presented below in Section 4.6, and in the cores presented in Chapters 2 and 3). More importantly, differences between COD in different sub-cores similar to those observed in ERDC 112Bx presented above in Section 4.3.1 show that there are problems with comparing absolute values between different cores, presumably because of the different conditions under which they have been stored. Because of these reasons, it is also very difficult to interpret the observed differences in COD between the samples of similar age from cores from the different sites, although I attempt a comparison below.

Figure 4.7 presents the core-top data for the ERDC cores plotted against water depth. Figure 4.7a displays COD as concentrations and Figure 4.7b COD as accumulation rates. I

Figure 4.7a. COD plotted against water depth in samples near the core-top from box cores from the Ontong-Java Plateau. COD is given as a concentration (as is the usual convention). Lines join samples from different sub-cores from the same box core. The lysocline depth is at around 3300-3500 m. The data appear in Table 4.5.

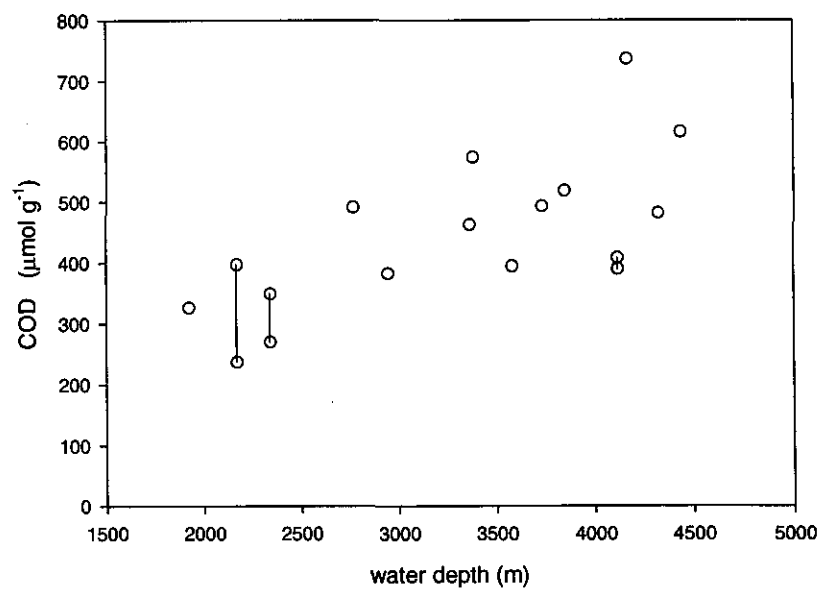


Figure 4.7b. As for Figure 4.7a, except that COD is given as an accumulation rate. Sedimentation rates are those used in Herguera and Berger (1994).

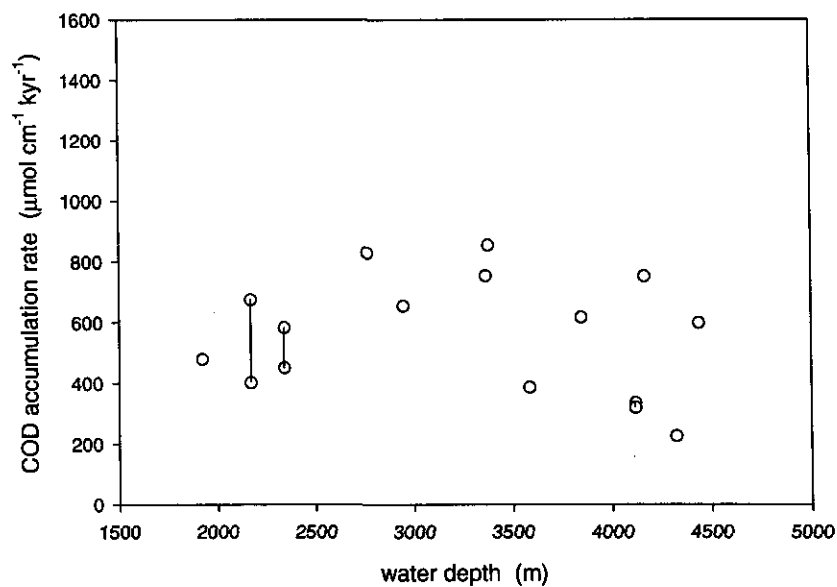


Figure 4.7c. As for Figure 4.7a, except samples are from depths in the core corresponding approximately to an age in the Last Glacial Maximum (estimated from interpolated radiocarbon ages (Berger and Killingley, 1982) or $\delta^{18}\text{O}$ curves (Yasuda, 1999)).

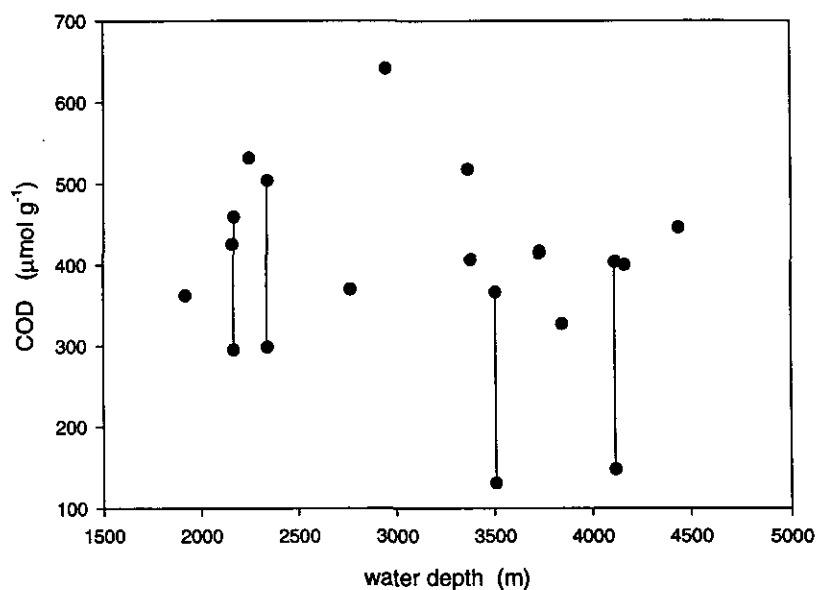
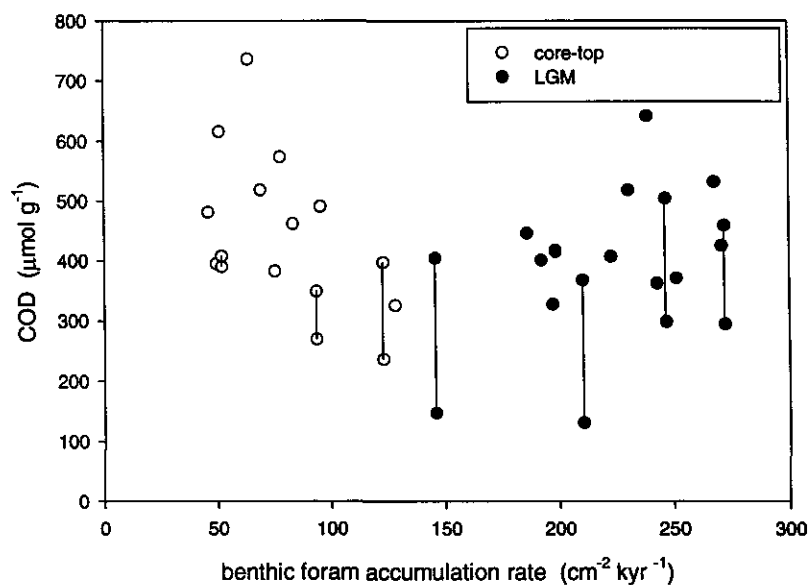


Figure 4.8. COD plotted against benthic foraminifer accumulation rates (Herguera and Berger, 1994) in samples near the core-top (open circles) and from depths corresponding approximately to an age in the Last Glacial Maximum (estimated from interpolated radiocarbon ages (Berger and Killingley, 1982) or $\delta^{18}\text{O}$ curves (Yasuda, 1999)) (solid circles) from box cores from the Ontong-Java Plateau. COD is given as a concentration (as is the usual convention). Lines join samples from different sub-cores from the same box core. The data appear in Table 4.5.



have divided the data into similar sample depths in the core to aid comparison of data that are at similar points on the decay curve discussed above in Section 4.3.1, and have not plotted values for samples from below a depth of 2 cm. The bottom water dissolved oxygen concentrations show no significant variation over the depth ranges of the cores (Geochemical Ocean Sections Study (GEOSECS) data) and therefore are not expected to have any measurable effect on the amount of organic matter that is preserved in the sediment. The data appear to indicate an increase in COD concentration with increasing water depth. This might be explained by the fact that concentration of CaCO_3 goes down with increasing water depth, thus COD concentrations are enhanced with reduced CaCO_3 content. Evidence for such an effect is provided by the accumulation rates of COD, which are fairly constant with increasing water depth (and decreasing total accumulation rate). This pattern is less clear below the lysocline, which is at a depth of around 3300-3500 m. However, Figure 4.7c shows the corresponding data for LGM samples, which appear to show no clear pattern between COD and water depth. Accumulation rates of benthic foraminifera (BFAR) have been shown to reflect the amount of organic carbon exported from the surface waters (Herguera and Berger, 1991; Herguera, 1992), and for these cores the BFAR's actually show a *decrease* with increase in water depth. I speculate that one might not necessarily expect a correlation between BFAR and COD, since COD may be a measurement of how much highly refractory organic matter remains in the sediment, that is not eaten by anything or attacked by bacteria. This may likely still be correlated to the rain rate of organic matter from the surface waters that reaches the sediment, but not as directly as this organic matter export would be expected to be related to BFAR. With respect to the relationship between COD and BFAR, the data from the ERDC cores are however paradoxical, since Figure 4.8 suggests that higher COD

concentration may correspond to higher BFAR in the LGM samples. There is no apparent correlation for the core-top samples, perhaps a result of ongoing diagenesis or inhomogeneous mixing in the top part of the cores, discussed above in Section 4.3.1. There does not appear to be any correlation between COD and distance from the equator, not even for cores from very similar water depths, although there is perhaps some evidence for higher COD in cores on the equator at greater water depth in LGM samples. This lack of correlation is perhaps surprising, given the significant increase in export of organic matter from surface waters above sites on and closer to the equator, although the lack of correlation may also be explained by the decay trend observed in the top part of the cores and/or differences produced by different storage conditions, as discussed above in Section 4.3.1.

4.6 COD in PLDS (eastern/central equatorial Pacific) box and piston cores

I measured COD at 5 or 10 cm intervals in six PLDS cores (Glockhoff 1982; Berger and Killingley, 1982), covering from the core tops to ages ranging from ~30-60 kyr. The site locations are given in Figure 4.1b and Table 4.1b. This study enabled a comparison of the core top-Holocene-glacial trends in COD at different sites in the open-ocean eastern equatorial Pacific, at different water depths and distances from the equator, and with varying clay, volcanic mineral, and CaCO₃ content. COD is plotted with $\delta^{18}\text{O}$ and CaCO₃ content (where available) for the six cores in Figure 4.9. PLDS 73PV, Figure 4.9a, from 1°N does indicate an increase, an approximate doubling, of COD in glacial conditions relative to the Holocene, an observation similar to the Ontong-Java Plateau cores ERDC 112Bx and ERDC 128Bx presented in Section 4.3 above, and the piston core records from RNDB 74P and ODP

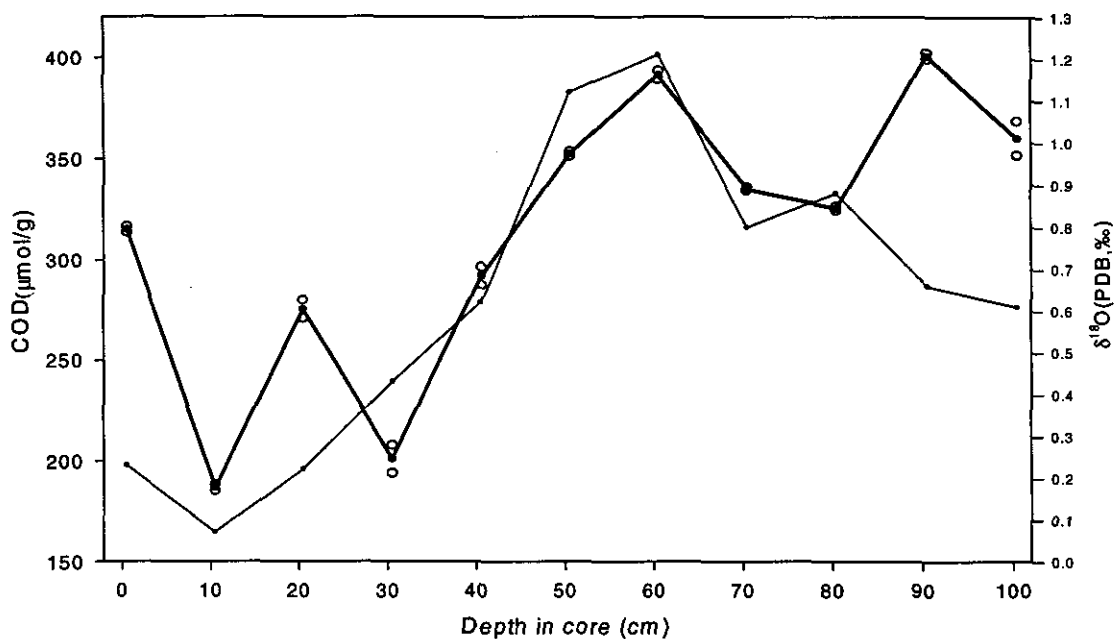


Figure 4.9a. COD (heavy line) in duplicate samples from the piston core PLDS 73PV ($1^{\circ}00.4'N$, $109^{\circ}18.9'W$, 3672 m) from the eastern equatorial Pacific. $\delta^{18}O$ in *N. dutertrei* (Herguera, 1999) is also plotted as an indication of age. $\delta^{18}O$ rises into the last glacial period.

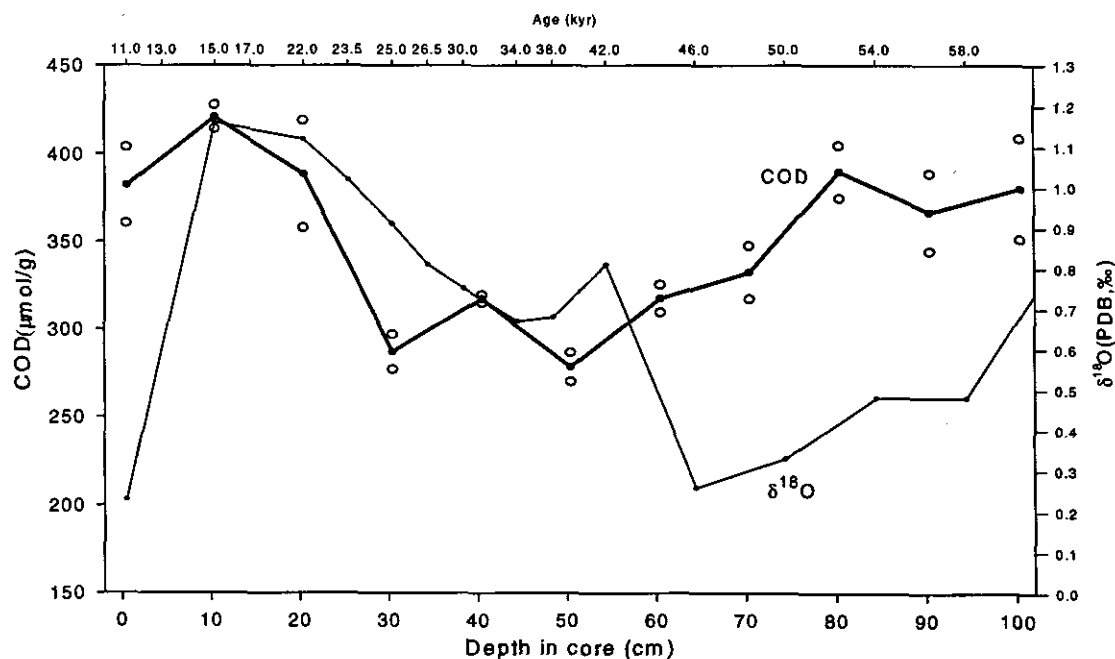


Figure 4.9b. COD (heavy line) in duplicate samples from the piston core PLDS 69PV ($1^{\circ}02.1'N$, $105^{\circ}35.0'W$, 3527 m) from the eastern equatorial Pacific. $\delta^{18}O$ in *N. dutertrei* is also plotted. Ages are from Herguera (1999).

849 in Chapter 3. There is however a data-point at 20-21 cm of higher COD than would be expected from this trend of lower Holocene COD increasing across the transition into the last glacial. PLDS 69PV in Figure 4.9b from a similar latitude and water depth has the Holocene missing, but also displays very similar glacial values of COD to PLDS 73PV. (In contrast, benthic foraminifer accumulation rates (BFAR's) are very similar in the Holocene and last glacial period for both PLDS 69PV and PLDS 73PV (Herguera, 1999), although one would not necessarily expect BFAR and COD to correlate, as discussed above in Section 4.5). In contrast, PLDS 16PV and 15PG from 3°19'S in Figures 4.9c and d do not appear to indicate any elevated COD in the last glacial period relative to the Holocene. (For these 2 cores, BFAR's do in fact show an increase in the last glacial (Herguera, 1999)). I do not have data from enough cores to demonstrate whether this is a true effect of latitude and sites this far south of the equator really do not show any clear increase in COD across the Holocene-LGM transition.

There is a COD spike in PLDS 15PG at a depth of 20 cm. It is unclear as to the cause of this spike, and it is not present at the same depth and similar age in neighboring PLDS 16PV. *The spike could be from the presence of minerals in volcanic clays from the East Pacific Rise, although when samples were analyzed with a Scanning Electron Microscope (SEM) for elemental abundances no evidence was found for more than trace amounts of minerals that could have produced such a spike.* The poor reproducibility of duplicate samples in this core at 20 cm and also at 30 cm may also be due to volcanic minerals. Notes taken during retrieval of the cores (Glockhoff, 1982) describe an FeOx layer between 18-33 cm, which may also coincide with reduced Fe and other reduced minerals that will undergo oxidation

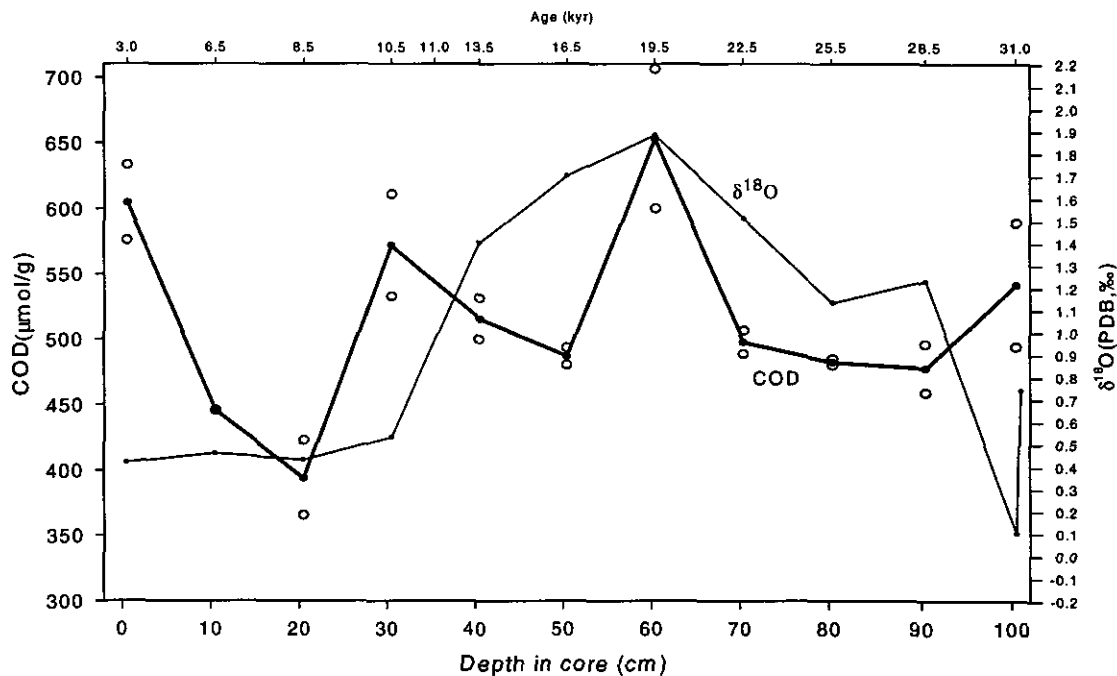


Figure 4.9c. COD (heavy line) in duplicate samples from the piston core PLDS 16PV (3°19.4'S, 102°03.5'W, 3251 m) from the eastern equatorial Pacific. $\delta^{18}\text{O}$ in *N. dutertrei* is also plotted. Ages are from Herguera (1999).

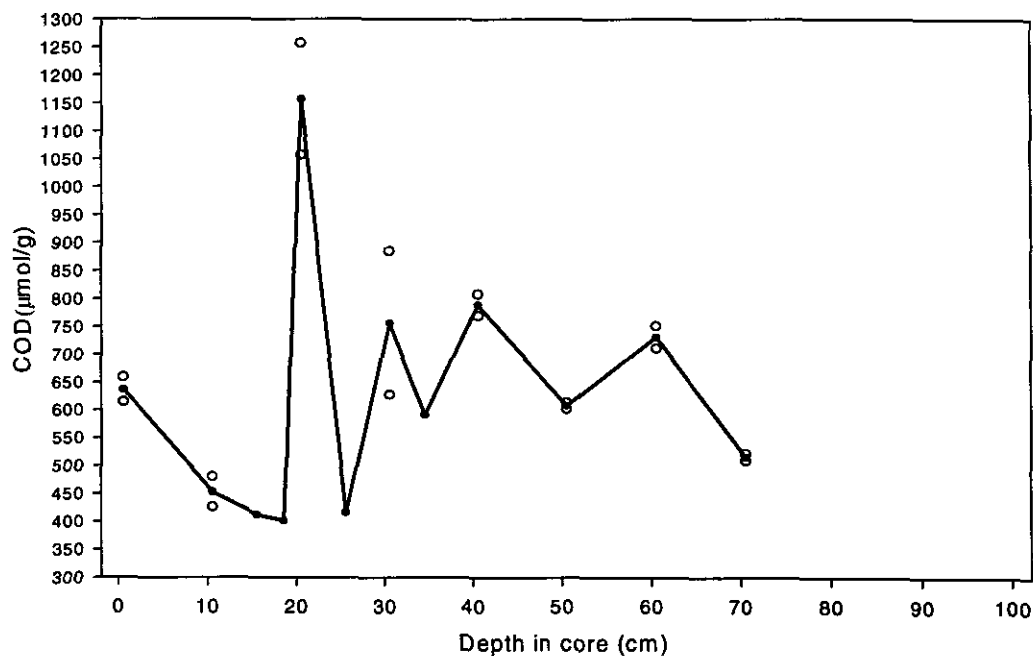


Figure 4.9d. COD (heavy line) in duplicate samples from the piston core PLDS 15PG (3°20.9'S, 102°15.1'W, 3222 m) from the eastern equatorial Pacific.

in the COD instrument. Reproducibility in duplicate samples is also poorer in many of the samples from PLDS 16PV and PLDS 69PV. Again, there was no indication of higher than background abundances of reduced minerals for these points when analyzed with an SEM.

Although at least the top part of the Holocene is missing in the six PLDS cores (and all of it in PLDS 69PV), a decay trend in COD similar to that observed in the ERDC cores presented above is present to a depth of around 10 cm. PLDS 92Bx and PLDS 107Bx in Figures 4.9e and f are from further west and north of the equator at water depths below 4500m. Since they lie close to the Clipperton Fracture Zone, the possible effects of the presence of volcanic minerals could be investigated. However, I did not observe any COD spikes in either core, and the reproducibility of duplicate samples was generally good, although poorer for some of the samples from PLDS 107Bx. At such deep sites, the preservation of CaCO_3 is poorer. The deeper site, PLDS 107Bx, which is also more than 6°N of the equator has very low CaCO_3 concentrations. The effect of such low CaCO_3 can clearly be seen in the COD concentrations relative to PLDS 92Bx and the other cores presented in this chapter. COD is as high as over $850 \mu\text{molO}_2/\text{g}$, at the base of PLDS 107Bx, which is more than double the high core-top value in PLDS 92Bx. The high COD value in PLDS 107Bx corresponds to $<5\%$ (wt) CaCO_3 . In both cores, there is some correlation between CaCO_3 concentration and COD, with COD generally increasing down-core as CaCO_3 decreases. Thus, it appears that as well as influencing absolute values of COD between different cores, CaCO_3 dissolution can affect the down-core COD trend, although the effects in the other cores discussed in this chapter are not large enough to cancel out or reverse the COD trends. Since in general CaCO_3 preservation improves in the last glacial, in cores where a significant rise in COD is observed the CaCO_3 concentrations may actually be reducing the

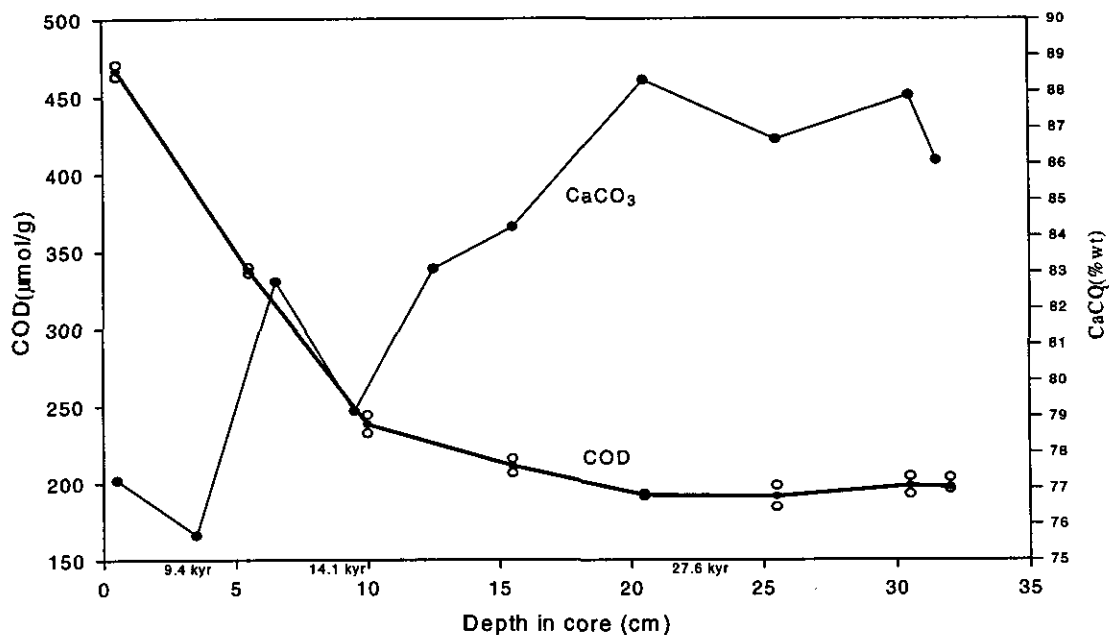


Figure 4.9e. COD (heavy line) in duplicate samples from the box core PLDS 92Bx ($3^{\circ}57.2'N$, $135^{\circ}58.7'W$, 4515 m) from the central equatorial Pacific plotted with calcium carbonate concentrations (W. Berger, pers. comm.). Ages are ^{14}C ages from Berger and Killingley (1982).

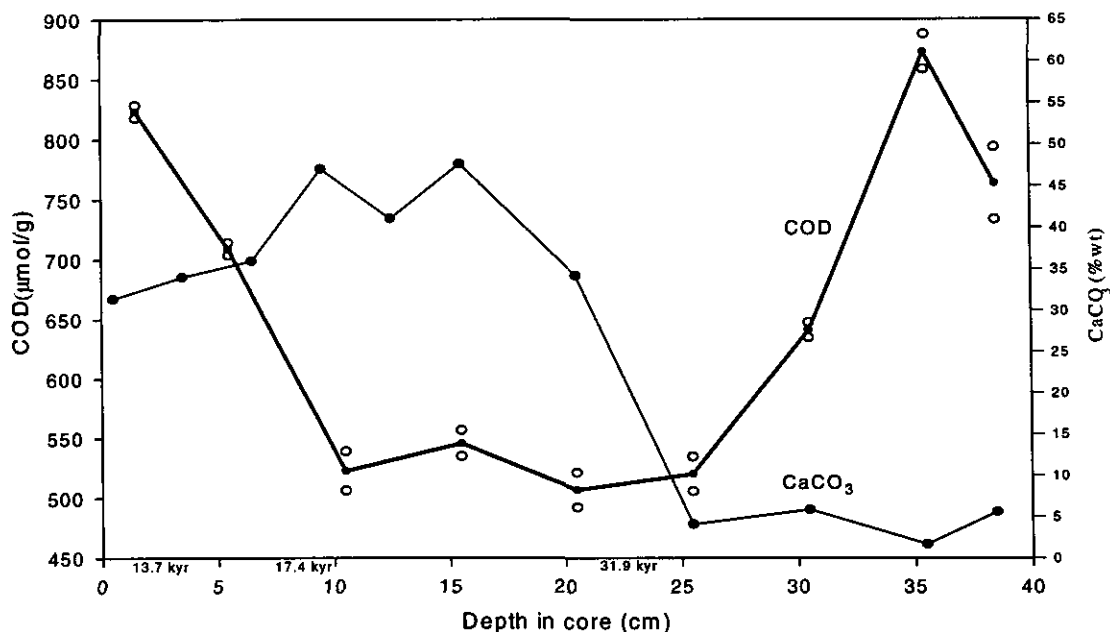


Figure 4.9f. COD (heavy line) in duplicate samples from the box core PLDS 107Bx ($6^{\circ}09.4'N$, $138^{\circ}16.6'W$, 4849 m) from the central equatorial Pacific plotted with calcium carbonate concentrations (W. Berger, pers. comm.). Ages are ^{14}C ages from Berger and Killingley (1982).

measured COD increase relative to the actual changes that occurred in the amount of organic matter initially deposited and buried in the sediment.

4.7 A 4 Million-Year COD record from the Ontong-Java Plateau and the eastern equatorial Pacific.

I measured COD in samples from the last ~4 Myr in ODP 806B (0°19.1'N, 159°21.7'E, 2519.9 m) from the Ontong-Java Plateau at roughly 50 kyr intervals (Figure 4.10) and in ODP 851B (2°42.2'N, 110°34.3'W, 3772.0 m) at roughly 100 kyr intervals (Figure 4.11). This resolution is too low to allow study of Milankovitch forcing on COD, and subsequently I am unable to say anything about whether the pronounced precessional forcing I observe in COD in RNDB 74P and ODP 849 for the last 400 kyr also exists for older ages. Poor reproducibility at some of the lower depths in 806B is probably an indication of redox reactions in the sediment, which requires further study. I observed pyrite in some of the 806B samples, below a depth of ~17 m. I observed no similar scatter in COD in 851B and did not observe any pyrite. In Figure 4.10 the COD for RNDB 74P, which was the survey piston-core for 806B, is also plotted for comparison with COD at older core depths in 806B, and Figure 4.11 shows data for 851B with higher resolution for the top ~450 kyr of that same core. For both locations, the data indicate that there may be some decay in the COD signal, possibly due to diagenesis of organic matter taking place on longer timescales than the 400 kyr records presented in Chapters 2 and 3. The differences between RNDB 74P and ODP 806B may also be an artifact of the effects of different storage conditions for the 2 cores, discussed above for ERDC 112Bx in Section 4.3.1.

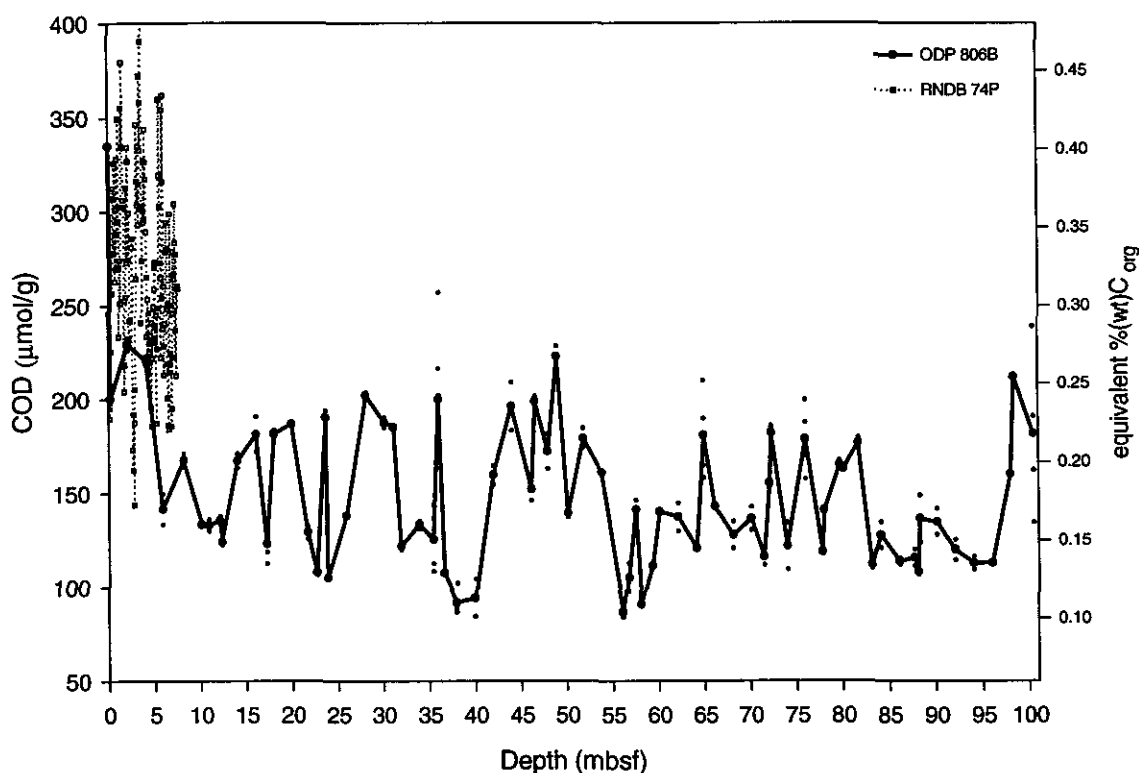


Figure 4.10. COD in ODP 806B ($0^{\circ}19.1'N$, $159^{\circ}21.7'E$, 2519.9 m) (solid line) (values shown for replicate samples) plotted with RNDB 74P ($0^{\circ}20'N$, $159^{\circ}22'E$, 2547m) (dotted line). Both cores are from the Ontong-Java Plateau. Scatter in COD at greater depths in 806B appears to be due to the presence of pyrite. The sampling interval in 806 B is approximately 50 kyr and the bottom sample has an age of ~ 4 Myr. The bottom of RNDB 74P has an age of ~ 395 kyr and the average sampling interval is 2-3 kyr.

The fact that the COD values in 851B also display lower values at greater depths, supports the conclusion that diagenesis of a fraction of the organic matter has taken place below the depths of the <400 ka samples. However, there are still significant swings in COD between high and low values at both locations. In the western equatorial Pacific, there appears to be more, higher frequency variability, with changes generally of less than a factor of 2, whereas in the east there are fewer peaks, even when taking into account that the time resolution in

sampling in ODP 851B is only about half of that in ODP 806B, but the amplitude of the peaks is generally greater. The average value in 851B is slightly higher (~15%) than in ODP

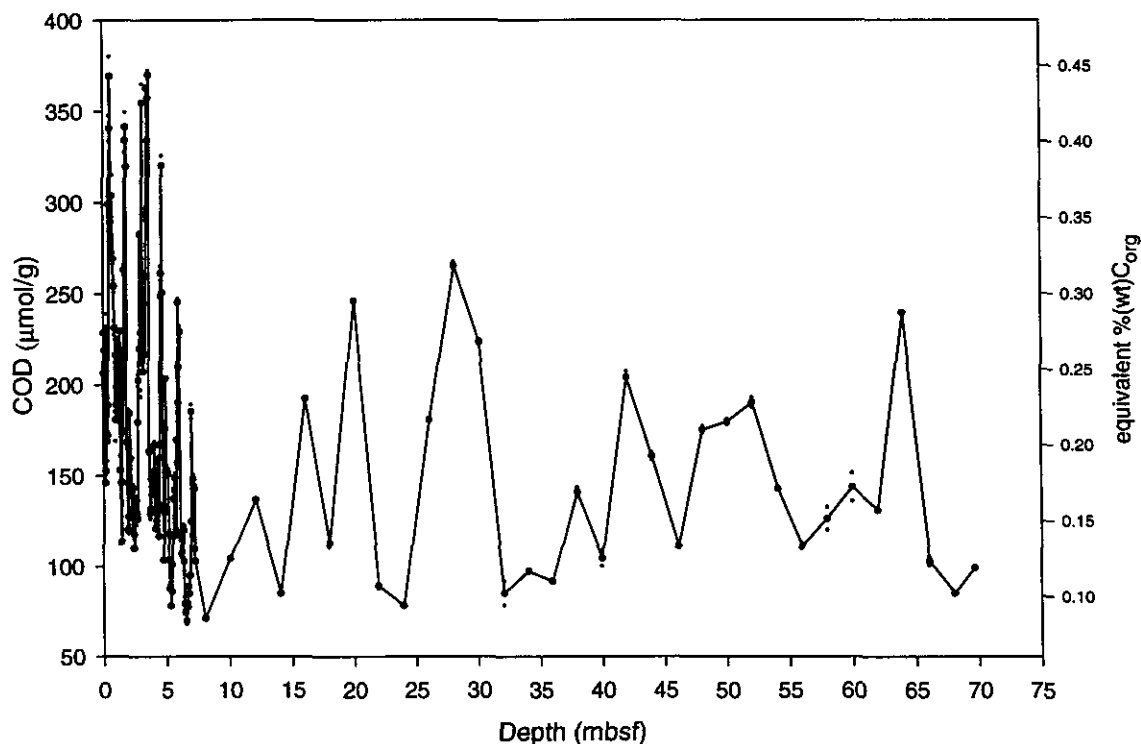


Figure 4.11. COD in ODP 851B (2°46.2'N, 110°34.3'E, 3772 m) from the eastern equatorial Pacific. The sampling interval is approximately 100 kyr and the bottom sample has an age of ~3.7 Myr. Higher resolution (an average interval of ~3-4 kyr) is shown for the top ~460 kyr of the core.

806B. This is actually the reverse of what is observed in COD in the late Pleistocene between the western and eastern equatorial Pacific, although again this difference could be due to the effects of storage conditions of the cores. The resolution of the COD data for both locations is insufficient to allow any conclusions as to whether COD would display a change in its behavior across the transition to significant Northern Hemisphere glaciation at around 2.7 Ma. The measurements in the Ontong-Java Plateau cores show that the investigation of Milankovitch variability in COD during and prior to the early Pleistocene, including earlier

in the Pliocene before the onset of significant Northern Hemisphere glaciation, and a comparison between the eastern and western equatorial Pacific, would be complicated by the possible occurrence of pyrite in ODP 806B.

Stax and Stein (1993) measured the total organic carbon content (TOC) in ODP Leg 130 cores (including ODP 806B) for the last ~25 Myr by making two measurements for each sample on a CHN Analyzer; measuring total carbon in the dry bulk sediment and organic carbon in carbonate free samples treated with 10% HCl. This method has the advantage that it eliminates the direct measurement of inorganic carbon and is not affected by inaccuracy when calibrating the total carbon technique. These are two major sources of error in many techniques used for measuring small concentrations of organic carbon in carbonate-rich samples. However, the loss of organic carbon through hydrolysis during the acid treatment cannot be quantified. For the last 4 Myr in ODP 806B, the Stax and Stein (1993) values lie between 0.05 and 0.27 %(wt), with an average of around 0.15 %(wt), which is comparable with my estimations of TOC from COD, although the lowest Stax and Stein values are smaller than the COD-derived values (the COD values provide an upper bound for TOC as discussed in Section 4.3.1). The close agreement between the two methods provides support for the validity of the COD method and perhaps more evidence for there being a real offset between TOC in RNDB 74P and ODP 806B.

Several ODP shipboard measurements of TOC in ODP 851B in samples that span the last 4 Myr also exist (Mayer et al., 1992, data provided on the CD-Rom), using a similar technique to Stein and Stax (1993). These are also in good agreement with the COD data.

The links between productivity and the concentration of magnetite in deep-sea sediments have been discussed by e.g. Tarduno (1994) and Yamazaki and Kawahata (1998). I did not

observe any correlation between magnetic susceptibility (magnetite has a high value of magnetic susceptibility) and COD in RNDB 74P, ODP 806B nor ODP 851B.

4.8 Summary

The data presented in this chapter have shown that there are complications when comparing absolute values of COD in different calcium carbonate-rich cores. There appears to be an effect from differences in storage conditions after retrieval of the cores from the sea floor, which can produce offsets between samples expected to have very similar COD (e.g. from sub-cores from the same box core), but does appear to preserve down-core COD trends. It is unclear which factors of storage conditions play a role in affecting COD, and ideally samples should be frozen and or dried as soon as possible after retrieval from the sea floor. It is also possible that COD measures the residual, highly refractory component of organic matter in the sediment, which is not eaten or attacked by bacteria and that the ratio of this component to the organic matter rain rate from the surface waters to the sediment is not constant so that COD is not necessarily higher in sites below more productive surface waters. The differences found between samples of similar ages from different cores complicates the study of the effects of factors such as water depth, calcium carbonate content, and distance from the equator. Because of this, the processes that cause differences between the cores studied here are often unclear and some of the data produced unexpected results, e.g. no indication of higher glacial COD in eastern equatorial Pacific cores at 3°S of the equator. (Generally, COD rises, sometimes by more than a factor of 2, from the mid-late Holocene into glacial conditions). A clear trend I observed in COD was a decay signal in the top 8-12 cm of the cores, roughly corresponding to the mixed layer. This may be a result of ongoing

diagenesis of this younger organic matter in the cores, uneven mixing by bioturbation, or it may reflect a true increase in the rain rate of organic matter from the surface waters from the early Holocene to present, which is not masked by either of the first two processes. COD appears to be dominated by the contribution from the fine fraction ($<63\mu\text{m}$), and the COD from the organic matter bound up in either the coccolithophore or foraminifer calcite lattice is very small (corresponding to $<\sim 0.08\%$ (wt) C_{org}). Generally, in the cores studied in this chapter, CaCO_3 preservation does not appear to be large enough to produce an observable effect on the absolute COD values or mask down-core trends. However, in deeper box cores from the Ontong-Java Plateau and particularly in two cores from the deep central equatorial Pacific with significant CaCO_3 dissolution, changes in CaCO_3 concentration do appear to drive the absolute value of COD and, in the piston cores, the down-core trend. Box and piston cores from the eastern equatorial Pacific did not indicate any significant influence on COD from reduced minerals of volcanic origin. However, at sediment depths of below $\sim 17\text{m}$ in an ODP core from the Ontong-Java Plateau it appears that pyrite causes anomalously high COD values and irreproducibility, which greatly complicates the study of older samples at this site. *Such a problem was not encountered in an ODP core from the eastern equatorial Pacific.* These longer records, into the Pliocene, display significant variations throughout the length of the record, with perhaps some down-core decay in COD, although the sampling resolution was too low to examine the role of Milankovitch forcing over this period on COD.

4.9. References

- Berger, W. H. and J. S. Killingley, Box cores from the equatorial Pacific: ^{14}C sedimentation rates and benthic mixing, *Marine Geology*, 45, 93-125, 1982.
- Glockhoff, C., Core descriptions for Eurydice Expedition: Equatorial Pacific and eastern Indian Oceans, *SIO Reference No. 79-21*, 1979.
- Glockhoff, C., Pleiades Expedition core descriptions: Eastern Tropical Pacific, *SIO Reference No. 82-13*, 1982.
- Hedges, J. I., and R. G. Keil, Sedimentary organic matter preservation: an assessment and speculative synthesis, *Marine Chemistry*, 49, 81-115, 1995.
- Herguera, J. C., and W. H. Berger, Paleoproductivity from benthic foraminifera abundance: Glacial to postglacial change in the west-equatorial Pacific, *Geology*, 19, 1173-1176, 1991.
- Herguera, J. C., Deep-sea benthic foraminifera and biogenic opal, glacial to postglacial productivity changes in the western Equatorial Pacific, *Marine Micropaleontology*, 19, 79-98, 1992.
- Herguera, J. C., and W. H. Berger, Glacial to postglacial drop in productivity in the western equatorial Pacific: Mixing rate vs. nutrient concentrations, *Geology*, 22, 629-632, 1994.
- Herguera, J. C., Last Glacial paleoproductivity from in the eastern equatorial Pacific: benthic foraminifera records, *Marine Micropaleontology*, 1999, in revision.
- Jahnke, R. A., S. R. Emerson, J. Cochran, J. Kirk, and D. J. Hirschberg, Fine scale distributions of porosity and particulate excess ^{210}Pb , organic carbon and CaCO_3 in surface sediments of the deep Equatorial Pacific, *Earth and Planetary Science Letters*, 77, 59-69, 1986.
- King, K., and P. E. Hare, Amino acid composition of the test as a taxonomic character for living and fossil planktonic foraminiferal changes near the Paleocene/Eocene boundary, *Micropaleontology*, 18, 285-293, 1972.
- Mayer, L., et al., *Proceedings of the Ocean Drilling Program Initial Report vol.*, 138, 1462 pp., Ocean Drill. Program, College Station, Texas, 1992.
- Prahl, F. G., L. A. Muehlhausen, and M. Lyle, An organic geochemical assessment of oceanographic conditions at Manop Site C over the past 26,000 years, *Paleoceanography*, 4, 495-510, 1989.
- Price, B. Equatorial Pacific sediments: A chemical approach to ocean history, Ph.D. thesis, Univ. of Calif. at San Diego, 1988.

- Stax, R., and R. Stein, Long-term changes in the accumulation of organic carbon in Neogene sediments, Ontong Java Plateau, *Proc. Ocean Drill. Prog. Sci. Results*, 130, 573-579, 1993.
- Stakes, D. S., D. Orange, J. B. Paduan, K. A. Salamy, and N. Maher, Cold-seeps and authigenic carbonate formation in Monterey Bay, California, *Marine Geology*, 159, 93-109, 1999.
- Suess, E., Interaction of organic compounds with calcium carbonate – II. Organo-carbonate association in recent sediments, *Geochim. Cosmochim. Acta*, 57, 147-157, 1973.
- Tarduno, J. A., Temporal trends of magnetic dissolution in the pelagic realm: gauging paleoproductivity?, *Earth Planet. Sci. Lett.*, 123, 39-48, 1994.
- Yamazaki, T. and H. Kawahata, Organic carbon flux controls the morphology of magnetofossils in marine sediments, *Geology*, 26, 1064-1066, 1998.
- Yasuda, M., Foraminifera as indicators of Quaternary carbonate saturation and productivity in the western equatorial Pacific, the last million years, Ph.D. thesis, Univ. of Calif. at San Diego, 1999, in prep.

4.10 Tables

Table 4.1.a. Site data for Ontong-Java Plateau cores.

Core	Water Depth (mbsf)	Latitude Longitude
ERDC 88Bx	1924	0° 2.9' S 155° 52.1' E
ERDC 113P	2163	1° 38.1' S 159° 13.2' E
ERDC 112Bx	2169	1° 37.5' S 159° 14.1' E
ERDC 120Bx	2247	0° 1.0' S 158° 41.6' E
ERDC 83Bx	2342	1° 24.1' N 157° 18.6' E
ERDC 79Bx	2767	2° 47.1' N 156° 13.8' E
ERDC 123Bx	2948	0° 1.3' S 160° 24.9' E
ERDC 125Bx	3368	0° 0.2' S 160° 59.9' E
ERDC 108Bx	3383	1° 44.8' S 160° 48.0' E
ERDC 135Bx	3509	0° 52.5' N 160° 59.6' E
ERDC 77Bx	3584	4° 55.0' N 156° 3.5' E
ERDC 128Bx	3732	0° 0.3' S 161° 25.6' E
ERDC 136Bx	3845	1° 6.0' N 161° 36.3' E
ERDC 139Bx	4118	1° 21.7' N 162° 23.6' E
ERDC 129Bx	4169	0° 0.4' S 161° 58.5' E
ERDC 141Bx	4325	2° 21.7' N 163° 42.4' E
ERDC 131Bx	4441	0° 1.6' S 162° 42.1' E
ODP 806B	2520	0° 19.1' N 159° 21.7' E
RNDB 74P	2547	0° 20' N 159° 22' E
RC17-177	2600	1° 45.3' N 159° 26.9' W

Table 4.1.b. Site data for eastern and central equatorial Pacific cores.

Core	Water Depth (mbsf)	Latitude Longitude
PLDS 66Bx	3497	0° 56.6' N 104° 06.1' W
PLDS 69PV	3527	1° 02.1' N 105° 35.0' W
PLDS 73PV	3672	1° 00.4' N 109° 18.9' W
PLDS 16PV	3251	3° 19.4' S 102° 03.5' W
PLDS 15PG	3222	3° 20.9' S 102° 15.1' W
PLDS 92Bx	4515	3° 57.2' N 135° 58.7' W
PLDS 107Bx	4849	6° 09.4' N 138° 16.6' W
ODP 851B	3772	2° 42.2' N 110° 34.3' W

Table 4.2. Data for piston-core RC17-177 from the Ontong-Java Plateau appearing in Figure 4.2.

COD	COD equivalent C _{org}	COD contribution of size fraction in bulk	COD equivalent C _{org}	size fraction	
μmol/g	%(wt)	μmol/g	%(wt)		
387.87	0.466	192.40	0.231	<63μm	
388.48	0.467	192.70	0.231	<63μm	
381.73	0.458	189.30	0.227	<63μm	
458.38	0.551			<63μm	peroxide treated
466.31	0.560			<63μm	peroxide treated
67.68	0.081			<63μm	Na hypochlorite treated
62.12	0.075			<63μm	Na hypochlorite treated
167.99	0.202	17.97	0.022	63-150μm	
205.24	0.247	21.96	0.026	63-150μm	
169.59	0.204			63-150μm	peroxide treated
170.89	0.205			63-150μm	peroxide treated
107.35	0.129	13.42	0.016	<150-250μm	
109.74	0.132	13.72	0.016	<150-250μm	
96.57	0.116			<150-250μm	peroxide treated
118.49	0.142			<150-250μm	peroxide treated
76.88	0.092	20.91	0.025	>250μm	
88.28	0.106	24.01	0.029	>250μm	
73.30	0.088			>250μm	peroxide treated
76.38	0.092			>250μm	peroxide treated
55.95	0.067			>250μm	Na hypochlorite treated
60.59	0.073			>250μm	Na hypochlorite treated
		total COD in bulk sample			
		260.00	0.312		

Table 4.3. Data for box core ERDC 112Bx appearing in Figure 4.3.

date analysed	sample description	depth interval in core cm	depth in core (mid-point) cm	C-14 age interpolated		C-14 age interpolated kyr	COD in duplicates $\mu\text{mol/g}$	COD average $\mu\text{mol/g}$	equivalent C _{org} %(wt)
				yr	yr				
951002	ERDC 112Bx1	0-1		4107		4.107	221.939		
951002	ERDC 112Bx1	0-1	0.5	4107		4.107	230.830	226.385	0.272
951003	ERDC 112Bx1	1-2	0.5	4223		4.223	194.548		
951003	ERDC 112Bx1	1-2	1.5	4223		4.223	193.802	194.175	0.233
980518	ERDC 112Bx1c	2-3	1.5	4340		4.340	230.338		
980518	ERDC 112Bx1c	2-3	2.5	4340		4.340	242.243	236.291	0.284
980522	ERDC 112Bx1	2-3	2.5	4340		4.340	200.543		
980522	ERDC 112Bx1	2-3	2.5	4340		4.340	198.209	199.376	0.239
950929	ERDC 112Bx37	3-4	3.5	4457		4.457	206.843		
950929	ERDC 112Bx37	3-4	3.5	4457		4.457	189.269	198.056	0.238
951003	ERDC 112Bx47	5-6	5.5	4690		4.690	189.305		
951003	ERDC 112Bx47	5-6	5.5	4690		4.690	183.269	186.287	0.224
950929	ERDC 112Bx47	7-8	7.5	4923		4.923	195.538		
950929	ERDC 112Bx47	7-8	7.5	4923		4.923	215.906	205.722	0.247
950929	ERDC 112Bx47	8-9	8.5	5040		5.040	121.352		
950929	ERDC 112Bx47	8-9	8.5	5040		5.040	139.823	130.588	0.157
950929	ERDC 112Bx47	10-11	10.5	5734		5.734	172.330		
950929	ERDC 112Bx47	10-11	10.5	5734		5.734	166.004	169.167	0.203
951003	ERDC 112Bx47	11-12	11.5	6080		6.080	162.463		
951003	ERDC 112Bx47	11-12	11.5	6080		6.080	147.470	154.967	0.186
950929	ERDC 112Bx47	12-13	12.5	6427		6.427	106.408		
950929	ERDC 112Bx47	12-13	12.5	6427		6.427	116.391	111.400	0.134
951003	ERDC 112Bx47	13-14	13.5	6774		6.774	137.592		
951003	ERDC 112Bx47	13-14	13.5	6774		6.774	129.151	133.372	0.160
951003	ERDC 112Bx47	16-17	16.5	7814		7.814	137.830		
951003	ERDC 112Bx47	16-17	16.5	7814		7.814	127.004	132.417	0.159
950929	ERDC 112Bx47	17-18	17.5	8161		8.161	147.674		
950929	ERDC 112Bx47	17-18	17.5	8161		8.161	168.403	158.039	0.190
950929	ERDC 112Bx47	18-19	18.5	8508		8.508	150.108		
950929	ERDC 112Bx47	18-19	18.5	8508		8.508	120.335	135.222	0.162

Table 4.3 continued										
950929	ERDC 112Bx47	19-20	19.5	8855	8.855	175.879	181.892	0.218		
950929	ERDC 112Bx47	19-20	19.5	8855	8.855	187.905	181.892	0.218		
980522	ERDC 112Bx47	20-21	20.5	9201	9.201	125.515				
980522	ERDC 112Bx47	20-21	20.5	9201	9.201	179.497	152.506	0.183		
951003	ERDC 112Bx47	20-21	20.5	9201	9.201	164.934	164.934	0.198		
951003	ERDC 112Bx47	21-22	21.5	9548	9.548	149.133				
951003	ERDC 112Bx47	21-22	21.5	9548	9.548	139.198	144.165	0.173		
950929	ERDC 112Bx47	23-24	23.5	10242	10.242	175.945	175.945	0.211		
951003	ERDC 112Bx47	25-26	25.5	10935	10.935	120.515				
951003	ERDC 112Bx47	25-26	25.5	10935	10.935	131.672	126.093	0.151		
950929	ERDC 112Bx47	26-27	26.5	11282	11.282	148.052	148.052	0.178		
950926	ERDC 112Bx47	27-28	27.5	11629	11.629	268.694				
950926	ERDC 112Bx47	27-28	27.5	11629	11.629	280.987	274.841	0.330		
951003	ERDC 112Bx47	27-28	27.5	11629	11.629	289.098				
951003	ERDC 112Bx47	27-28	27.5	11659	11.659	229.618	259.358	0.312		
950929	ERDC 112Bx47	29-30	29.5	12323	12.323	207.648				
950929	ERDC 112Bx47	29-30	29.5	12323	12.323	175.339	191.493	0.230		
951003	ERDC 112Bx47	30-31	30.5	12669	12.669	179.372				
951003	ERDC 112Bx47	30-31	30.5	12669	12.669	167.640	173.506	0.208		
951003	ERDC 112Bx1	31-32	31.5	13016	13.016	317.714				
951003	ERDC 112Bx1	31-32	31.5	13016	13.016	338.983	328.349	0.394		
951003	ERDC 112Bx47	32-33	32.5	13363	13.363	227.680				
951003	ERDC 112Bx47	32-33	32.5	13363	13.363	234.285	230.983	0.277		
950929	ERDC 112Bx47	33-34	33.5	13710	13.710	315.126				
950929	ERDC 112Bx47	33-34	33.5	13710	13.710	296.305	305.715	0.367		
980515	ERDC 112Bx47	34-35	34.5	14056	14.056	296.759				
980515	ERDC 112Bx47	34-35	34.5	14056	14.056	292.858	294.808	0.354		
950926	ERDC 112Bx47	35-36	35.5	14403	14.403	302.059				
950926	ERDC 112Bx47	35-36	35.5	14403	14.403	326.735	314.397	0.378		
951002	ERDC 112Bx47	35-36	35.5	14403	14.403	288.917				
951002	ERDC 112Bx47	35-36	35.5	14403	14.403	341.482	315.200	0.379		
951002	ERDC 112Bx47	37-38	37.5	15097	15.097	264.976				
951002	ERDC 112Bx47	37-38	37.5	15097	15.097	275.806	270.391	0.325		
980518	ERDC 112Bx5	0-1	0.5	4107	4.107	430.358				

Table 4.3 continued

980518	ERDC 112Bx5	0-1	0.5	4107	4.107	440.189	435.273	0.523
971216	ERDC 112Bx?	2-3	2.5	4340	4.340	391.089		
971216	ERDC 112Bx?	2-3	2.5	4340	4.340	402.689	396.889	0.477
980515	ERDC 112Bx5	5-6	5.5	4690	4.690	372.938		
980515	ERDC 112Bx5	5-6	5.5	4690	4.690	325.839	349.389	0.420
980518	ERDC 112Bx5	10-11	10.5	5734	5.734	300.375		
980518	ERDC 112Bx5	10-11	10.5	5734	5.734	300.096	300.236	0.361
980518	ERDC 112Bx5	15-16	15.5	7468	7.468	292.759		
980518	ERDC 112Bx5	15-16	15.5	7468	7.468	285.569	289.164	0.347
980518	ERDC 112Bx5	20-21	20.5	9201	9.201	287.153		
980518	ERDC 112Bx5	20-21	20.5	9201	9.201	287.593	287.373	0.345
980515	ERDC 112Bx5	25-26	25.5	10935	10.935	394.101		
980515	ERDC 112Bx5	25-26	25.5	10935	10.935	400.125	397.113	0.477
980522	ERDC 112Bx5	30-31	30.5	12669	12.669	412.868		
980522	ERDC 112Bx5	30-31	30.5	12669	12.669	405.368	409.118	0.491
971216	ERDC 112Bx?	34-35	34.5	14056	14.056	458.085		
971216	ERDC 112Bx?	34-35	34.5	14056	14.056	459.725	458.905	0.551
980522	ERDC 112Bx5	36-37	36.5	14750	14.750	488.805		
980522	ERDC 112Bx5	36-37	36.5	14750	14.750	434.318	461.562	0.554

depth in core (mid-point) cm	Corg(%) B.Price (1988) %(wt)	depth in core (mid-point) cm	CaCO3(%) B.Price (1988) %(wt)	depth in core (mid-point) cm	sand M.Yasuda (1999) %(wt)
1	0.300	0.5	86.30	0.5	26.3
3	0.181	3.5	84.18	0.5	52.4
5	0.150	7.5	85.84	3.5	40.0
7	0.180	11.5	85.51	7.5	43.0
9	0.167	15.5	85.16	11.5	35.0
11	0.131	19.5	85.91	11.5	35.0
13	0.141	23.5	84.44	15.5	42.0
15	0.122	27.5	79.09	15.5	42.0
17	0.106	31.5	77.95	19.5	44.8

Table 4.3	continued					
19	0.111	35.5	81.20	23.5	37.0	
21	0.094			27.5	29.0	
23	0.103			31.5	23.3	
25	0.099			35.5	23.5	
27	0.105					
29	0.133					
31	0.182					
33	0.233					
35	0.258					
37	0.265					

Table 4.4. Data for box core ERDC 128Bx appearing in Figure 4.4.

date analysed	sample description	depth interval in core	depth in core (mid-point)	COD in duplicates	COD average	equivalent Corg
		cm	cm	$\mu\text{mol/g}$	$\mu\text{mol/g}$	%(wt)
980521	ERDC 128Bx2	1-2	1.5	478.387		
980521	ERDC 128Bx2	1-2	1.5	505.807	492.097	0.591
980521	ERDC 128Bx3	5-6	5.5	414.965		
980521	ERDC 128Bx3	5-6	5.5	454.669	434.817	0.522
980521	ERDC 128Bx2	11-12	11.5	299.973		
980521	ERDC 128Bx2	11-12	11.5	304.044	302.009	0.363
980521	ERDC 128Bx2	15-16	15.5	260.381		
980521	ERDC 128Bx2	15-16	15.5	249.084	254.733	0.306
980521	ERDC 128Bx2	21-22	21.5	293.168		
980521	ERDC 128Bx2	21-22	21.5	306.220	299.694	0.360
980521	ERDC 128Bx2	25-26	25.5	324.794		
980521	ERDC 128Bx2	25-26	25.5	335.941	330.368	0.397
980521	ERDC 128Bx2	31-32	31.5	360.928		
980521	ERDC 128Bx2	31-32	31.5	393.888	377.408	0.453
980515	ERDC 128Bx2	35-36	35.5	431.933		
980515	ERDC 128Bx2	35-36	35.5	397.069	414.501	0.498
980518	ERDC 128Bx2	41-42	41.5	597.365		
980518	ERDC 128Bx2	41-42	41.5	585.062		
980518	ERDC 128Bx2	41-42	41.5	591.215	591.214	0.710

depth in core (mid-point)	CaCO ₃ (%) M.Yasuda (1999)
cm	%(wt)
0.5	77.95
2.5	79.80
5.5	80.34
8.5	84.44
11.5	83.77
15.5	81.35
19.5	82.30
24.5	78.02
29.5	79.50
34.5	77.20
38.5	80.4
39.5	80.29

Table 4.5. Data for ERDC cores appearing in Figures 4.7 and 4.8.

Date analysed	sample description	depth interval in core	depth in core mid-point	COD average $\mu\text{mol/g}$	equivalent Corg % (wt)	benthic foram (BF) abundance ¹	CT SAR ¹	COD AR $\mu\text{mol/cm}^2\text{kyr}$	Corg MAR $\text{g/m}^2\text{kyr}$	BF AR $\text{\#}/\text{cm}^2\text{kyr}$	water depth
		cm	cm			$\text{\#}/\text{g}$	$\text{g}/\text{cm}^2\text{kyr}$				m
Core-top samples											
971126	ERDC 88Bx	1-2	1.5	325.418	0.391	87.12	1.47	478.365	57.456	128.07	1924
971216	ERDC 112Bx	2-3	2.5	396.889	0.477	72.27	1.70	674.711	81.040	122.86	2169
980518	ERDC 112Bx1c	2-3	2.5	236.291	0.284	72.27	1.70	401.694	48.247	122.86	2169
971016	ERDC 83Bx	2-3	2.5	348.493	0.419	56.06	1.67	581.983	69.902	93.62	2342
980515	ERDC 83Bx2c	2-3	2.5	269.523	0.324	56.06	1.67	450.104	54.062	93.62	2342
971014	ERDC 79Bx	2-3	2.5	490.603	0.589	56.55	1.69	829.120	99.586	95.57	2767
971126	ERDC 123Bx	2-3	2.5	382.392	0.459	44.00	1.71	653.890	78.539	75.24	2948
971126	ERDC 125Bx	0-1	0.5	461.807	0.555	51.19	1.63	752.745	90.412	83.44	3368
971216	ERDC 108Bx	2-3	2.5	573.452	0.689	52.32	1.49	854.444	102.627	77.96	3363
971106	ERDC 77Bx	1-2	1.5	394.095	0.473	50.41	0.98	386.213	46.388	49.40	3585
980521	ERDC 128Bx2	1-2	1.5	492.097	0.591						3732
971216	ERDC 136Bx	2-3	2.5	517.840	0.622	58.11	1.19	616.230	74.015	69.15	3848
971216	ERDC 139Bx	1-2	1.5	407.216	0.489	63.06	0.82	333.917	40.107	51.71	4118
980522	ERDC 139Bx1c	1-2	1.5	389.310	0.468	63.06	0.82	319.234	38.343	51.71	4118
971126	ERDC 129Bx	0-1	0.5	736.017	0.884	62.50	1.02	750.738	90.171	63.75	4169
971126	ERDC 141Bx	2-3	2.5	480.695	0.577	97.86	0.47	225.927	27.136	45.99	4324
971126	ERDC 131Bx	0-1	0.5	615.173	0.739	52.69	0.97	596.718	71.672	51.11	4441
LGM samples											
971126	ERDC 88Bx	35-36	35.5	362.003	0.435	127.10	1.47	691.789	83.091	242.89	1924
971216	ERDC 112Bx	34-35	34.5	458.905	0.551	123.10	1.70	1014.180	121.813	272.05	2169 deglacial
980515	ERDC 112Bx	34-35	34.5	294.808	0.354	123.10	1.70	651.526	78.255	272.05	2169 deglacial
971106	ERDC 113P	28-29	28.5	425.017	0.510	124.00	1.68	928.237	111.491	270.82	2158
971126	ERDC 120Bx	37-38	37.5	531.646	0.639	121.20	1.70	1174.938	141.122	267.85	2247

Appendix A.

The combustion oxygen demand method: Instrument performance and calibration.

A.1. Introduction and Theoretical Background.

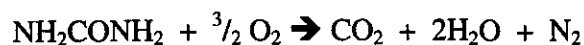
The combustion oxygen demand (COD) method measures the total amount of oxygen consumed upon complete combustion of the sample. In general, the amount of O₂ consumed in the combustion process will depend on the abundances of oxidizable elements in the sample and the difference in their oxidation states before and after combustion. Potentially important oxidizable elements in sediments include C, H, N, S, Fe and Mn. The observed COD is equivalent to a weighted average of the abundances of reduced forms of these elements in the samples.

Possible oxidation products for carbon include CO and CO₂, while possible oxidation products for hydrogen include H₂O and H₂. Complete combustion of carbon is promoted using a platinum on alumina catalyst. During the calibrations with potassium hydrogen phthalate (KHP) (HOCOC₆H₄COOK) (see below, Section A.3 and Figure A.4) and benzoic acid (C₆H₅COOH), the yields of CO and H₂ must have been small, otherwise I would not have obtained good agreement between predicted (the prediction assumed complete combustion to H₂O and CO₂) and observed oxygen consumption. One way to test for CO and H₂ production under a wider range of circumstances, would be to pass the exhaust from the combustion through a quadrupole mass spectrometer, which I did not attempt during my thesis studies.

From thermodynamic and kinetic considerations (Glassman, 1987) one would expect most of the nitrogen in the samples to react to form N₂ or NO, although small yields of N₂O and NO₂ are also possible. NO actually also has paramagnetic properties, which make it behave like N₂ in the COD instrument. As an example, if sediment carbon contained a C/N ratio of 6.6 (the classic "Redfield" ratio) then the O₂/C combustion ratio would vary from 1.11 to 1.18 depending on whether the final product is N₂ or NO, respectively. Given that organic N tends to undergo preferential remineralization relative to organic C during its descent through the water column and subsequent burial in the sediment, then the differences in oxygen consumption produced by different scenarios of oxidation state changes of the nitrogen upon combustion would be even smaller than this. I investigated the extent of N oxidation by measuring the oxygen consumed on burning 110 μL aliquots of different concentrations of urea (NH₂CONH₂) solutions in water purified by a "milli-Q" system, to boost the N/C ratio.

There are a number of possible ways in which urea can combine with oxygen during combustion in the COD instrument at 950°C. In each case, complete oxidation to CO₂ and H₂O is assumed. The most reduced oxidation product is N₂ and the most oxidized is HNO₃:

(i) When only N₂ is formed:



(ii) HNO₃ is formed:

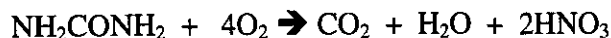


Figure A.1 shows the number of moles of O₂ consumed per mole of N in urea for different concentrations of urea solutions. Importantly, the straight line produced from the urea solutions indicates that the oxidation state change that takes place is consistent from one combustion to the next for different amounts of nitrogen. The slope of the regression fit is consistent with the N being oxidized to a combination of N₂ and NO, with possibly a small amount of NO₂ formed. Again, a study of the combustion exhaust with a quadrupole mass spectrometer may be helpful in determining the nature of the oxidation state changes of the nitrogen.

We expect sulfur to oxidize to a mixture of SO₂ and SO₃ (Glassman, 1987). The oxidation of SO₂ to SO₃ can be catalyzed using vanadium pentoxide (V₂O₅) or other catalysts operated at temperatures of a few hundred degrees Celsius (Glassman, 1987), but at higher temperatures V₂O₅ favors oxidation to SO₂. No catalysts for S oxidation were used in the COD instrument. I tested for the oxidation state changes of sulfur by pyrolyzing known amounts of pyrite and elemental sulfur and measuring oxygen consumption. No catalyst was used in the COD apparatus.

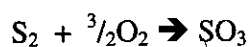
The results for elemental sulfur are presented in Figure A.2. There are a number of possible ways in which sulfur can combine with oxygen during combustion in the COD instrument at 950°C. Sulfur can combine with oxygen to produce just SO₂ or just SO₃, or a combination of the two:

(i) Just SO₂ is formed:



1 mole S₂ combines with 2 moles O₂.

(ii) Just SO₃ is formed:



1 mole S₂ combines with ³/₂ moles O₂.

Again, as with urea, the straight line indicates that the oxidation state change that takes place is consistent from one combustion to the next for different amounts of sulfur. The slope of the regression fit for the curve indicates that the S is being oxidized to SO₂. I also carried out some combustions with samples of pyrite and these confirmed that S is converted to SO₂.

In the carbonate-rich equatorial Pacific sediments, we expect the organic material will be the dominant reservoir of reduced elements in the form of reduced C, H, and N. Here the combustion oxygen demand should be closely related to organic carbon content. The correspondence will not be perfect, however, as COD is sensitive also to the C/H, C/O, and C/N ratio of the organic material. It is likely that COD in moles O₂ per gram sample will exceed organic carbon content in moles organic C per gram sample O₂ by 10 to 30%.

Figure A.1. Measured O₂ consumption for 110 μ L aliquots of different concentrations of urea (NH₂CONH₂) solutions in water purified by a “milli-Q” system with the slope of the regression fit.

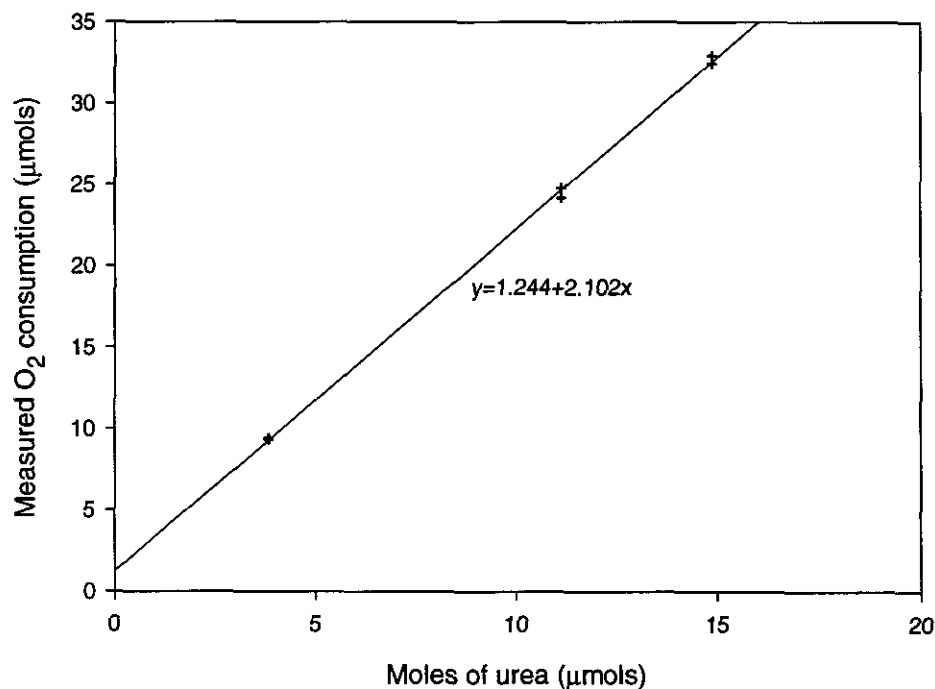


Figure A.2. Measured O₂ consumption for different masses of elemental sulfur with the slope of the regression fit.

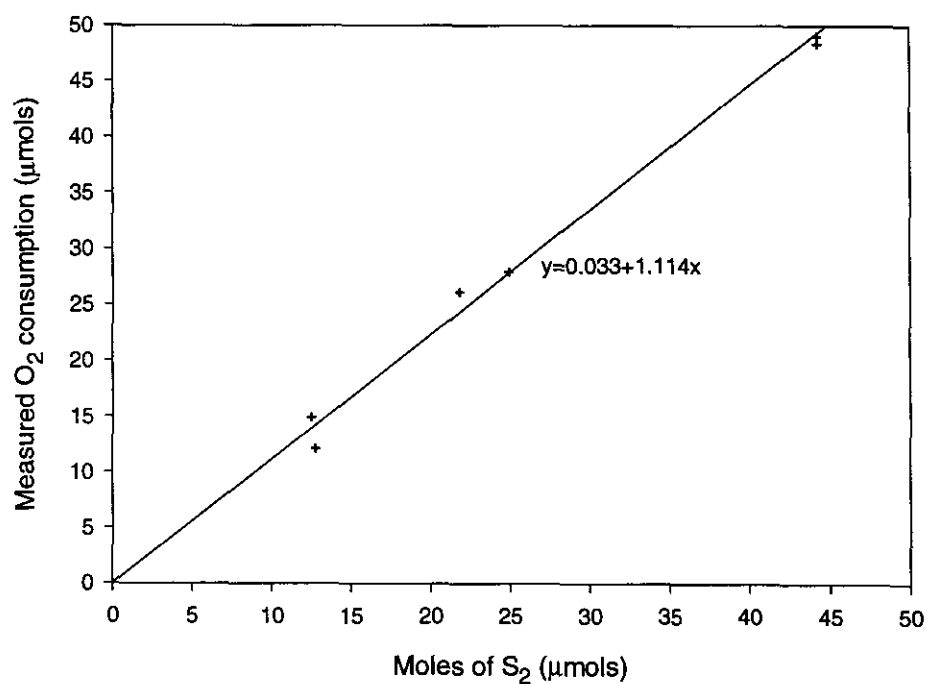
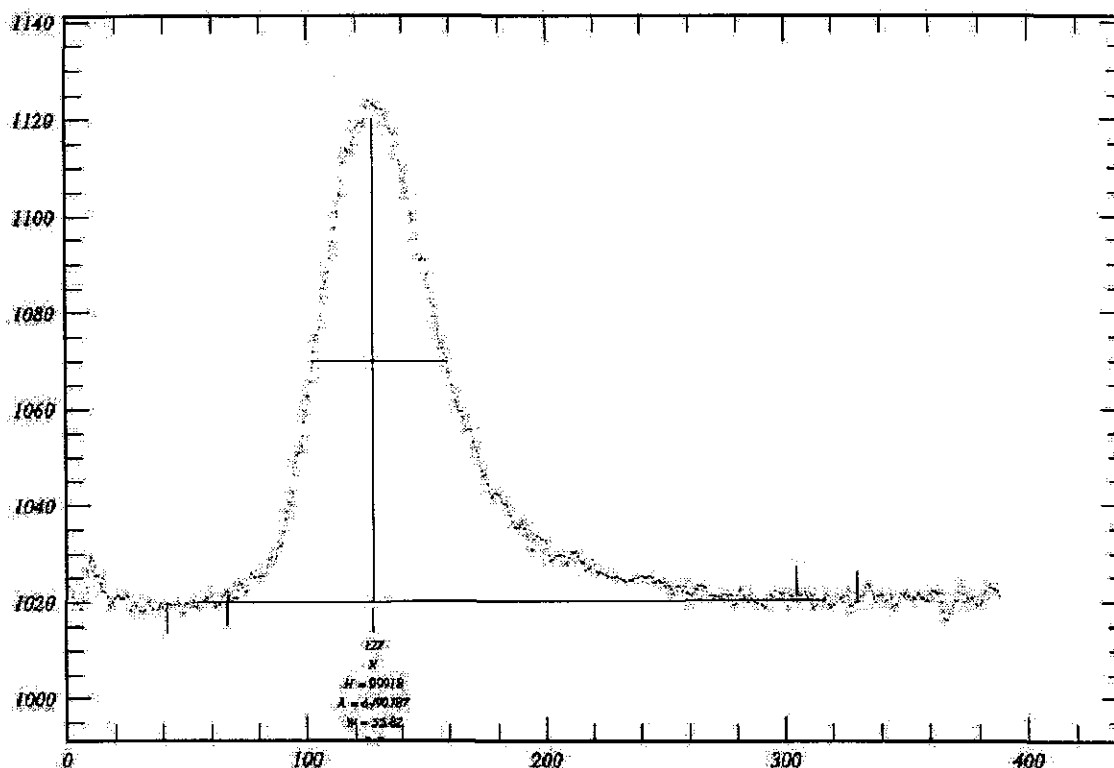
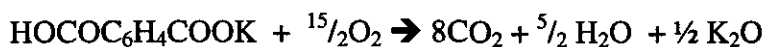


Figure A.3. A typical oxygen depletion peak obtained for the combustion of 40.23 mg of carbonate-rich sediment sample from ODP 851B on the Ontong-Java Plateau. The area of the peak corresponds to an oxygen consumption of 6.77 $\mu\text{mol O}_2$. The peaks were integrated on a Sun Microsystems Sparcstation 20 computer using adapted software developed for gas chromatograph peaks (P. Salameh, pers. comm.).



and it was impossible with the microbalance to accurately weigh out the small masses of KHP solid which would have an oxygen consumption over the range of such sediment samples. Assuming complete oxidation (which was promoted by the platinum on alumina pellets used to pack the tube in the oven just downflow of where the sample sits during combustion), KHP combines with oxygen upon combustion according to the following equation:



Hence from the formula weight, the KHP consumes 0.03672 moles of O_2 per gram of KHP. When combusting KHP standard solutions, the amount of O_2 consumed thus ranges from 5.5 μmol s to 47.7 μmol s.

During the course of each day that the COD instrument was operated it was calibrated by combustion of four or five of the different KHP standards. The aliquots of KHP solution were dried under a heat lamp for at least 30 minutes before being placed in the analyzer. This drying was necessary because the analyzer produced a signal from water vapor. (Although the reason for this observed behavior is unclear, a possible The H_2O vapor disappears in the

Figure A.4. Calibration curve for 100 μL aliquots of KHP (potassium hydrogen phthalate) solution.

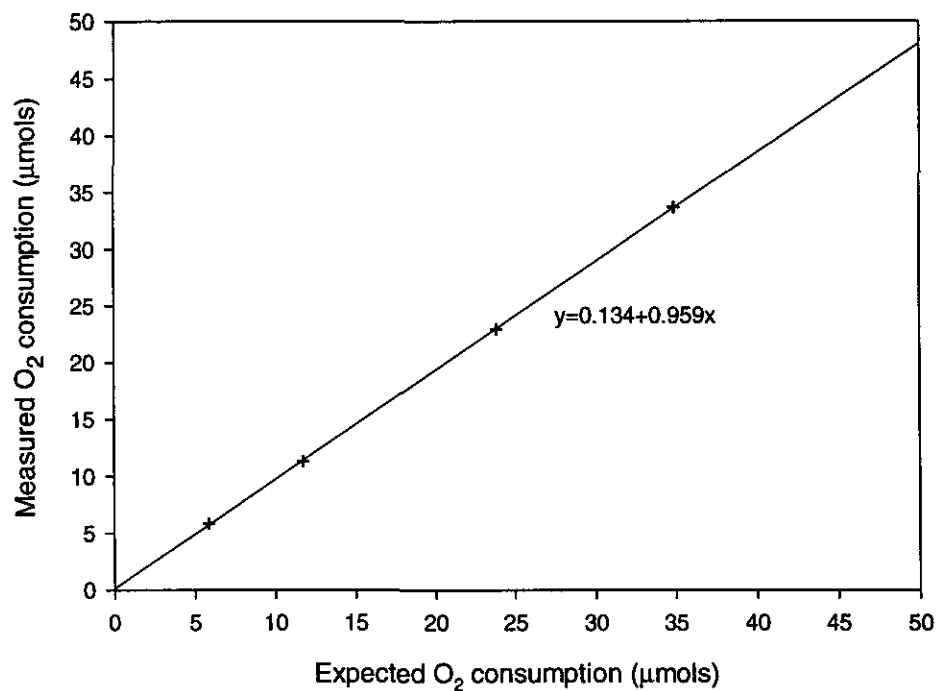
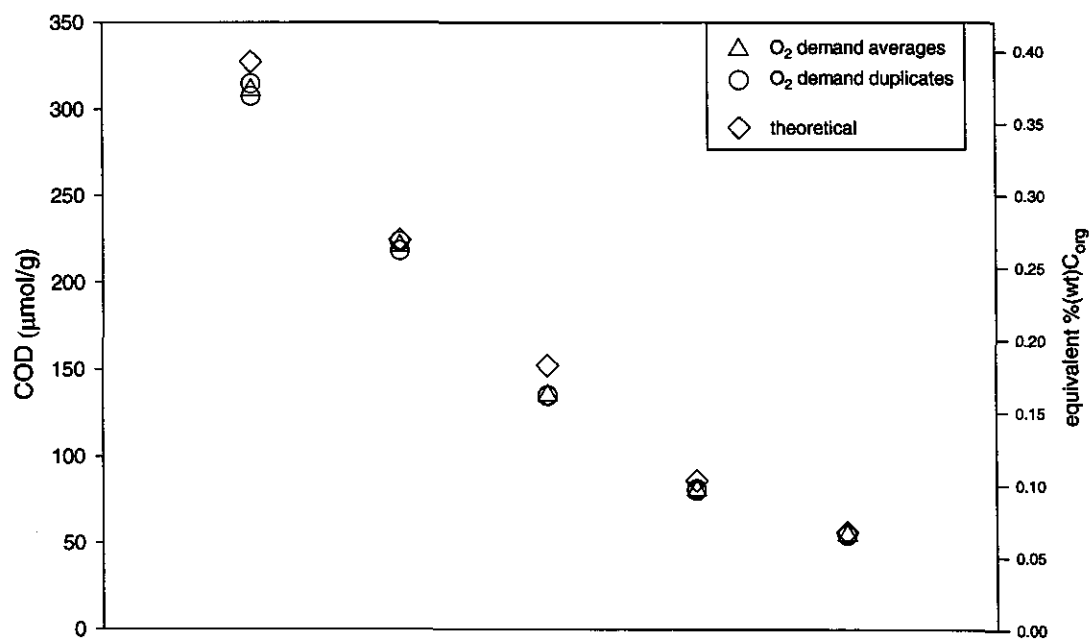


Figure A.5. COD measured in duplicate samples from standards made up from aliquots of KHP (potassium hydrogen phthalate) solution in water purified by a “milli-Q” system on calcium carbonate. The diamonds show the expected oxygen consumption based on the oxidation state change under complete oxidation of the C and H in the KHP.



trap, but the O_2/N_2 ratio is retained). A calibration curve, such as that shown in Figure A.4, was plotted each day from the amounts of O_2 consumed and the gradient of the curve used to scale all the results from that day.

Figure A.5 shows the performance of the COD instrument on standards made up from aliquots of the KHP solutions on calcium carbonate.

A.4. References

Glassman, *Combustion*, Academic Press Inc., Orlando, USA, 1987.